Department of Materials Science and Nanotechnology

PhD program Materials Science and Nanotechnology

Cycle XXXVIII

Sulfation and crosslinking of tamarind seed polysaccharide: physico-chemical characterization and biological evaluation

Sabrina Ziliani

833069

Tutor: Prof. Carlo Antonini

Co-tutor: Dr. Marco Sansò, Dr.ssa Sabrina Bertini

Coordinator: Prof. Francesco Cimbro Montalenti

ACADEMIC YEAR 2024/2025

Finanziato dall'Unione europea NextGenerationEU

Ministero dell'Università e della Ricerca

Italiadomani PIANO NAZIONALE DI RIPRESA E RESILIENZA

A mio Papà

I. TABLE OF CONTEXTS

II. ABSTRACT

My PhD project was funded by the University of Milano-Bicocca and the pharmaceutical company IFBS-Istituto Farmaco-Biologico Sperimentale in collaboration with Istituto di Ricerche Chimiche e Biochimiche G. Ronzoni.

The project was based on the chemical modification of the polysaccharide extracted from the seed kernels of *Tamarindus indica* L., tamarind seed polysaccharide (TSP). TSP is a neutral and water-soluble polysaccharide composed of a β-(1,4)-D-glucan backbone with α-(1,6)-D-xylose branches that are partially substituted with β-(1,2)-D-galactose. It is used as a stabilizer, thickener, gelling agent, and binder in food and pharmaceutical industries, due to its physical, chemical, and biological properties like broad pH tolerance, biocompatibility, high thermal stability, and non-carcinogenicity. Particularly, it is employed in the ophthalmic field in the formulation of eyes drop used for the treatment of the Dry-Eyed Disease (DED).

However, the high viscosity of TSP and the absence of charges on the sugar chain make the solubilization of this polysaccharide difficult. For this reason, a chemical modification of TSP is conducted adding sulfated groups on the chain to improve its workability, the physical and biological properties.

Several synthetic approaches were explored to identify the optimal sulfation conditions and to obtain sulfated samples with varying degrees of substitution, while preserving the native polysaccharide structure. The chemical and physical properties of the sulfated products were characterized by using various analytical techniques to confirm the success of the synthesis and to achieve a comprehensive characterization of the synthesized products. Physical, rheological, and morphological studies were conducted on the modified samples. Furthermore, NMR spectroscopy and mass spectrometry were applied to hydrolyzed products to investigate their chemical structure. Mucoadhesion with the glycoprotein mucin was evaluated through rheological measurements and zeta potential analysis, as reported in the literature. Finally, biological assays, such as the MTT test, were performed to assess the cytotoxicity of the synthesized samples, in collaboration with the Department of Pharmacy, University of Pisa.

The sulfated products exhibited higher solubility than native TSP, with molecular weight ranging from 700 to 1000 kDa, a sulfation degree of two to four groups per repeating unit, and pseudoplastic behavior. A preliminary mucoadhesion study revealed an unexpected interaction between S-TSP and mucin, suggesting a potential mechanism through which

the interactions sulfated TSP and mucin with biomolecules might occur. Moreover, no cytotoxic effects were detected in sulfated products.

After establishing the sulfation of TSP, the research focused on the possibility of cross-linking and/or derivatizing TSP to obtain a biopolymer capable of absorbing liquids, modulating enzymatic activities to enhance its residence time in biological systems, and exhibiting new rheological properties. The products were synthesized using 1,4-butanediol diglycidyl ether (BDDE) as a crosslinked agent, at different concentrations, in order to obtain both hydrogels and soluble modified samples. Their physio-chemical properties were analyzed using various analytical techniques, depending on their different solubility and viscosity profiles.

Morphological, physical and spectroscopic analysis were performed on the modified samples. The rheological properties, including viscosity and moduli G' (storage or elastic modulus) and G" (loss or viscous modulus) were measured to characterize the rheological behavior of the functionalized products. The cytotoxicity and the pharmacological potential of the samples were also evaluated using *in vitro* assays conducted at the Department of Pharmacy, University of Pisa. Hydrolyzed samples, obtained with xyloglucanase treatment, were analyzed by NMR spectroscopy and mass spectrometry. MALDI-TOF analysis was performed during my research period at KU Leuven University, Belgium.

In conclusion, the hydrogel products exhibited higher viscosity than native TSP, as expected, with G' values exceeding G'', confirming their gel-like behavior. For the lower viscosity products, the molecular weights were similar to or slightly lower than those of TSP, likely due to a partial depolymerization during synthesis. These results were confirmed by viscosity values which remained similar to or slightly lower than TSP. Following enzymatic degradation of the synthesized samples, the BDDE content, calculated from NMR spectra, ranged from 2 to17%. MALDI-TOF spectra revealed oligosaccharide structures containing crosslinked BDDE as well as monolinked BDDE, demonstrating that the crosslinker can attach TSP on both sides, forming a crosslink, or on only one side, generating a pendant structure. As expected, with increasing of the BDDE concentration, more crosslinked oligosaccharide structures were observed in the spectra compared to monolinked or not linked fragments.

In summary, during my PhD, I successfully chemically modified TSP to enhance its properties and thoroughly characterized the physio-chemical and biological properties of the synthetized products.

III. LIST OF ABBREVATIONS

ATR	Attenuated Total Reflectance
BDDE	1,4-Butanediol diglycidyl ether
BDPE	1,4-Butanediol di-(propan-2,3 diolyl)
BSD	Backscatter Detector
BSE	Back Scattered Electrons
COSY	Correlation Spectroscopy
CP	Cross Polarization
C-TSP	Crosslinked Tamarind Seed Polysaccharide
DED	Dry Eye Disease
DEPT	Distortionless Enhancement by Polarization Transfer
DLS	Dynamic Light Scattering
DMEM	Dulbecco's Modified Eagle Medium
DMF	N,N-dimethylformamide
DMSO	Dimethyl Sulfoxide
DOSY	Diffusion Ordered SpectroscopY
DS	Degree of sulfation
ECM	Extracellular Matrix
ESI	ElectroSpray Ionization
FBS	Fetal Bovine Serum
FDA	Food and Drug Administration
FID	Free Induction Decay
FTIR	Fourier Transform Infrared Spectroscopy
GA	Glutaraldehyde
GAGs	Glycosaminoglycans
Gal	Galactose
GC	Gas Chromatography
Glc	Glucose
GPC	Gel Permeation Chromatography
HA	Hyaluronic Acid

HBSS	Hank's Balanced Salt Solution
HCE	Human Corneal Epithelium
HILIC	Hydrophilic Interaction Liquid Chromatography
HP-SEC	High Performance Size Exclusion Chromatography
HSQC	Heteronuclear Single Quantum Correlation
IBD	Inflammatory Bowel Diseases
IPRP	Ion-Pair Reversed Phase
LALS	Low Angle Light Scattering
LC	Liquid Chromatography
LOQ	Limit Of Quantitation
LPS	Lipopolysaccharide
LS	Light Scattering
LVE	Linear Viscoelastic Region
MALDI	Matrix Assisted Laser Desorption Ionization
MAS	Magic Angle Spinning
Mn	Number Average Molecular Weight
MS	Mass Spectrometry
MTT	(3-[4,5-dimethylthiazol-2-yl]-2,5-diphenyltetrazolium bromide
Mw	Weight Average Molecular Weight
NMR	Nuclear Magnetic Resonance
NOESY	Nuclear Overhauser Effect Spectroscopy
NRE	Non-Reducing End
PBS	Phosphate Buffering Saline
PCS	Photon Correlation Spectroscopy
PDI	Polydispersity Index
Q-TOF	Quadruple-Time-Of-Flight
RALS	Right Angle Light Scattering
RE	Reducing End
R_h	Hydrodynamic Radius
ROS	Reactive Oxygen Species

RT	Room Temperature
SEM	Scanning Electron Microscopy
SE	Secondary Electron
SED	Secondary Electron Detector
SO_3·Py	Sulfur trioxide pyridine complex
SR	Swelling Ratio
STMP	Sodium Trimetaphosphate
S-TSP	Sulfated Tamarind Seed Polysaccharide
TDA	Triple Detector Array
TEER	Transepithelial Electrical Resistance
TOF	Time-Of-Flight
TOCSY	Total Correlation Spectroscopy
TSP	Tamarind Seed Polysaccharide
Xyl	Xylose
Zp	Zeta Potential

IV. LIST OF FIGURES

V. LIST OF TABLES

VI. LIST OF EQUATIONS

VII. PUBLICATIONS

Published:

Ziliani, S.; Alekseeva, A.; Antonini, C.; Esposito, E.; Neggiani, F.; Sansò, M.; Guerrini, M.; Bertini, S. Synthesis and Physiochemical Properties of Sulphated Tamarind (*Tamarindus indica* L.) Seed Polysaccharide. *Molecules,* **2024**, *29*, 5510. https://doi.org/10.3390/molecules29235510

Submitted:

Ziliani, S.; Esposito, E.; Antonini, C.; Bray, G.; Citi, V.; Calderone, V.; Neggiani, F.; Sansò, M.; Tagliaro, I.; Guerrini, M.; Bertini, S. Synthesis, physio-chemical and biological properties of 1,4-butanediol diglycidyl ether-functionalized Tamarind (*Tamarindus indica* L.) seed polysaccharide, *International journal of biological macromolecules,* **2025.**

VIII. SUBMITTED PATENT

Ziliani, S.; A.; Antonini, C.; E.; Neggiani, F.; Sansò, M.; Bertini, S. "A functionalized tamarind seed polysaccharide and a preparation process thereof" / "polisaccaride di semi di tamarindo funzionalizzato e procedimento per la sua preparazione"

IX. CONFERENCES

- *Eurocarb22, 2025, Gdańsk, Poland.* Oral presentation: "Tamarind seed polysaccharide hydrogel cross-linked with BDDE". Bertini, S., Ziliani, S., Antonini, C., Tagliaro, I., Esposito, E., Cosentino, C., Neggiani, F., Sansò, M.

- *XIX Convegno-Scuola sulla Chimica dei Carboidrati (XIX CSCC 2025), Pontignano, Italy.* Poster: "Synthesis and physio-chemical properties of crosslinked Tamarind (*Tamarindus indica* L.) seed polysaccharide." Bertini, S., Ziliani, S., Antonini, C., Tagliaro, I., Esposito, E., Guerrini, M., Sansò, M.

- *6th EPNOE Junior Scientist Meeting 2024, Vienna, Austria.* Pitch and poster: "Synthesis and physio-chemical properties of crosslinked tamarind (*Tamarindus indica* L.) seed polysaccharide." Ziliani, S., Antonini, C., Bertini, S., Esposito, E., Sansò, M., Neggiani, F.

- *31st International Symposium on the Chemistry of Natural Products and 11th International Congress on Biodiversity (ISCNP31 & ICOB11), Naples, Italy.* Oral presentation: "Synthesis and physio-chemical properties of sulphated tamarind (*Tamarindus indica* L.) seed polysaccharide". Bertini, S., Ziliani, S., Alekseeva, A., Antonini, C., Esposito, Guerrini, M., E., Neggiani, F., Sansò, M.

- *XVIII Convegno-Scuola sulla Chimica dei Carboidrati (XVIII CSCC 2023), Pontignano, Italy.* Oral presentation: "Synthesis and physio-chemical properties of sulphated tamarind (*Tamarindus indica* L.) seed polysaccharide." Ziliani, S., Antonini, C., Bertini, S., Esposito, E., Guerrini, M., Sansò, M. (2023)".

- *VLAG 17th Summer Course Glycosciences 2023*, *Wageningen, Netherlands*. Poster: "Synthesis and physio-chemical properties of sulphated tamarind (*Tamarindus indica* L.) seed polysaccharide." Ziliani, S., Antonini, C., Bertini, S., Esposito, E., Guerrini, M., Sansò, M. (2023)".

X. INTERDISCIPLINARY COURSE

- *Basic of biobased processes and biorefineries,* University of Milano-Bicocca, Prof.ssa Paola Branduardi.

- *Literature review: how to make a good bibliography,* University of Milano-Bicocca, Dr. Michele Balzarini, Dr.ssa Stefania Fraschetta and Dr.ssa Margherita Zambotto.

CHAPTER 1 – INTRODUCTION

1.1. Polysaccharides

1.1.1. Chemical composition and classification

Polysaccharides are macromolecules composed of long chains of monosaccharide units, linked together by O-glycosidic bonds in either linear or branched chains. They play an essential role in various physiological process such as adhesion, cell-cell communication, cell signal transduction, blood coagulation, fertilization and molecular recognition within the immune system (Yu et al., 2018; F. Zhang et al., 2011). Additionally, they provide structure support, protection, energy storage, lubrification and stimuli responsiveness (Gopinath et al., 2022; Z. Liu et al., 2008).

Natural polysaccharides are derived from different sources, including plants, algae, microorganism and also animals (Mohammed et al., 2021). In recent years, these biopolymer have been produced through fermentation or extracted from biomass to promote a sustainable development and replacing conventional petroleum-based polymers (Benalaya et al., 2024). Moreover, plant derived polysaccharides have gained their importance due to their affordability and availability from renewable sources (Chinta et al., 2025).

Polysaccharides can be divided in two categories: homopolysaccharides composed of the identical monomer unit and heteropolysaccharides, which consist of different monosaccharides (Mohammed et al., 2021). The most frequently occurring monosaccharides in nature are hexoses, six-carbon sugars, and pentoses, five-carbon monomers (Maji, 2019). D-glucose is the main sugar present in polysaccharides; however, D-fructose, D-galactose, L-galactose, D-mannose, L-arabinose, and D-xylose are also common. Moreover, several monosaccharide derivatives occur naturally amino sugars such as D-glucosamine and D-galactosamine and their derivatives like N-acetylneuraminic acid and N-acetylmuramic acid, as well as sugar acids such as glucuronic and iduronic acids (Mohammed et al., 2021).

Polysaccharide may consist of linear chain of the same monosaccharides, as for the cellulose, or by different units, such as hyaluronic acid (HA). They may also exhibit branching structure either composed of the same sugars, as in glycogen, or of mixed monosaccharides as in galactoxyloglucans (Benalaya et al., 2024; Dumitriu, 2004).

Polysaccharides can also be classified according to the charge of their sugar chain: neutral polymers with no charge, such as cellulose; positively charged polysaccharides, such as chitosan; and negatively charged polysaccharides, such as alginate, heparin, hyaluronic acid, and pectin (Z. Liu et al., 2008). The latter group also includes glycosaminoglycans (GAGs), which are key components of the cell surface and the extracellular matrix (ECM). GAGs comprise, in addition to heparin and hyaluronan, heparan sulfate, chondroitin sulfate, dermatan sulfate, and keratan sulfate (Sasisekharan et al., 2006).

1.1.2. Applications and uses of polysaccharides

The structural polysaccharide characteristics, such as the type of monosaccharides components, chain length and the branching, degree of substitution, molecular weight (Mw), strongly influence their properties including solubility, physiological activity, chemical reactivity, and biodegradability (Dumitriu, 2004).

Owing to this structural variability as well as their safety, biocompatibility, and nontoxicity, polysaccharides have been widely applied in several fields, such as food, environmental, cosmetic, pharmaceutical and biomedical industry (Benalaya et al., 2024). Examples of their diverse applications are illustrated in Figure 1-1.

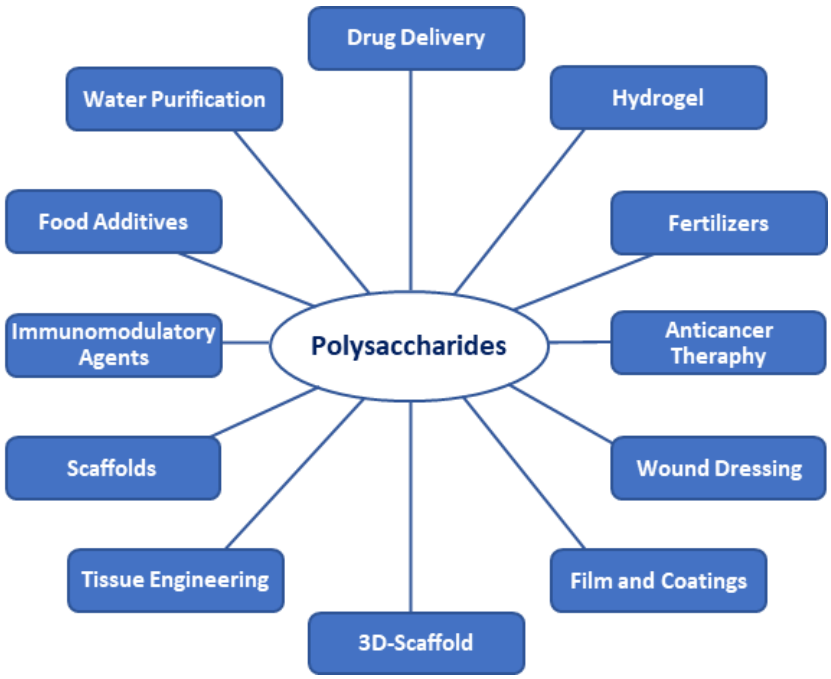

Figure 1-1. *Schematic representation of different polysaccharides' applications.*
Adapted from Tudu & Samanta, 2023.

Polysaccharide are used as food additives to improve the rheological and textural properties of the products, enhance their nutritional value, to preserve the food (Nakashima et al., 2018; Muthukumar et al., 2021).

In pharmaceutical field, they are employed for drug delivery, tissue engineering, and wound dressing applications (Sinha & Kumria, 2001; Bragd et al., 2004). They are widely formulated as hydrogel and nanoparticles to targeted drug release, to improve the therapeutic efficacy and reduce side effects (Gopinath et al., 2018; Xu et al., 2024)

Moreover, polysaccharide-based hydrogels are used as scaffolds for cell culture and in 3D-bioprinting (Vatanpour et al., 2022). They are applied in therapeutic applications as immunomodulator, anticancer, and antimicrobial agents (Schepetkin & Quinn, 2006; Fan et al., 2017).

Beyond food and medicine, polysaccharides are utilized as a promising alternative to synthetic plastics due to their ability to form biodegradable films and coatings (Shafqat et al., 2020). In agriculture, they are utilized as bio-based fertilizers, soil stabilizers, and plant growth enhancers, promoting sustainable farming practices (Chiaregato et al., 2022). Furthermore, polysaccharide-derived flocculants have applications in water purification, to remove pollutants and improve water quality (Qi et al., 2021).

1.1.3. Limitations and future perspectives

Although polysaccharides possess various properties and promising potential, they also present limitations and challenges. Since polysaccharides are typically derived from natural sources, there are some challenges regard their extraction and purification due to the presence of other compounds, such as proteins and lipids, resulting in a costly production process (Mohammed et al., 2021). Therefore, the development of cost-effective production systems using renewable resources and more efficient extraction methods is necessary (Jabeen & Atif, 2024).

Furthermore, the high variability of polysaccharides lead to batch-to-batch variations, susceptibility to microbial contamination, and uncontrolled rate of hydration and degradation (Saidin et al., 2018). Another limitation is their poor mechanical strength, which limit applications requiring durability of robust materials (Jabeen & Atif, 2024).

Fortunately, some of these challenges can be solved through chemical modifications such as grafting, cross-linking, and the introduction of functional groups, for examples *via* sulfation, phosphorylation or carboxymethylation and as well as by blending with other

polymers, thereby expanding the potential applications of polysaccharide (Mohammed et al., 2021; Jabeen & Atif, 2024).

Finally, understanding the relationship between the structure and configuration of polysaccharides and their resulting biological activities remains a significant challenge, requiring further research and investigations (A. Wang et al., 2023).

Moreover, further clinical studies are necessary to evaluate the *in vivo* safety of polysaccharides and to determine their long term efficacy and non-toxicity affects (Salehi & Rashidinejad, 2025).

1.2. Tamarind seed polysaccharide (TSP)

1.2.1. Origin and chemical composition

In this PhD thesis, the research focused on Tamarind seed polysaccharide (TSP), one of the most abundant and structurally complex natural polymers. TSP is a galactoxyloglucan extracted from the seed kernel of the of *Tamarindus indica* L. (Raj & Lee, 2024), a long-life evergreen tree of tropical and subtropical plant, widely distributed in Africa, Asia and America (Sudjaroen et al., 2005).

The tamarind fruit, also known as the tamarind pod, shown in Figure 1-2, contains 30-50% pulp, 25-40% seed and 11-30% shell and fiber. Each seed is composed of the testa, the outer seed coat, and the kernel or endosperm, which account for approximately 20-30% and 70-75% of the seed, respectively (Geethalaxmi et al., 2024).

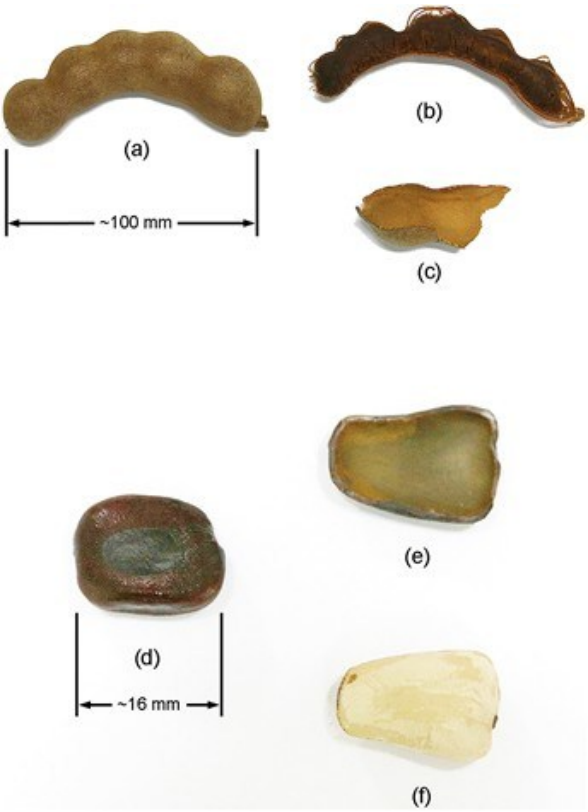

Figure 1-2. *Tamarind pod and its compositions.*
(a) pod, (b) pulp, (c) shell, (d) seed, (e) testa, and (f) kernel adapted from *Noraphaiphipaksa et al., 2016*.

The different parts of tamarind plant have various uses and applications (Ghaffaripour et al., 2017). The leaves are commonly consumed as vegetables, while the pulp has high edible values due to its content of sugars, amino acids, minerals and vitamins (H. Zhang

et al., 2024). Additionally, the dried powdered pulp and its juice extract are employed in the food industry as a natural preservatives (Mansingh et al., 2021).

Initially, the seeds of this plant were considered waste products of the tamarind pulp industry, due to the presence of some antinutritional components such as total phenols, tannins, and phytic acids, which are mainly concentrated in the seed coat (Nagar et al., 2022). In contrast, the seed kernel contains 65-73% polysaccharide, 15-20% protein and 6-8% lipid (H. Zhang et al., 2024). Consequently, extraction processes for obtaining TSP from the endosperm of seeds have been developed, thereby increasing the value of these by products and reducing overall waste (Mansingh et al., 2021).

TSP is a neutral, water-soluble polysaccharide consisting of a β-(1,4)-D-glucan backbone with α-(1,6)-D-xylose branches, which are partially substituted with β-(1,2)-D-galactose (Sonawane et al., 2015), as illustrated in Figure 1-3.

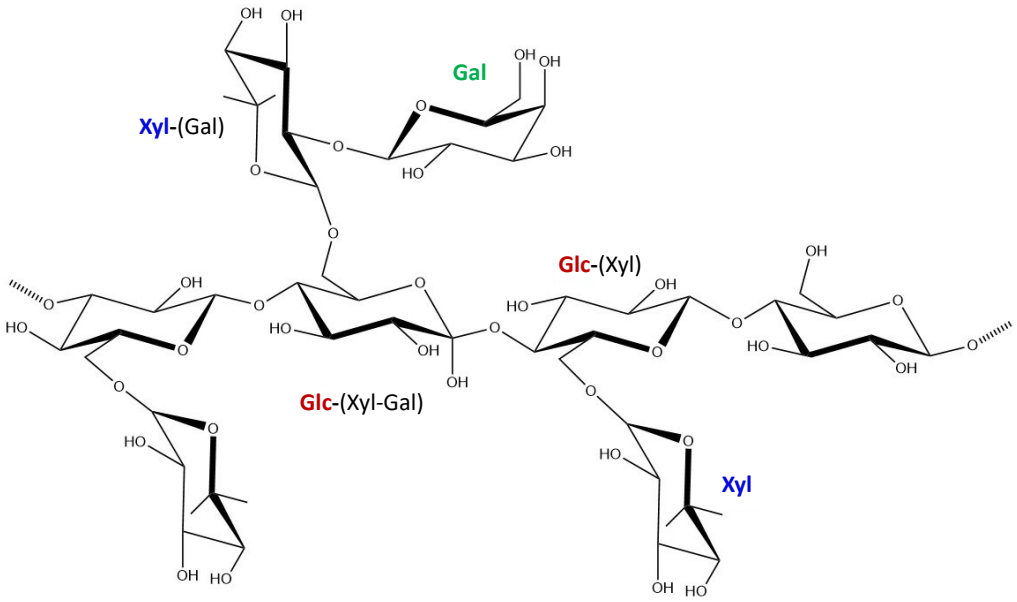

Figure 1-3. *Chemical structure of tamarind seed polysaccharide (TSP).*
TSP is composed of a β-(1,4)-D-glucan backbone, with α-(1,6)-D-xylose branches, partially substituted with β-(1,2)-D-galactose. The colored residues and abbreviations in bold correspond to the observed monosaccharide, while the linked monosaccharides are shown in parentheses. Glc—glucose; Xyl—xylose; Gal—galactose.

The molar ratio of glucose, xylose and galactose in TSP has been reported as 3.1:1.7:1.0 (Majeed et al., 2019), however variations exist in literature as the monosaccharide composition is influenced by the origin of the seeds and the extraction methods (H. Zhang et al., 2024).

Furthermore, depending on the distributions of xylose and galactose along the cellulosic backbone, TSP can exhibit different subunit structures, including heptasaccharide

(Glc_4Xyl_3), octasaccharide (Glc_4Xyl_3Gal), and nonasaccharide ($Glc_4Xyl_3Gal_2$) (H. Zhang et al., 2020). Small amounts of arabinose residues have also been detected in TSP, likely resulting from contamination by arabinan or arabinoxylan in plant seeds (H. Zhang et al., 2020).

1.2.2. Extraction Methods of TSP

The extraction methods significantly influence the monosaccharide composition, chemical structure, conformation, and functional properties of biopolymers. Various pretreatments and extraction methods have been studied to identify the optimal conditions to obtain high yield and purity of TSP (Morales et al., 2019).

Prior to the TSP extraction, the seeds are washed with water and dried. Subsequently, different pretreatments such as roasting, soaking, filtration, boiling, and autoclaving are applied to separate the testa, which is rich in tannins, from the kernel, thereby enhancing the purity of the extracted polysaccharide (Mansingh et al., 2021; Geethalaxmi et al., 2024). Currently, the main extraction methods for TSP include hot water, organic acid extraction, high pressure extraction, subcritical water and enzymatic ultrasound-assisted extraction (H. Zhang et al., 2024), which are briefly described below.

- Hot water extraction is a traditional and widely used method for polysaccharide isolation, that uses water to extract polar polysaccharides from plants materials. In this process, tamarind seed powder is first solubilized in water and then added to boiling distilled water. The resulting solution is centrifugated, and the supernatant is precipitated with pure alcohol. The precipitate is subsequently washed with ethanol and air-dried. (Geethalaxmi et al., 2024; H. Zhang et al., 2024). This method requires simple equipment and low operational cost; however, it is time-consuming, and typically yields polysaccharides of relatively low purity (Crispín-Isidro et al., 2019).
- Organic acid method is commonly used approach for extracting TSP. In this method, an acid solution is added to the extract to break down cell walls and degrade crude fiber structures, thereby facilitating the release of polysaccharides. Additionally, this process promotes isoelectric precipitation of proteins, reducing amino acids content and increasing the purity of TSP (Z.-B. Wang et al., 2014). The main limitation of this method is that the acid conditions may result in a partial degradations of the polysaccharide (H. Zhang et al., 2024).

- High pressure extraction applies pressures ranging from 100 to 1000 MPa to polysaccharides at temperatures below 50°C, disrupting the structure of the raw material, and thereby increasing extraction yields (Geethalaxmi et al., 2024). This method allows shorter extraction time, higher extraction efficiency and lower energy consumption. However, the high pressure would may affect the molecular weight, viscosity, water absorption index and water solubility of TSP (Xie et al., 2021)
- Subcritical water method operates at temperatures between 100 and 374°C keeping water in a liquid state using high pressure (Limsangouan et al., 2019). The elevated temperatures improve TSP extraction yield, and this method is relatively inexpensive and more ecological compared to other processes. However, extensive hydrolysis of TSP may occur, resulting reduced Mw and apparent viscosity (Geethalaxmi et al., 2024).
- Enzymatic ultrasound-assisted extraction combines protease enzyme which hydrolyze proteins with ultrasound to improve the polysaccharide extraction (Muthusamy et al., 2021; Nagar et al., 2022). This method improves the purity of TSP but sonication can lead to a partial depolymerization of the polysaccharide (Geethalaxmi et al., 2024).

Nowadays, the most commonly used method for TSP extraction is the organic acid method, while auxiliary techniques, such as high pressure and subcritical water extraction can be employed to reduce the extraction time and increase yield (H. Zhang et al., 2024). However, all these methods show common limitations, including non-selective degradation of TSP and disruption of its molecular structure; therefore, further research is required to optimize these extraction processes (Geethalaxmi et al., 2024).

1.2.3. Physicochemical and biological properties

TSP is a water-soluble polysaccharide that assumes a random coil conformation in aqueous solutions (H. Zhang et al., 2020). It can also easily form aggregates depending on the degree of galactose side-chain substitution (Raj & Lee, 2024). Indeed, literature indicates that partial degalactosylation of TSP promotes the formation of large aggregates due to hydrophobic interactions (R. Guo et al., 2022).

At low concentration, TSP exhibits Newtonian behavior in solution, whereas at higher concentrations it shows a viscoelastic property. In this state, viscosity decreases with

increasing shear rate, as the TSP chains align with the flow direction, reducing flow resistance (Kaur et al., 2012; Chinta et al., 2025). TSP is not able to forms gels on its own, even at high concentrations; however, gel formation can occur in the presence of alcohol, sugar, salts, or polyphenols (Yamatoya et al., 2020).

Generally, TSP has a Mw in the range of 400-1000 kDa, however, this value can be influenced by factors such as the source of raw materials, the analytical techniques used for the Mw determination and the extraction and purification methods. (H. Zhang et al., 2024).

TSP also shows a good physical stability under various conditions (Shao et al., 2019). Its apparent viscosity remains relatively stable across a wide pH range, at elevated temperatures and in presence of salts and sucrose (Shao et al., 2019; H. Zhang et al., 2024).

Moreover, TSP solutions can be sterilized by autoclaving without undergoing thermal degradation, unlike hyaluronic acid, which is advantageous from a production prospective (Yoon & Lee, 2019).

TSP shows both emulsion stabilizing and emulsifying properties, as well as the ability to inhibit ice recrystallization (Yamatoya et al., 2020; X. Sun et al., 2023).

Furthermore, TSP possesses important characteristics such as excellent drug-loading capacity, bioadhesivity, biocompatibility, non-carcinogenicity and non-irritating properties (Xie et al., 2023; Chinta et al., 2025). It also exhibits various biological activities, including antioxidation, antibacterial, anti-inflammatory, antitumor and regulation of intestinal flora (Ren et al., 2022; H. Zhang et al., 2024).

Finally, the “mucin-like” molecular structure of TSP confers mucoadhesive and mucomimetic properties, enabling interactions with the glycoproteins present in the mucus layer, called mucins (Uccello-Barretta et al., 2013).

Unlike other polysaccharides, such as glycosaminoglycans, TSP is resistant to degradation by physiological enzymes; however, it can be depolymerized by the enzyme endo-β-(1,4)-glucanase produced by fungi or plants (H. Zhang et al., 2020). This group of enzymes includes: xyloglucanase, which hydrolyses β-1,4 bond (H. Zhang et al., 2020), and cellulase, which cleaves both the β-1,4 linkage between glucose units and 1,2-linked xylose and galactose (Ejaz et al., 2021).

1.2.4. Applications

TSP has a wide range of applications, Figure 1-4, across different fields due to its unique properties and its recognition as safe by the regulatory authorities in several countries (Chinta et al., 2025).

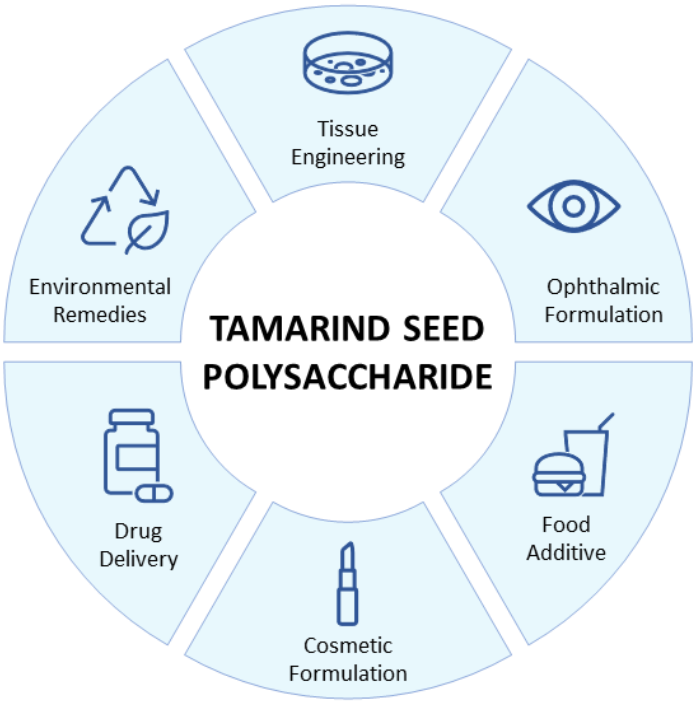

Figure 1-4. *Schematic representation of TSP's applications.*

TSP is extensively used in the food industry as a thickening, stabilizing and emulsifying agent in soups, dairy products, and baked goods (Nagar et al., 2022). It also possesses gelling properties similar to pectin, making it a more economical alternative in the production of jam, jellies, and marmalades (Marathe et al., 2002).

Moreover, its high water-holding capacity and antimicrobial activity enhances the texture and shelf life of processed foods (Xie et al., 2020). Due to its non-toxic nature, TSP is also employed as a dietary fiber supplement with potential prebiotic benefits and it is used gluten-free product formulations, due to its similarity to gluten (Jang et al., 2018).

In pharmaceutical field, TSP has been employed as versatile excipient for drug delivery system in various conventional dosage forms such as suspensions, emulsions, tablets, beads, gels and nanoparticles (Raj & Lee, 2024).

It has also been explored in ophthalmic formulations, particularly in artificial tear solutions and ocular drug delivery for the treatment of the Dry Eye Disease (DED) owing

to its high mucoadhesive properties and compatibility with ocular physiology (Nozari & Ramin, 2021). Its branched structure allows adhesion to glycoprotein mucins of the ocular surfaces, resulting in increased residence time (Uccello-Barretta et al., 2013; Alotaibi et al., 2024).

Furthermore, TSP has demonstrated a synergistic effects when combined with HA, improving HA stability and mucoadhesive properties in ophthalmic applications, as well as in intra-articular injections for arthritis (Uccello-Barretta et al., 2010; Yoon & Lee, 2019). Notably, the ophthalmic company Farmigea S.p.A. has developed the eye drops Xyloial®, a TSP and HA formulation, capable of lubricating, hydrating and stabilizing the ocular surface.

Moreover, TSP has been studied for potential applications in wound dressings, tissue engineering scaffolds, and as a component of bioadhesive hydrogel (Mansingh et al., 2021). Its ability to promote cell adhesion and proliferation highlight its promise in regenerative medicine (Sanyasi et al., 2014).

Due to TSP's hydrating and film-forming properties it has been used in cosmetic formulations including skin creams, lotions, and hair care products (Semenzato et al., 2015). It helps retain moisture in the skin, enhancing hydration and improving elasticity (Amnuaikit et al., 2019). Furthermore, its non-irritant nature makes it suitable for products for sensitive and anti-aging applications (Khongkow et al., 2024).

Finally, TSP has also been employed in wastewater treatment and environmental remediation, due to its ability to absorb pollutant molecules (Mansingh et al., 2021; Cui et al., 2024).

1.2.5. Limitations and future perspectives

Despite its numerous advantages, TSP also presents certain limitations that can affect its applications. One of the main challenges lies in its high viscosity, resulting from its high molecular weight, which can complicate processing and formulation, especially in pharmaceutical and food industries where precise control of consistency is required (H. Zhang et al., 2024). Furthermore, the rigid cellulose backbone and the absence of ionic groups contribute to its poor water solubility, thereby restricting its versatility in some applications (Yamatoya & Shirakawa, 2003; Sri et al., 2025). Additionally, the physicochemical properties of TSP exhibits variability depending on factors such as

extraction techniques, environmental conditions, and the origin of the seed (Chawananorasest et al., 2016).

From an economic perspective, the extraction and purification process of TSP can be costly and time-consuming, involving multiple steps to remove impurities and obtain the desired level of purity. Large-scale production therefore requires optimization strategies to improve both yield and cost-effectiveness (Geethalaxmi et al., 2024). Additionally, regulatory approval of TSP-based products in the pharmaceutical and food industries can be challenging, since safety and efficacy must be evaluated before commercialization (Gopinath et al., 2022).

Although TSP is generally recognized as biocompatible and non-toxic, potential allergenic or immunogenic responses in certain individuals cannot be entirely excluded. Further studies are required to assess its long-term safety, particularly in novel biomedical and therapeutic applications (Sonawane et al., 2015). To enhance the commercial viability of TSP in various fields, advancements in processing methods, formulation strategies, and regulatory standardization will be essential. Moreover, chemical modifications of the TSP such as grafting, crosslinking, or functional group substitution can be a solution to improve its physicochemical and functional properties, thereby expanding its potential applications (Raj & Lee, 2024; H. Zhang et al., 2024).

1.3. Chemical modifications of polysaccharides

Modifications of polysaccharides are used to enhance their properties and broaden their applications, as well as to overcome some of their limits and drawbacks (T. Liu et al., 2023). The main approaches used for polysaccharides modification include physical, biological and chemical methods (Chen et al., 2024).

Physical modification is a convenient and effective strategy that relies on physical interactions between polysaccharides or other biomolecules to form new structures. However, these interactions are generally reversible and they do not significantly increase the chemical reactivity and the biological activity of the polysaccharide (B. Zhang et al., 2022).

Biological modification represents a highly specific and environmentally friendly approach, involving enzymatic reactions under mild conditions. Nevertheless, this method is limited by the cost of the enzymes and the relatively low efficiency (Chen et al., 2024).

Chemical modification involves the introduction or the removal of functional groups along sugar chain. Although, this approach requires a large of reagents and careful control of reaction conditions, it allows efficient alteration of the physiochemical and biological properties of the polysaccharide (Mukherjee et al., 2022).

Depending on the functional groups introduced, changes in molecular structures, molecular weight, solubility, rheological behavior and biological activities can be achieved (Chakka & Zhou, 2020; Deng et al., 2020).

The presence of reactive functional groups in polysaccharides, such as hydroxyl, amino, and carboxylic acid groups, allows various chemical modifications including sulfation, acetylation, phosphorylation, selenization, carboxymethylation and crosslinking (Y. Ren et al., 2019; T. Liu et al., 2023).

In this PhD thesis, TSP was chemically modified through sulfation and crosslinking reactions, to enhance its functional properties, expand its range of applications and address its limitations.

1.3.1. Sulfation

Sulfated polysaccharides are negatively charged biopolymers naturally occurring in various organism and exhibit diverse biological and chemical properties. The two main classes of naturally sulfated polysaccharides are glycosaminoglycans (GAG), with the exception of hyaluronic acid, and marine algae polysaccharide extracted (Muthukumar et al., 2021). GAGs interact with a wide range of proteins involved in both physiological and pathological process including cell signaling and development, angiogenesis, axonal growth, tumor progression, metastasis and anti-coagulation (Gandhi & Mancera, 2008; Shi et al., 2021). Moreover, these sulfated polymers regulate blood clotting and play key roles in pathogens attachment, neuronal growth, cancer cell apoptosis and many several other biological functions (Bedini et al., 2017). Sulfated polysaccharides from marine algae, such as carrageenan, ulvan, fucoidan, possess important biological activities, including antitumor, antiviral, antioxidant, antimicrobial, anticoagulant, and immune-inflammatory effects (Ngo & Kim, 2013; Hans et al., 2021). The growing scientific and industrial interest to these polysaccharides is due to their abundance and renewable origin; however, their application remains challenging because of different factors such as seasonality, variability, differences among algae species and the extraction difficulties (Ray et al., 2021; Martins et al., 2023). Furthermore, some marine polysaccharides contain, sulfated fractions with high bioactivity but low natural content, which limits their use in large-scale biomedical applications (T. Liu et al., 2023).

For these reasons, chemical sulfation has been explored as a strategy to introduce sulfated groups into other polysaccharides with distinct physiochemical properties such as high molecular weight or branched structure to enhance their biological activities and develop new biopolymers not found in nature. Studies have demonstrated that sulfated polysaccharides often exhibit enhanced anticoagulation, antitumor and antioxidant activity compared to their non-sulfated counterparts (Mazepa et al., 2022; Rizkyana et al., 2022). Moreover, sulfation can improve polysaccharide solubility, moisture absorption, and the water retention capability (Chinta et al., 2025).

1.3.1.1. Sulfation chemical reaction

Sulfation is an esterification reaction that involves the hydroxyl groups of the sugar chain and an acylating agent (Mukherjee et al., 2022).

The extent of derivatization is expressed as the degree of sulfation (DS), which depends on several factors, including the reaction type and conditions, time and temperature, the polysaccharide structure, the nature of reagent and solvent and the reagent-to-substrate molar ratio (Mukherjee et al., 2021). Moreover, the regioselectivity of sulfation reactions is influenced by both steric and electronic effects (Mukherjee et al., 2022).

The most common sulfation methods employed dimethyl sulfoxide (DMSO) or N,N-dimethylformamide (DMF) as solvents and use reagents as chlorosulfonic acid-pyridine, sulfamic acid, concentrated sulfuric acid, and trioxide-pyridine (Z. Wang et al., 2018; T. Liu et al., 2023). A brief description of these methods is provided below.

- Chlrosulfonic acid-pyridine method is commonly used for obtaining sulfated polysaccharides with a high degree of substitution (Berezhnaya et al., 2024). The sulfating reagent is prepared by adding chlorosulfonic acid dropwise to anhydrous pyridine in an ice bath due to the high exothermicity of the reaction (Chen et al., 2024). The resulting complex is then added to a solution of polysaccharide in an organic solvent. Because the reaction is exothermic, the temperature must be carefully controlled (Niu et al., 2023). Moreover, the reagent is strongly acid, so the concentration of the reagent and the time of the reaction have to be optimized to a depolymerization of the polysaccharide (Berezhnaya et al., 2024). Although this method yields high substituted product, chlorosulfonic acid is flammable, toxic, and unstable and it reacts violently with water (T. Liu et al., 2023).
- Sulfamic acid method involves the addition of the sulfamic acid to a polysaccharide dissolved in DMF at high temperature (Niu et al., 2023). Due to the low reactivity of sulfamic acid, catalysts such as pyridine, urea and acetamide are required to achieve a higher DS. This method is less commonly than the other sulfation techniques (T. Liu et al., 2023).
- Concentrated sulfuric acid method is one of the classic sulfation approaches. The reagent is prepared by mixing concentrated sulfuric acid with n-butanol. Ammonium sulfate and the polysaccharide are then added at low temperature (Niu et al., 2023). The advantages of this method are the use of less toxic reagents, relatively stable reaction conditions and minimal side reactions (Z. Wang et al., 2018). Nonetheless,

the strong acidity may lead to polysaccharide depolymerization and carbonization (Berezhnaya et al., 2024).

- Sulfur trioxide-pyridine (SO_3·Py) method is a milder sulfation process (T. Liu et al., 2023). The reaction is carry out by adding the SO_3·Py complex to a polysaccharide solution in an organic solvent, usually DMF (Berezhnaya et al., 2024). This method can achieve a high DS without affecting the molecular weight of the polysaccharide (Jana et al., 2021; Mukherjee et al., 2021), however the main limitation is the high cost of the reagent (T. Liu et al., 2023).

Usually, following sulfation, polysaccharide is typically recovered through a neutralization, ethanol precipitation and dialysis step (Caputo et al., 2019).

In this PhD project, TSP was sulfated using the sulfur trioxide-pyridine method, which enables the introduction of sulfate groups with a high degree of substitution while preserving the molecular weight of the polysaccharide.

1.3.1.2. Biological effects of sulfation

The different biological effects of polysaccharides' sulfation are widely reported in literature and they include anti-coagulant, antioxidant, antitumoral, anti-viral, immunomodulatory activities, as showed in Figure 1-5 below (Ngo & Kim, 2013).

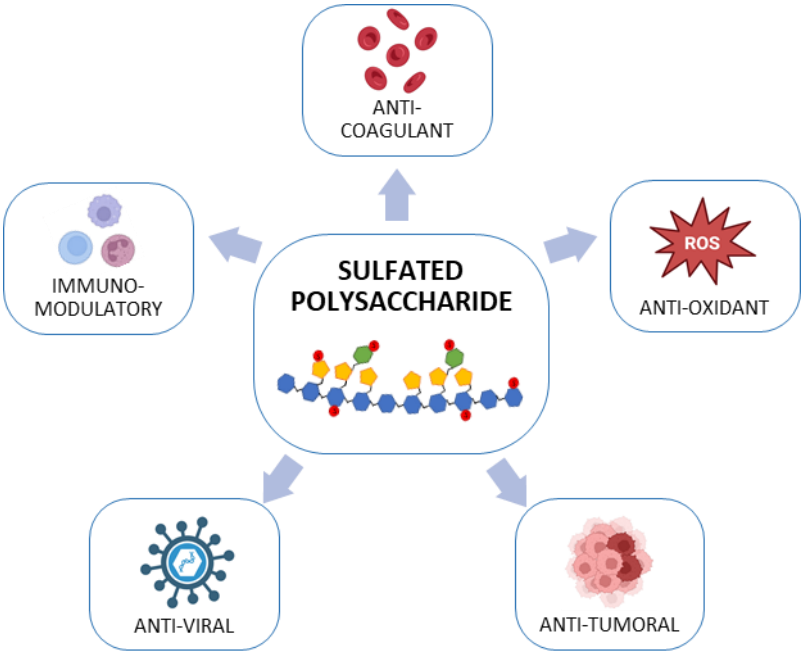

Figure 1-5. *Biological effects of sulfated polysaccharides.*

- Anticoagulant activity: coagulation is critical physiological process in hemostasis and anticoagulants play a key role in preventing the formation of thrombus (Z. Wang et al., 2018). The anticoagulant effect of sulfated polysaccharides is mediated by electrostatic interactions between the negatively charged sulfated groups and the positively charged amino acids residues of coagulation protease inhibitors, such as antithrombin (Mukherjee et al., 2022). Studies has reported that a higher DS allows these interactions due to an increased density of the negative charges, resulting in more effective binding to target proteins (Liang et al., 2018). One of the most used anticoagulant molecules is heparin, but it can also be harmful because it can cause bleeding and thrombocytopenia. Therefore, chemically sulfated polysaccharide are being investigated as safer alternatives to heparin (Niu et al., 2023).
- Antioxidant activity: antioxidants protect cells and tissues from damage caused by reactive oxygen species (ROS) which can contribute to cancer, atherosclerosis, and DNA damage (Dharmaraja, 2017). The antioxidant properties of polysaccharides are attributed to the hydrogen- and electron-supplying ability of the sugar chains (Niu et al., 2023). According to literature, the presence of the sulfated groups on the polysaccharide chain enhance antioxidant activity compared to the unmodified polysaccharide, likely due to improved radical scavenging efficiency (Z. Wang et al., 2018).
- Antitumoral activity: polysaccharides are used in antitumoral therapies due to their ability to inhibit the tumor cell proliferation, induce apoptosis and activate the immune system against cancer cells (Zong et al., 2012). Sulfated polysaccharides enhance immune recognition and facilitate the elimination of the tumor cells, exhibiting a high antitumoral activity compared to their non-sulfated counterparts (L. Wang et al., 2009).
- Antiviral activity: sulfated polysaccharides show higher anti-viral activity than unmodified polysaccharides. The negatively charged sulfate groups interact with biomolecules on the surface of host cells or viruses. This includes preventing viral adsorption and invasion, avoiding viral release from host cells and promoting viral neutralization (Bouhlal et al., 2011; Niu et al., 2023).
- Immunomodulatory activity: polysaccharides can induce the production of immune factors and enhance overall immune function (Y. Wang et al., 2010). Studies have shown that sulfated polysaccharides exhibit immunoregulatory activity protecting immune organs, promoting the differentiation of immune cells and stimulating the

secretion of cytokines (Gao et al., 2019). Additionally, sulfated polysaccharides have been reported to interact more strongly with macrophages compared to unmodified polysaccharides further enhancing their immunomodulatory potential (Yu et al., 2017).

1.3.1.3. TSP Sulfation

Chemical modification of TSP by the introduction of sulfated groups is desirable to extend the processability and the applicability of this biopolymer.

Owing to its high molecular weight and the absence of charged substituents, TSP solutions are often highly viscous, and complete solubilization can require prolonged stirring and, in some case, even heating (Raj & Lee, 2024). For these reasons, formulations containing TSP are typically prepared at low concentrations to facilitate the dissolution step, which represents a limitation for certain pharmaceutical and other applications.

The incorporation of sulfated groups on the sugar backbone can improve polysaccharide solubility, due to the alter of chain conformation (Z. Wang et al., 2018).

Moreover, sulfation can allow specific interactions with proteins or cellular receptors, significantly increasing the biological activity and potential applications of the biopolymer, such as using sulfated TSP derivatives as glycosaminoglycan mimics (Niu et al., 2023).

Compared to naturally sulfated polysaccharides from marine algae, TSP is a low-cost byproduct of tamarind seed pulp industry (Sonawane et al., 2015). It possess a well-defined structure but retains considerable complexity (L. Ren et al., 2022). Moreover, its high molecular weight, compared to those from marine algae, makes TSP an attractive biopolymer for chemical modification to enable new applications (Kang et al., 2022).

Indeed, previous studies reported that polysaccharides with higher molecular weights often exhibit enhanced immunomodulatory, antioxidant and anticoagulant properties (Mukherjee et al., 2022; M. Yang et al., 2022)

In addition, a higher degree of branching in polysaccharides can improve antioxidant properties as the increased number of reactive sites that facilitates the scavenging free radicals (Tian et al., 2020).

For these reasons, a chemical sulfation of TSP was performed in this PhD study, to improve its processability and functional properties, thereby expanding its potential.

1.3.2. Crosslinking

Crosslinking modifications allow the formation of hydrogels, three dimensional structures based on natural or synthetic polymers capable of absorbing large amounts of water or biological fluids without dissolving or altering their morphology (Uman et al., 2020; Paiva et al., 2024). Crosslinking can also be employed for the development of films and membranes, fibers, porous and sponge-like structures and micro- and nanoparticles (Reddy et al., 2015). Recently, crosslinked structures based on natural biopolymers such as proteins and polysaccharides have attracted considerable interest by due to their non-toxicity, biodegradability and biocompatibility (Maiti et al., 2024). In literature, several examples of crosslinked polysaccharides can be found, based on cellulose, pullulan, hyaluronic acid, alginate and chitosan (Reddy et al., 2015). This type of modification can indeed enhance the mechanical properties and stability of polysaccharides, broadening their applications in different various fields such as biomedical engineering, pharmaceuticals, food technology and environmental science (Reddy et al., 2015; Li & Lin, 2021).

1.3.2.1. Methods of crosslinking

Crosslinking processes are generally classified into chemical, physical, and enzymatic methods (Paiva et al., 2024), which are briefly described below.

- In chemical crosslinked hydrogels, covalent bonds between polymeric chains are formed through reactions with crosslinking agents (Paiva et al., 2024). This method provides the three dimensional network, with enhanced chemical, mechanical and structural stability even under external *stimuli* such as variations in temperature, ionic strength or pH (Alavarse et al., 2022). Several crosslinker have been reported in literature for the preparation of polysaccharide-based hydrogels, including glutaraldehyde (GA), epichlorohydrin, 1,4-Butanediol diglycidyl ether (BDDE), sodium trimetaphosphate (STMP), Polyvinyl alcohol (PVA), divinyl sulfone and the natural crosslinker genipin (Paiva et al., 2024).
- Physically crosslinked hydrogels are formed through weak interactions such as mechanical chain entanglements, hydrogen bonding, van der Waals force, hydrophobic interactions, or electronic interactions. These interactions are reversible and can be disrupted by environment changes such as pH or temperature (Uman et

al., 2020). Unlike chemical hydrogels, physical hydrogels are prepared without the use of crosslinkers or initiators (Qin et al., 2019).

- Enzymatic-mediated crosslinking reactions generate covalent bonds and linkages in a highly specific manner under mild conditions. The main limitation of this method are its high costs and the chemoselectivity of the enzymes, which can react only in the presence of substrate containing a specific functional group (Paiva et al., 2024).

1.3.2.2. Crosslinkers

In chemical crosslinking, different types of crosslinkers with various reactivities can be employed to obtain polysaccharide-based hydrogels based. A brief description of the most used crosslinkers is reported.

- Aldehydes crosslinkers are common reagents used for hydrogel formation. Among them, one of the most frequently employed in biodegradable hydrogels based on chitosan and proteins is glutaraldehyde (GA), a low-cost and easily available crosslinking agent (Paiva et al., 2024). GA is a bifunctional aldehyde with a low molecular weight that exhibits high affinity toward amine, thiol and imidazole functional groups (Pal et al., 2013). However, GA has shown cytotoxicity effects; therefore, low concentrations have to be used to minimize the risk of unreacted compound formation (Alavarse et al., 2022).
- Trisodium trimetaphosphate (STMP) is a cyclic polyphosphate salt used for polysaccharide crosslinking. It exhibits low toxicity and good safety, with no reported adverse effects on humans, although its crosslinking efficiency is lower compared to other crosslinkers (Alavarse et al., 2022).
- Genipin is a bicyclic molecule that hydrolyzes in aqueous solutions to form two reactive aldehydes, which can easily react with polysaccharides under mild conditions to yield stable products. Despite being a natural crosslinker, genipin is expensive, exhibits slow reaction kinetics and it requires are and further studies to fully evaluate its safety (Yu et al., 2021; Paiva et al., 2024).
- Epichlorohydrin is a crosslinked agent used with polysaccharides and polyamines (Dehabadi & Wilson, 2014). It contains an epoxy ring and a chloromethyl group, which react with hydroxyl groups on sugar chains (Zafar et al., 2022). Its main limitation is cytotoxicity which reduces its use in biomedical or food application (Maiti et al., 2024).

- Divinyl-sulfone is a bifunctional alkylating agent with two reactive vinyl groups that can form covalent bonds between polymer chains (Faivre et al., 2021). The main drawbacks are its high reactivity and toxicity (De Boulle et al., 2013).
- 1,4-Butanediol diglycidyl ether (BDDE) is a well-established epoxy crosslinking agent used primarily for the formation of HA hydrogels (Wojtkiewicz et al., 2024). Under alkaline conditions, the epoxide groups of BDDE can react with amine, hydroxyl, and sulfhydryl functional groups, leading to the formation of secondary amines, ethers, or thioethers, respectively (Qiu et al., 2024). BDDE exhibits significantly lower toxicity compared to other ether-bond crosslinking agents as divinyl sulfone (De Boulle et al., 2013) and epichlorohydrin (Li et al., 2021).

1.3.2.3. Crosslinked polysaccharide applications

Crosslinked polysaccharides are widely used in various applications due to their properties, such as the swelling capability, high viscosity, 3D structures and enhanced stability (Alavarse et al., 2022). Figure 1-6 illustrates examples of crosslinked polysaccharides.

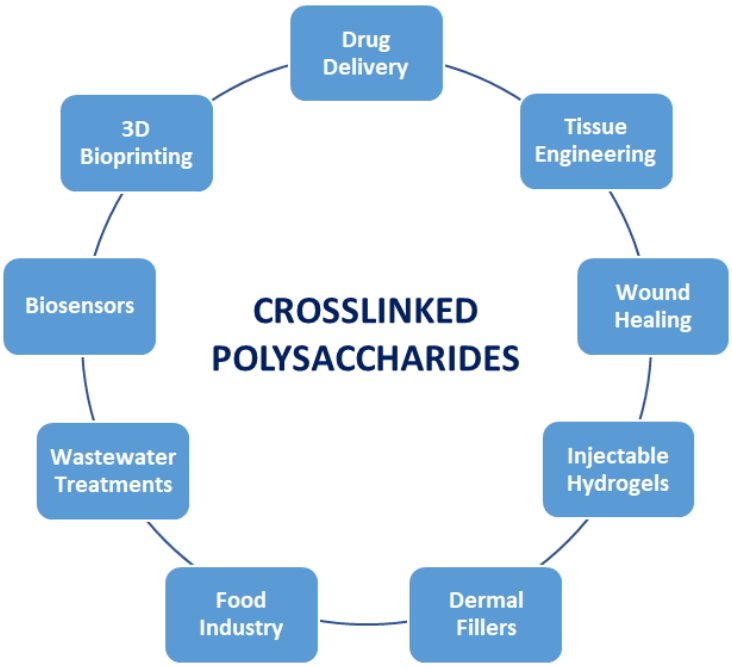

Figure 1-6. *Schematic representation of crosslinked polysaccharide applications.*

- Polysaccharide hydrogels are frequently used in drug delivery. Pharmaceutical compounds can be encapsulated within the network and released in a sustained way (Esposito et al., 2020). Moreover, hydrogel can respond to specific environmental *stimuli* such as changes in temperature, pH or irradiation, to release drugs, which has been shown to improve efficacy while reducing adverse effects in the human body (Mohanty et al., 2024).
- Hydrogels are commonly applied in tissue engineering, due to their similarity to the extracellular matrix. They can create a biocompatible environment for cells growth, regulate living cells and organs and promote tissue repair and regeneration thank to their permeability to oxygen and nutrients (Q. Yang et al., 2022; Mohanty et al., 2024).
- Polysaccharide hydrogels are used in wound healing, as they protect wounds against external contaminants. Moreover, they can incorporate antimicrobial and inflammatory agents, which accelerate the wound healing process (X. Zhang et al., 2021).
- Injectable hydrogels are low viscosity polysaccharide solutions that can form gels *in situ*, due to a transition solution to gel. They are used for local delivery with minimal invasiveness to target sites (Lee, 2018).
- Hydrogels, especially hyaluronic acid-based ones, are applied in cosmetic field as dermal filler to anti-aging treatments and corrections of facial imperfections, due to their swelling capability and biocompatible and no-toxic properties (Fallacara et al., 2017).
- In food industry, polysaccharide-based hydrogels are used in the food packaging due to their favorable mechanical, food preservation and environmental friendliness (Manzoor et al., 2022). Additionally, antimicrobials, antioxidants, flavorings, colorants, and bioactive components can be encapsulating in the 3D structure of hydrogels and released over time (Kwan & Davidov-Pardo, 2018).
- The mechanical properties, swelling capability and stability of polysaccharide hydrogels make them eco-friendly alternative for wastewater treatments. They are used as sorbents to remove of pollutants such as dyes, oxyanions, pesticides, phenols, pharmaceutics and heavy metals in wastewater (Ghiorghita et al., 2022).

- The volume of hydrogel can change significantly in response to external *stimuli*. For this reason, they are used as sensors capable of detecting, for example, change in pH, pressure, temperature, glucose levels or the presence of specific biomolecules (Li & Lin, 2021).
- Polysaccharide hydrogels are used as bioinks in 3D bioprinting due to their rheological and structural properties. They can be printed into structures for applications in tissue engineering and organ-on-chip systems (Damiri et al., 2025).

1.4. Analytical methods for polysaccharides characterizations

Polysaccharides exhibit a complex structure due to their molecular complexity which arises from the monosaccharide composition, linkage patterns, degree of branching, functional groups and molecular weight distribution (Q. Guo et al., 2019). For this reason, the characterization of polysaccharides can be challenging, yet it is essential for understanding the functional, conformational, and physiological properties of these biopolymers (Salehi & Rashidinejad, 2025). Various analytical methods are employed to elucidate the structure of polysaccharides and to examine their physical and biological properties.

In this PhD thesis, various techniques, reported in Figure 1-7 and described below, were used to investigate TSP and its modified products.

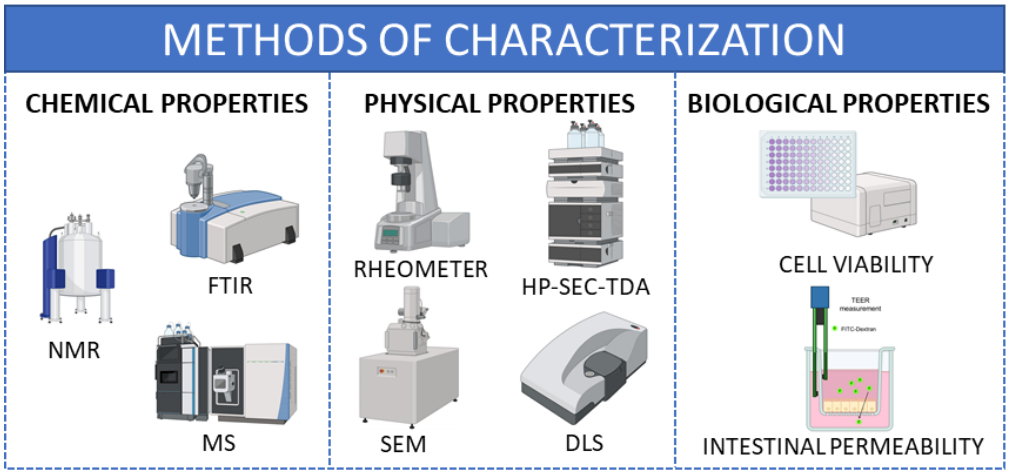

Figure 1-7. *Analytical methods used for the characterization of TSP and its modified products*

The identification of the functional groups and the composition of the polysaccharide is typically studied using spectroscopy and spectrometry techniques. Physicochemical properties, such as distribution of the molecular weight, can be determined through chromatographic methods. Moreover, the rheological behavior of polysaccharides can be assessed by rheological analysis. Dynamic Light Scattering (DLS) is employed to measure the surface charge and the particle size of the polymers. The morphology of the samples is examined by the Scanning Electron Microscope (SEM). Finally, the biological properties of polysaccharides are investigated through *in vitro* methods, based on cells culture.

1.4.1. Spectroscopic techniques

1.4.1.1. Nuclear Magnetic Resonance (NMR)

Nuclear Magnetic Resonance (NMR) spectroscopy is an analytical technique that provides detailed structural information on chemical and natural compounds. It is widely used for the study of complex polysaccharides, obtaining information about monosaccharide composition, the linkage and substitution patterns, sequence distribution, and the quantification of functional groups (Alba & Kontogiorgos, 2021).

NMR measures the absorption of radio frequency radiation (100 to 1000 MHz) from nuclei of molecules immersed in a static magnetic field (B_0), that possess a non-zero quantum spin number (I) such as ^{13}C and ^{1}H (I = 1⁄2) (Cheng & and Neiss, 2012).

From this analysis, three fundamental parameters can be obtained to provide information on the structure of molecules and polymers (Cheng & and Neiss, 2012; Alba et al., 2018):

- chemical shift (δ), expressed in ppm, which reflects the degree of shielding of a nucleus by its surrounding chemical environment; local magnetic fields generated neighboring nuclei influence the resonance frequency of the observed nucleus;
- signal intensity, which depends on the concentration of the species analyzed and the number of scans performed during the experiment;
- coupling constant, a parameter describing the interaction between nuclei due to the molecular structure, which is independent of the applied magnetic field.

The NMR signal is generated using the pulse method, in which all nuclei of the same species are simultaneously excited by a radio frequency pulse. The energy absorbed by the nuclei is gradually transferred to neighboring atoms through longitudinal relaxation, or spin-lattice (T1), which takes into account for energy exchanges between the spin system and the molecular environment, and transverse relaxation, or spin-spin (T2), resulting from the loss of phase coherence among nuclear spins (Sinnott, 2013). The emitted signal, known as FID (Free Induction Decay), is a sinusoidal signal that decays exponentially over time due to these relaxation processes that restore the equilibrium situation. To extract the individual frequencies, it is necessary to apply a mathematical operator called "Fourier transform" which produces the NMR spectrum (Q. Guo et al., 2019; Alba & Kontogiorgos, 2021).

The main experiments for conformational analysis include one-dimensional (1D) methods, such as ^{1}H and ^{13}C NMR as well as two-dimensional techniques including

Heteronuclear Single Quantum Correlation (HSQC), Correlation Spectroscopy (COSY), Total Correlation Spectroscopy (TOCSY) and Nuclear Overhauser Effect Spectroscopy (NOESY) experiments. Solid state NMR can be also employed to characterize powder samples.

^{1}H NMR is typically the first experiment performed, providing information about the protons of sugar residues. The chemical shift of polysaccharides are generally in the range of 1-6 ppm: with anomeric protons are observed in the region 4.2-5.8 ppm and sugar ring between 3.2-4.6 ppm (Cheng & and Neiss, 2012; Alba et al., 2018). The main limit of this experiment is the signal overlap in the of 3.0-5.0 ppm region which complicates the interpretation of the spectra (Alba & Kontogiorgos, 2021).

^{13}C NMR shows lower sensitivity compared to ^{1}H; therefore, higher concentrations of polysaccharides are required. However, this can lead to high viscosity solutions for biopolymers with high molecular weights (Sinnott, 2013). To overcome this limitation, enzymatic degradation can be performed on the polysaccharide to reduce its molecular weight without affecting any chemical modifications that maybe be present (Nizzolo et al., 2024). Nevertheless, ^{13}C NMR provides a wider distribution of the peaks compared to the overlapping signals in ^{1}H NMR. In ^{13}C spectra, the anomeric carbons are observed in the range of 90-110 ppm while ring carbons between 60 and 80 ppm (Cheng & and Neiss, 2012). Moreover, most of the ^{13}C experiments are proton-decoupled spectra meaning that the interactions between ^{1}H and ^{13}C nuclei are removed, resulting in singlets signals. The main limitation of this approach is that is not possible to compare the intensity of CH_3, CH_2, CH or C peaks and it does not allow differentiation between CH_3, CH_2, CH or quaternary carbons (Q. Guo et al., 2019). However, in ^{13}C-DEPT (Distortionless Enhancement by Polarization Transfer) experiment, these differences can be distinguished as CH and CH_3 groups present positive peaks whereas CH_2 negative peaks (Alba & Kontogiorgos, 2021).

^{1}H-^{13}C HSQC (Heteronuclear Single Quantum Correlation) correlates protons with directly bonded carbons, and these correlations are represented by cross-peaks. In these spectra, the ^{1}H chemical shifts are observed along the horizontal axis while the ^{13}C chemical shifts appear on the vertical axis (Alba & Kontogiorgos, 2021). HSQC-DEPT can also be performed, in which the cross-peaks corresponding to CH_2 groups have negative intensity values (Q. Guo et al., 2019).

COSY experiments provide information about correlation between adjacent protons on the sugar ring. In COSY spectra, ^{1}H spectrum is plotted along both axes, and the

correlations are represented by cross-peaks that are symmetrical respect to the diagonal (Alba & Kontogiorgos, 2021). In TOCSY analysis, correlations between all coupled proton within a spin system are observed and the NOESY experiment reveals correlations between protons through space (Cheng & and Neiss, 2012).

In these types of experiments, polysaccharides are studied in solution, typically dissolved in D_2O, if water soluble, or in DMSO if soluble in organic solvents (Cheng & and Neiss, 2012). However, some polysaccharides, that exhibit very low solubility, cannot dissolve, for example when forming hydrogel. In such cases, solid state NMR can be used for structural characterization.

^{13}C Cross Polarization with Magic Angle Spinning, CP-MAS, is a solid-state NMR technique commonly used to study sample structure. In CP, magnetization is transferred from ^{1}H nuclei to ^{13}C nuclei to enhance sensitivity (Apperley et al., 2012). With MAS, the sample is spun at 54.7°, improving spectra resolution (Bai et al., 2010).

The spin-lattice relaxation time, ^{1}H T1ρ, provides information about the populations of nuclei in phase, which is related to the structure of the samples: crystalline samples exhibit high T1ρ values (100 ms), whereas amorphous samples show lower T1ρ values (10 ms) (Separovic & Sani, 2020).

1.4.1.2. Attenuated Total Reflection Fourier-Transform Infrared Spectroscopy (ATR FT-IR)

Fourier Transform Infrared Spectroscopy is an analytical technique used to characterize the molecular structure of polysaccharide by applying electromagnetic radiation in the infrared region, which induces the vibration of covalent bonds. Each functional groups exhibit a characteristic frequency vibration, corresponding to a specific infrared absorption bands (Berthomieu & Hienerwadel, 2009; Alba & Kontogiorgos, 2021). In FTIR experiments, a spectrum of infrared light is directed towards the samples and an interferometer splits and recombines the beam to generate an interferogram. The Fourier Transform is then used to process the interferogram and generate a spectrum in which each adsorption band corresponds to a specific functional groups (Berthomieu & Hienerwadel, 2009; Moore, 2017).

Attenuated Total Reflection (ATR) is a FTIR method, in which the sample is placed on a crystal, typically made of diamond, silicon or germanium. Infrared light passes through the crystal and reflects internally due to mirrors within the spectrometer, generating an

evanescent wave that penetrates the samples 0.5-5 μm into the sample. The light absorbed by the sample and it is then measured (Moore, 2017; Tiernan et al., 2020). Typically, the infrared spectrum is recorded in the range between 4000 cm^{-1} and 400 cm^{-1} with specific absorption regions corresponding to characteristic chemical bonds. For example, in polysaccharides, alcohols bonds (O-H) stretching vibrations appear between 3200-3600 cm^{-1}, alkanes stretching (C-H) between 2850-2950 cm^{-1}, aromatics (C-H) stretching between 3000-3100 cm^{-1} and carboxyl groups (C=O) stretching between 1700-1750 cm^{-1} (Mallick, 2023). In Table1-1 the typical FTIR adsorption bands for functional groups are reported (Khan et al., 2018).

Table 1-1. *Typical FTIR wavelength for functional groups. Adapted from Khan et al., 2018.*

Wavelength (cm^{-1})	**Functional groups**
3200-3600	O-H stretching
2500-3000	Carboxyl O-H
3300-3500	N-H stretch
3500-3500	O=C-N-H
2220-2260	Nitrile (CN)
2850-2950	C-H stretch
3010-3100	=C-H stretch
1620-1680	C=C stretch
1690-1740	Aldehyde C=O
1680-1750	Ketone C=O
1735-1750	Ester C=O
1710-1780	Carboxyl acid C=O
1630-1690	Amide C=O
2700-2800	Aldehyde C-H stretch

1.4.2. Mass Spectrometry (MS) techniques

Mass spectrometry (MS) is an analytical technique used for structural analysis and determination of polysaccharide monomer composition. This method offers various advantages compared to other analytical techniques, such as high sensitivity, detection specificity, and low sample consumption (Zaia, 2004). The mass spectrometer consists of three main components: an ion source, which generates ions; a mass analyzer, which separates the ionized species based on their mass-to-charge ratio (*m/z*); and a detector, which produces an electrical signal proportional to the ion abundance (Hoffmann &

Stroobant, 2007). The data are displayed in a mass spectrum where the detector signal is plotted as a function of *m/z* (Zaia, 2004).

Ionization sources include chemical ionization, electron ionization, the fast atom bombardment, while the most used methods are electrospray ionization (ESI) and matrix assisted laser desorption/ionization (MALDI) (Glish & Vachet, 2003). The most frequently mass analyzer are time-of-flight (TOF), which separates ion based on their velocity and the quadrupole system (Kailemia et al., 2014).

During the ionization, ions can be generated either in positive or negative mode, depending on the nature of the samples. Indeed, oligosaccharides containing acidic functional groups such as sulfate, carboxylate and phosphate are analyzed in negative ion mode (Kailemia et al., 2014).

In ESI ionization, a diluted solution of the sample is passed through a capillary to which a potential of 1-4 kV is applied. This potential difference generates charged droplets, that are dried using a flow of heated gas. As the solvent evaporates, the ions, are introduced into the mass analyzer (Glish & Vachet, 2003; Kailemia et al., 2014). This method can be coupled with liquid chromatography (LC) which separate samples based on their molecular size or their chemical properties (Fenn & McLean, 2011). The sensitivity of this technique decreases with the increasing molecular weight of the oligosaccharides, and its efficiency is lower for neutral samples (Kailemia et al., 2014).

In MALDI ionization, the sample solubilized in organic solvent is mixed with a matrix, dried, and then spotted on a MALDI target or the matrix can be deposited and dried on the target plate first, and then the sample is spotted on the matrix layer. The dry mixture is subsequently irradiated with a UV laser, which is absorbed by the matrix which transfers energy to the oligosaccharides, leading to ion formation (Fenn & McLean, 2011; Kailemia et al., 2014). Compared to ESI, MALDI exhibit higher sensitivity, efficiently ionizes higher molecular weight samples and shows better tolerance to contaminants (Kailemia et al., 2014). The main limitation is that the higher energy transfer to the analytes which can cause a fragmentation of some functional groups in the samples (Zaia, 2004).

Among mass analyzers, time-of-flight (TOF) is one of the most commonly used. Ions are accelerated through a fixed potential into a TOF drift tube of defined length and ions with lower *m/z* ratios achieve higher velocities and therefore reach the detector first (Glish & Vachet, 2003).

Another widely used mass analyzer is the quadruple (Q), in which a dynamic electric field is applied to filter ions based on their *m/z* ratio. This method offers higher selectivity compared to TOF, and it is particularly suitable for complex mixtures or high mass samples (Hoffmann & Stroobant, 2007). Moreover, quadruples are commonly paired with ESI system, whereas TOFs are used with MALDI. These two methods can also be combined in quadrupole time-of-flight (Q-TOF) instrument to enhanced the analytical performance (Glish & Vachet, 2003).

Tandem mass spectrometry, MS/MS, can be employed to obtain more detailed structural information on oligosaccharide. In this technique ions of a specific mass (*m*) or charge (*z*) are selected in the initial stage and subsequently fragmented in a second stage, providing additional structural information (Glish & Vachet, 2003).

As previously mentioned, ESI can be coupled with chromatography separation, such as high-performance liquid chromatography (HPLC) or electrophoresis. In this approach, samples are separated according to their molecular size or chemical properties at different retention times, and then they are analyzed in MS (Kailemia et al., 2014). Among the chromatographic approaches, hydrophilic interaction liquid chromatography (HILIC), and ion-pair reversed phase liquid chromatography (IPRP-LC) are usually used for the separation of oligosaccharides.

HILIC chromatography is based on a hydrophilic stationary phase typically silica, and a hydrophobic mobile phase, usually a mixture of an organic solvent, commonly acetonitrile, and water in varying proportions (Kohler et al., 2022). Separation is based on different polarity of the samples, which depend on factors such as molecular size, and the presence of specific chemical groups in the sugar chain, such as sulfated groups and N-acetylation content. However, the main limitations of this technique are the poor peak shapes, low resolution and reproducibility (D.-Q. Tang et al., 2016; Kohler et al., 2022).

IPRP-HPLC is commonly used for the separations of oligosaccharides containing strongly anion group, such as sulfated, as in heparin (Doneanu et al., 2009).

To improve the retention of charged samples on the stationary phase, typically octadecyl (C18) columns, ions are added to the mobile phase (Kailemia et al., 2014). Samples are eluted based on their charge and this method is sensitive to sulfate distribution and steric hindrance (Doneanu et al., 2009).

1.4.3. Chromatographic methods

Size Exclusion Chromatography (SEC), also known as Gel Permeation Chromatography (GPC), is a chromatographic technique that separates molecules based on their size, or more precisely, their hydrodynamic volume, which is the effective volume a molecule occupies when solvated. Separation relies on physical principles rather than chemical interactions and it is achieved using a column packed with a porous stationary phase, typically composed of silica particles or polymeric gels, forming a three-dimensional network with a defined pore size. Molecules elute at different rates according to their size: larger molecules elute more quickly, while smaller ones are retained longer within the pores resulting in delayed elution (Mori, 1999; Wu, 2003).

The SEC system consists of a pump, preceded by a degasser to remove any air bubbles from the mobile phase. The sample, usually dissolved in the mobile phase, is injected into the system either manually or *via* an autosampler. The solution then elutes through the column, where separation occurs, and is subsequently detected by one or more detectors. The acquired signal, referred as a chromatogram, is analyzed digitally using dedicated software (Lough & Wainer, 1995).

SEC can be used to determine the molecular weight of polymers, which differs from that of small molecules because polymers are composed of chains with repeating units that may have vary in length. Consequently, average molecular weights are considered.

Two key parameters are typically obtained from SEC analysis: the weight-average molecular weight (Mw), derived from the weighted average, and the number-average molecular weight (Mn), representing the statistically most probable value. The ratio between these two values defines the polydispersity index (PDI), which indicates the width of the molecular weight distribution. For instance, a polymer with a PDI of 1 is monodisperse, meaning all chains have the same length (Mori, 1999; Alba & Kontogiorgos, 2021).

However, chromatograms obtained from SEC do not directly provide molecular weight distributions; they only show sample concentration as a function of elution volume or retention time. Therefore, system calibration is required to determine molecular weights (Wu, 2003).

There are two types of calibration: conventional (or relative) and universal.

In conventional calibration, standard samples with known molecular weights, referred to as narrow standards due to their nearly unitary polydispersity, are used to construct a

calibration curve, plotting the logarithm of Mw against elution volume or retention time. This curve can then be used to determine the molecular weight of the analyte based on its elution time.

This technique offers several advantages: it is easy to set up, requires only a single detector, provides good precision, and allows estimation of sample concentrations, as they are not treated as variables. However, it has also several limitations: each polymer requires its own calibration curve, structural changes such as branching can introduce errors, and no information about molecular structure is obtained (Lough & Wainer, 1995; Mori, 1999).

Universal calibration was first introduced by Benoit in 1967. He observed that, by considering the intrinsic viscosity ([η]), defined as the ratio of the polymer specific viscosity to its concentration at infinite dilution, many polymers, with different molecular structures, follow the same calibration curve. This calibration also relies on a series of standards with known molecular weights and viscosities, as well as two coupled detectors: one sensitive to concentration and one to viscosity. A calibration curve is then constructed by plotting the product between the logarithmic value of the molecular weight and the intrinsic viscosity, *versus* elution volume can then be built. Using this curve, the hydrodynamic volume of an unknown sample can be determined (Lough & Wainer, 1995; Wu, 2003).

This technique is highly sensitive to both high and low molecular weights, and their determination is based on actual intrinsic viscosities, allowing polymer structure characterization. However, its main limitations include potential chemical or electrostatic interactions during column separation, which can lead to inaccurate results, and the requirement for standards with molecular weights similar to the sample being analyzed (Mori, 1999).

High-Performance Size Exclusion Chromatography with Triple Detector Array (HP-SEC-TDA) uses high-performance instrumentation, providing better control over pressure conditions and eliminating the need for calibration due to the presence of three complementary detectors: light scattering (LS), a refractometer, and a viscometer. The light scattering measures the hydrodynamic radius and radius of gyration (Rg), which is the radius of a sphere that can encompass the entire molecule, using two detectors: RALS (Right Angle Light Scattering – 90°) and LALS (Low Angle Light Scattering – 7°). The refractometer measures the analyte concentration during chromatography, and the viscometer determines intrinsic viscosity (Yau, 1979; Wu, 2003).

The combined use of these three sensors enables a comprehensive analysis of molecular structure, providing in a single run the molecular weight distribution, intrinsic viscosity, and molecular weight.

Each detector is associated with a specific equation (1), (2), (3) as following reported:

$$\text{Refractometer} \rightarrow A = K_1 \frac{dn}{dc} C \quad (1)$$

$$\text{Viscometer} \rightarrow A = K_2[\eta]\, C \quad (2)$$

$$\text{Light scattering} \rightarrow A = K_3\, M_w \left(\frac{dn}{dc}\right)^2 C \quad (3)$$

Where A represents the area of the chromatogram peaks, C is the sample concentration, dn/dc is the refractive index increment, which can be found in the literature for common polymers or determined directly using HP-SEC-TDA, and K represents instrument constants that depend solely on the detector geometry.

These constants are established during system calibration by injecting a known standard, such as pullulan, for which all parameters ([η], Mw, C, and dn/dc) are known. Once the calibration constants K for each detector are determined, the sample of interest can be analyzed, provided that its concentration and/or dn/dc in the chosen solvent are known (Lough & Wainer, 1995).

This technique also provides empirical constants logK and *a* for a polymer at a specific temperature and in a specific solvent. These constants are part of the Mark–Houwink equation (4), which correlates intrinsic viscosity ([η]) and molecular weight (M), and is presented as follows (H. Zhang et al., 2020):

$$[\eta] = K\, M^{\alpha} \quad (4)$$

The constants K and *a* are used to understand the chain structure and the behavior in specific solvent and temperature of polymers: K is related to the flexibility of the intrinsic chain and *a* reflects the geometric chain (Vega et al., 2001). The value of *a* gives information about the shape of the polymer in solution: if *a* is about 0, the polymer showed a compact structure as tight coil, if *a* is between 0.5 and 0.8, the polymer is defined as random coil, and if *a* is higher than 1 the polymer form rigid rod coil (Rosen, 1993).

1.4.4. Rheological analysis

In rheology experiments, materials are subjected to a shear stress (τ) expressed in Pascal, which is defined as the ratio between the tangential force (F) and the surface of the body (A) on which it acts, as the following expression shows (Mezger, 2015):

$$\tau = \frac{F}{A} \qquad (5)$$

The shear stress is applied at a specific rate, called the shear rate or flow gradient ($\dot{\gamma}$), expressed in s^{-1}. It is defined as the ratio between the tangential speed (v) on the top plane and the distance between the upper and lower surface (h) (Mezger, 2015):

$$\dot{\gamma} = \frac{v}{h} \qquad (6)$$

Depending on the physical nature of the material, different stress response behaviors can be observed. In purely elastic solids, deformation is instantaneous, fully reversible, and directly proportional to the applied stress. These materials return to their original equilibrium rate once the stress is removed (Han, 2007).

In contrast, purely viscous liquids exhibits flow in response to the applied shear stress which is time-dependent and irreversible as the energy applied to induce deformation is dissipated as friction (Irgens, 2013).

Viscoelastic materials display intermediate behavior between purely viscous liquid and a purely elastic solid. Their deformation is time dependent and can be considered as the sum of both viscous and elastic components (Irgens, 2013).

Liquid-like systems, such as liquids and semi-solids, exhibit behavior described by Newton's laws. According to Newton, a fluid at rest can be considered as an infinite series of parallel molecular layers. When a tangential force is applied, the upper layer moves in the direction of the force and transmits motions to the lower layers. These layers, however, move at a lower speed, resisting the motion of the fluid. This phenomenon is due to a material property called viscosity (η), expressed in Pa·s, and defined as the ratio between shear stress and shear rate, as described by the following equation (7) (Irgens, 2013; Mezger, 2015):

$$\eta = \frac{\tau}{\dot{\gamma}} \qquad (7)$$

This equation can be represented on a graph, known as a flow curve, Figure 1-8, which shows shear stress as a function of shear rate. When the curve is a straight line, the fluid is defined as Newtonian, and its viscosity is constant (green curve in Figure 1-8), meaning it does not depend on the applied flow conditions and corresponds to the slope of the curve. This behavior is typical of water or organic solvents. However, there are fluids whose viscosity varies depending on the shear rate; these are called non-Newtonian fluids. They can be divided into two categories: pseudoplastic (shear thinning) and dilatant (shear thickening) fluids (Mezger, 2015; Ramli et al., 2022).

Pseudoplastic materials are characterized by a decreasing slope of the flow curve, in fact, their viscosity decreases as the shear rate increases (red curve in Figure 1-8), although it remains constant at very low and very high shear rates. Two linear regions, known as Newtonian plateaus, can be identified: the zero-shear viscosity η_0 (at low shear rates) and the infinite-shear viscosity η_∞ (at high shear rates), which can be obtained using the Carreau-Yasuda model (Han, 2007; Alba & Kontogiorgos, 2021).

This group typically includes dispersions of long-chain polymers, which, at rest or under low shear stress, are randomly dispersed in the solvent. When shear stress is applied, the chains align in the direction of the force, allowing better layer slippage and thus a decrease in viscosity (Irgens, 2013).

Dilatant fluids, on the other hand, exhibit the opposite behavior, as their viscosity increases with increasing shear rate (blue curve in Figure 1-8). This behavior is typical of highly concentrated solutions, where under high shear stress, particles tend to agglomerate and resist flow, leading to an increased viscosity. They are called dilatant because they tend to expand in volume when force is applied (Mezger, 2015).

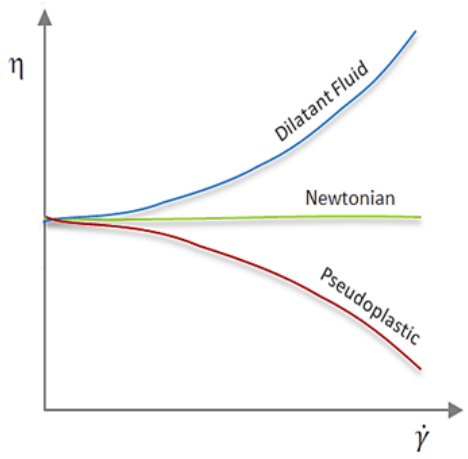

Figure 1-8. *Representation of flow curves of Newtonian and no-Newtonian fluids.* The viscosity versus the shear rate is reported. Adapted from Mezger, 2015.

Flow curves can be obtained using a rheometer. This instrument is equipped with a motor that allows the rotation of a shaft connected to a geometry capable of applying stress to the sample. The most common geometries are the plate–plate system, mainly used for more gel-like materials, and the double-gap or concentric cylinder system, used for less viscous solutions. In both cases, the lower support remains fixed, and only the upper part connected to the motor moves. The motor can apply rotations in both directions, generating either unidirectional or oscillatory stresses. In the case of oscillatory stresses, the instrument can control both the amplitude and the frequency of the applied stress (Han, 2007; Mezger, 2015).

Using a rheometer, it is possible to measure the elastic moduli, the storage modulus, G′, and the loss modulus, G″, both expressed in Pascal. These values are obtained through a strain sweep test, also known as an amplitude sweep, during which the sample is subjected to increasing shear stress while keeping temperature and oscillation frequency constant. Samples in which G″ is greater than G′ exhibit a fluid-like behavior (viscoelastic liquid), whereas when G′ exceeds G″, the samples exhibit the solid-like behavior (viscoelastic solid). This test helps identify the range of shear rates in which the material shows linear viscoelastic behavior, meaning no structural damage is observed. This range is referred to as the Linear Viscoelastic Region (LVE) (Figure 1-9), which is essential for determining the appropriate shear rate levels for a subsequent test called the frequency sweep (Mezger, 2015).

In amplitude sweep curves, it is sometimes possible to observe a flow point, where the G′ and G″ curves intersect, and the values become equal. Beyond this point, the moduli switch roles: the previously lower modulus becomes higher than the other, indicating that the sample has undergone structural damage that alters its physical nature (Figure 1-9) (Ramli et al., 2022).

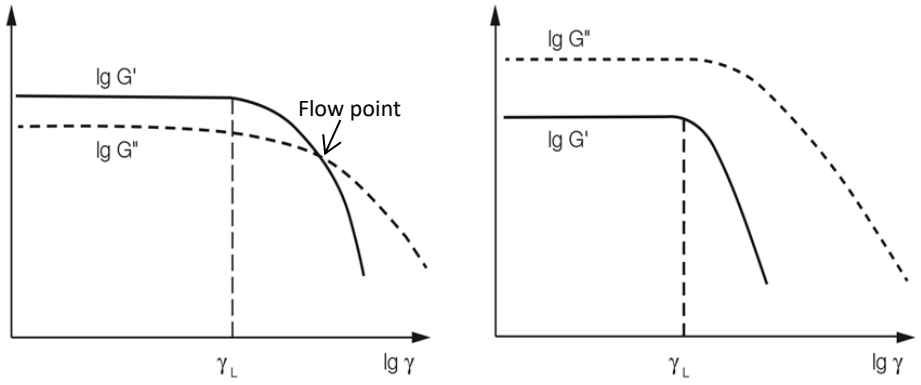

Figure 1-9. *Representation of the curve obtained after the amplitude sweep test*.
The curve of a solid-like materials (G'>G'') is observed in the graph at the left, where a flow point is also detected; at right the amplitude sweep of a liquid-like materials (G''>G') is reported. Adapted from Mezger, 2015.

Once the LVE is identified, a frequency sweep test can be conducted. In this test, the sample is subjected to oscillatory stress at variable angular frequencies. This allows the measurement of the material's viscoelasticity and provides insights into the internal structure of polymers and the long-term stability of dispersions by evaluating how the sample behaves over time. High frequencies simulate short-term or fast motion, while low frequencies simulate long-term or resting behavior.

The results of these tests are typically presented in logarithmic scale graphs, where angular frequency (ω), expressed in radians per second (rad/s), or frequency (f) in Hertz (Hz), is plotted against G′ and G″ (Mezger, 2015).

To evaluate the behavior of the tested material, the values of G′ and G″ at high and low frequencies are measured: if at low frequencies G″ > G′, the sample behaves primarily viscously and if at high frequencies G′ > G″, the material exhibits primarily elastic properties.

To assess the long-term stability of dispersions, G′ and G″ values in the low-frequency region are considered. If G′ > G″, this indicates a solid-like structure, often due to a stable network of interactions, suggesting good physical stability of the dispersion. Conversely, if G″ > G′, the material is liquid-like and susceptible to phase separation.

In frequency sweep graphs, a crossover point, where G′ and G″ intersect, may be present. This point can be linked to the resistance of a formulation over time: the lower the frequency at which the crossover occurs, the more long-lasting and stable the tested sample is, since frequency is inversely proportional to time (Ramli et al., 2022).

1.4.5. Dynamic Light Scattering (DLS)

Dynamic Light Scattering, also known as Photon Correlation Spectroscopy (PCS), is an instrument used to measure the Zeta potential (Zp) and hydrodynamic radius (Rh) of particles. The Zp is a parameter that refers the surface change density of particles or nanoparticles (Berne & Pecora, 2013). Depending on its value, repulsion or aggregation phenomena due to electrostatic forces can occur: at values lower than -30 mV and higher than +30 mV no aggregation events happen due to the repulsion of the charges (Stetefeld et al., 2016). To measure the Zp, an electric field is applied between the electrodes of the cell containing the sample in solution, and then a laser beam passes through it. The charged particles move towards the electrode with opposite charge, causing a variation in the frequency of the light scattered by the sample. From this variation, it is possible to calculate the electrophoretic mobility (μ), which is used to calculate the Zeta potential through the Henry equation (8):

$$\mu = \frac{2\,\varepsilon\,\zeta\,f(k\,a)}{3\,\eta} \qquad (8)$$

where ε is the dielectric constant, ζ the zeta potential, f(k a) is the Henry function and η the solvent viscosity (Berne & Pecora, 2013; Stetefeld et al., 2016).

Trough the DLS it is also possible to determine the hydrodynamic radius of the particles, their size, based on the irradiation of a solution and the subsequent measurement of scattering light (Stetefeld et al., 2016). During the experiment, a laser beam is applied to the sample and the variations in intensity of scattered light generated by random motion of particles, known as Brownian motions, are measured over time. This allows to determine the hydrodynamic radius of the particles because, at the same temperature and viscosity, smaller particles move faster, producing rapid changes in scattering intensity, while larger particles move more slowly, generating smaller intensity variations (Berne & Pecora, 2013; Feng et al., 2023).

1.4.6. Scanning Electron Microscope (SEM)

Scanning electron microscopy is a technique that allows the acquisition of images with magnifications beyond the resolution limit of optical microscopy, by exploiting the interaction between an electron beam and the atoms of the sample (Vernon-Parry, 2000). The SEM mainly consists of: a source from which the electron beam is generated, a

column containing a system of lenses necessary to control the beam, a series of detectors that collect the signal generated from the interaction between beam and sample to reconstruct the images, a sample holder and a vacuum system, generated by a vacuum pump and a turbomolecular pump, to prevent the beam from encountering obstacles such as gas molecules, with which would interact with it and reduce the image resolution. The lenses used are of electromagnetic type, as electrons cannot pass through the glass, and divided into two categories: condensing lenses, the first encountered by the electrons in the column, used to determine the size of the beam and used to focus the beam on the sample (Zhou et al., 2007).

The signals obtained from a SEM analysis are: back-scattered electrons (Back Scattered Electrons, BSE), secondary electrons (SE) and X-rays (Goldstein et al., 2012).

BSE are generated as a result of elastic interaction between the electron beam and the nuclei of the atoms constituting the sample. They are collected by the Backscatter Detector (BSD) which generates a grayscale image based on the sample composition. Darkest areas correspond to elements with a lower atomic number while the lighter areas correspond to heavier elements (Zhou et al., 2007).

Secondary electrons are emitted from the material as a result of impact with the electron beam. In this case, the interaction is inelastic, during which part of the energy is dissipated; therefore, these electrons have a lower energy level than the back-diffused ones. For this reason, only electrons close to the sample surface can produce a signal which is picked up by the Secondary Electron Detector (SED). The image obtained allows a detailed view of the sample surface and its topography (Goldstein et al., 2012).

X-rays have a characteristic energy for each element in the samples, allowing for qualitative and semi-quantitative analysis (Vernon-Parry, 2000).

1.4.7. In vitro system

In vitro models play an important role in the preclinical evaluation of chemical compounds, providing a controlled, reproducible, and ethically sustainable system to study their biological effects, mechanisms of action, and potential toxicity (Ediriweera et al., 2019). These models typically involve cultured cell lines, primary cells, 2D or 3D cultural systems, and organ system that mimic specific physiological environments, allowing the studies of parameters such as cytotoxicity, genotoxicity, oxidative stress, inflammation, metabolic activity, and barrier integrity (C. Zhang et al., 2024). Moreover, advanced models such as co-culture systems, organoids, and organ-on-a-chip

technologies have been developed to improve the similarity of physiological environments, especially in pathological conditions, in order to obtain more accurate results of *in vivo* outcomes (Saeidnia et al., 2015).

In vitro systems can be used to understand compound mechanism in the cellular pathways and their interaction with receptors and enzymes without the need for animal testing (Adler et al., 2011). Despite some limitations in replicating the complexity of whole organisms, *in vitro* approaches are important for early-stage screening and for the determination of certain biological properties of chemical compounds.

1.4.7.1. Cell viability in vitro test

The MTT (3-[4,5-dimethylthiazol-2-yl]-2,5-diphenyltetrazolium bromide) assay is a well-established and widely used colorimetric test for assessing cell viability, proliferation, and cytotoxicity in various biological and pharmacological studies (Ghasemi et al., 2021). This assay is based on the evaluation of cellular mitochondrial function by measuring the activity of succinate dehydrogenase enzymes present in metabolically active cells. Indeed, these enzymes are able to convert the yellow tetrazolium salt MTT into insoluble purple formazan crystals, which can be quantified by measuring the absorbance at a specific wavelength (Larramendy & Soloneski, 2018). This reaction occurs only in living cells with functional mitochondria, making the assay an indirect measure of cell viability and metabolic integrity (Buranaamnuay, 2021).

During the test, cells, previously treated with the test compounds, are incubated with MTT and then the resulting formazan crystals are solubilized using an appropriate solvent, typically dimethyl sulfoxide (DMSO) or isopropanol. The absorbance of the resulting purple solution is measured typically at 570 nm, and this value is proportional to the number of viable cells in the culture, allowing to determine cell proliferation or the cytotoxic effects of tested compound (Ghasemi et al., 2021; Larramendy & Soloneski, 2018).

The MTT assay is a simple, cost-efficient, and reproducible test, making it particularly suitable for high-throughput screening. However, some limitations include sensitivity to variations in metabolic state, difficulties in removing cell culture media from the plate wells, and the requirement to solubilize formazan in organic solvent (Larramendy & Soloneski, 2018). Despite these drawbacks, the MTT assay remains a valuable tool in toxicological evaluations, drug development, and cancer research.

1.4.7.2. In Vitro Models for Intestinal Permeability

Cell-based assays are used for studying the intestinal permeability *in vitro*, providing valuable insight into the absorption, transport, and barrier function of compounds across the intestinal epithelium, including under pathological condition such as inflammatory bowel diseases (IBD) (Dunleavy et al., 2023). The most commonly used models are monolayers of human colorectal adenocarcinoma cell lines, such as Caco-2 and HT29-MTX, which differentiate over time to form tight junctions and microvilli (Srinivasan et al., 2015).

Permeability is typically evaluated by measuring transepithelial electrical resistance (TEER), which reflects the integrity of the cell monolayer, and by monitoring the transport of marker molecules, such as or fluorescein isothiocyanate-dextran (FITC-dextran) across the cell layer. A decrease in TEER or an increase in the permeability of the markers indicates a compromise in barrier integrity (Malik et al., 2025). These *in vitro* models are important for preclinical studies to understand the mechanisms of absorption, predict oral bioavailability, and assess the impact of inflammatory stimuli, microbial metabolites, or pharmacological agents on gut barrier function (Artursson et al., 2001).

CHAPTER 2 - SYNTHESIS AND CHARACTERIZATION OF SULFATED TAMARIND SEED POLYSACCHARIDE

As previously reported, Tamarind seed polysaccharide (TSP) is a neutral water-soluble galactoxyloglucan isolated from the seed kernel of *Tamarindus indica* L. with average Mw 600–800 kDa. It is applied as a stabilizer, thickener, gelling agent and binder in food and pharmaceutical industries and in the ophthalmic field in the formulations of synthetic eye drops used for the treatment of the Dry Eye Disease (DED), due to its important physical, chemical and biological properties.

Despite the above, there is room to further improve TSP properties and processing. Owing to its high molecular weight and the absence of charged substituents, the solution containing the polysaccharide can become very viscous, and solubilization of TSP requires a long time, and sometimes even heating. For these reasons, formulations containing TSP at low concentrations are often prepared to facilitate the dissolution step, representing a limitation for some applications in the pharmaceutical field and beyond. TSP chemical modification by sulfated groups is desirable to extend processability and applicability. In particular, the sulfated modification can allow the formation of specific binding to proteins or receptors, significantly increasing the biological activity and the potential applications of the biopolymer.

The aim of this chapter is to determine the best conditions for TSP sulfation by tuning the extent of sulfation while maintaining high molecular wights. The chemical structure, the molecular size and the degree of sulfation (DS) were characterized by using a range of complementary physico-chemical techniques. Moreover, the stability toward enzymatic degradation by xyloglucanase, viscosity and mucoadhesive properties of S-TSP were evaluated.

TSP was sulfated in a one-step process using dimethyl formamide as a solvent, and sulfur trioxide-pyridine complex as a sulfating reagent. Studies of chemical structure, molecular weight distribution and viscosity were conducted to characterize the synthesized products. The sulfation degree was established by conductimetric titration; the sulfate group distribution was studied by NMR spectroscopy and liquid chromatography-mass spectrometry, and sulfated TSP oligomers were obtained by enzymatic degradation with cellulase and/or xyloglucanase. Sulfated products showed higher solubility than TSP,

Mws in the range of 700–1000 kDa, a sulfation degree of two to four per subunit and pseudoplastic behavior. A preliminary study of mucoadhesion revealed the unexpected interaction of S-TSP with mucin, providing a route by which sulfated TSP interactions with biomolecules may be influenced.

2.1. Chemical sulfation of TSP

2.1.1. Synthesis strategy

TSP sulfation synthesis was performed in dimethylformamide, DMF, using sulfur pyridine complex (SO_3·Py), modifying the sulfation methods of Nguyen (Nguyen et al., 2021) and Lang and Crescenzi (Lang et al., 1992). The chemical sulfation mechanism of TSP can be described as an electrophilic attack of the hydroxyl groups of the polymer on the SO_3·Py reagent as shown in Figure 2-1.

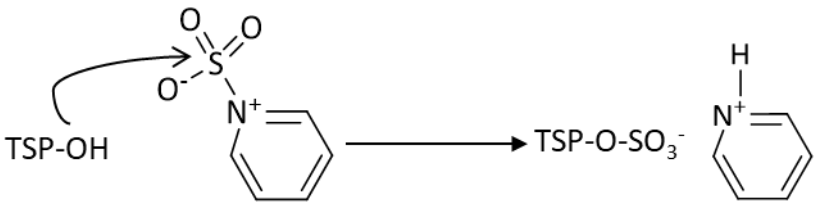

Figure 2-1. *The chemical sulfation mechanism of TSP.*

In contrast with the published method, dry TSP was directly solubilized in DMF and was not precipitated in a gelatinous state before adding the reagent. Initially, the reaction was performed at room temperature (RT) and at 50°C as reported by Lang and Crescenzi (Lang et al., 1992), at the same concentration of reagents and with a TSP/ SO_3·Py molar ratio of 1:1. The sample obtained at room temperature, S-TSP_1, showed a lower degree of sulfation than the product sulfated at 50°C, S-TSP_1a (Table 2-1). However, S-TSP_1a showed lower absolute zeta potential and lower molecular weight, as reported in Table 2-1 and Table 2-2 respectively, due to depolymerization of the product caused by the higher temperature. For this reason, the sulfation synthesis with higher concentration of reagent were performed at room temperature. TSP was solubilized at two different concentrations, 10 mg/mL and 5 mg/mL, to evaluate how this parameter influenced synthesis. As reported in Table 2-1, different TSP/ SO_3·Py molar ratios were tested to obtain S-TSP with different sulfation degrees.

Table 2-1. *Reaction conditions for sulfated TSP, S-TSP, synthesis (molar ratio and concentration), resulting in sulfation degree and zeta potential.*

Sample	Temperature (°C)	TSP/ SO_3·Py molar ratio	TSP concentration in DMF (mg/mL)	Sulfation Degree (DS)*	Zeta potential (mV)
TSP	-	-	-	-	-0.70±0.16
S-TSP_1	RT	1:1	10	2	-43.0±1.02
S-TSP_1a	50°C	1:1	10	3	-37.8±3.12
S-TSP_2	RT	1:2	10	3	-47.4±2.41
S-TSP_3	RT	1:2	5	4	-58.1±3.12

*by conductimetric titration; RT: room temperature

2.1.2. Conductimetric titration

By conductimetric titration, the sulfation degree (DS) was determined (Equation 9 in paragraph 2.7.2.5.), considering that 21 hydroxyl groups can be sulfated on the repeating unit of TSP. The DS values are reported in Table 2-1. By increasing the reagent, an increase in DS was observed, as expected. S-TSP_1 and S-TSP_2 show, respectively, DS of two and three and S-TSP_3 DS of four, meaning that a lower TSP concentration also leads to an increase in DS.

2.1.3. Zeta potential

Qualitative analysis of the sulfation reaction was performed measuring sample Zp, a parameter typically obtained by model-dependent transformation of the measured electrophoretic mobility used to estimate the surface charge of the polymers (Ladiè et al., 2021). As expected, the Zp of neutral TSP is equal to 0 mV, while negative Zp values were determined for the sulfated TSP products (Table 2-1). Additionally, the absolute Zp value correlated with the degree of sulfation obtained by conductimetric titration: −43 mV for S-TSP_1, −47 mV for S-TSP_2 and −58 mV for S-TSP_3 (Table 2-1).

2.1.4. Fourier-transform infrared spectroscopy (FT-IR)

TSP sulfation was also confirmed by FT-IR spectroscopy. The pristine TSP FT-IR spectrum (Figure 2-2) showed the typical profile of this polysaccharide (Chawananorasest et al., 2016). The wide absorption peak from about 3600 cm^{-1} to 3000 cm^{-1} corresponded to the stretching vibration of hydroxyl groups (O–H) induced by inter- or intramolecular motion. The peak at 2890 cm^{-1} was due to C–H stretching and bending vibrations including CH, CH_2 and CH_3. The band at 1640 cm^{-1} is due to the small traces of uronic

acid in the TSP and the peaks from 1550 cm^{-1} to 1300 cm^{-1} were also related to C–H bands (L. Ren et al., 2022). The peak from 1150 to 897 cm^{-1} was attributed to C–O–C stretches (Chawananorasest et al., 2016). In S-TSP compounds, the presence of the sulfated groups was confirmed by the formation of two new bands in the spectra at 807 cm^{-1} and 1227 cm^{-1}, assigned to S=O and C–O–S stretching vibrations, respectively (Lang et al., 1992). The intensities of these bands increased with increasing DS, from S-TSP_1 to S-TSP_3.

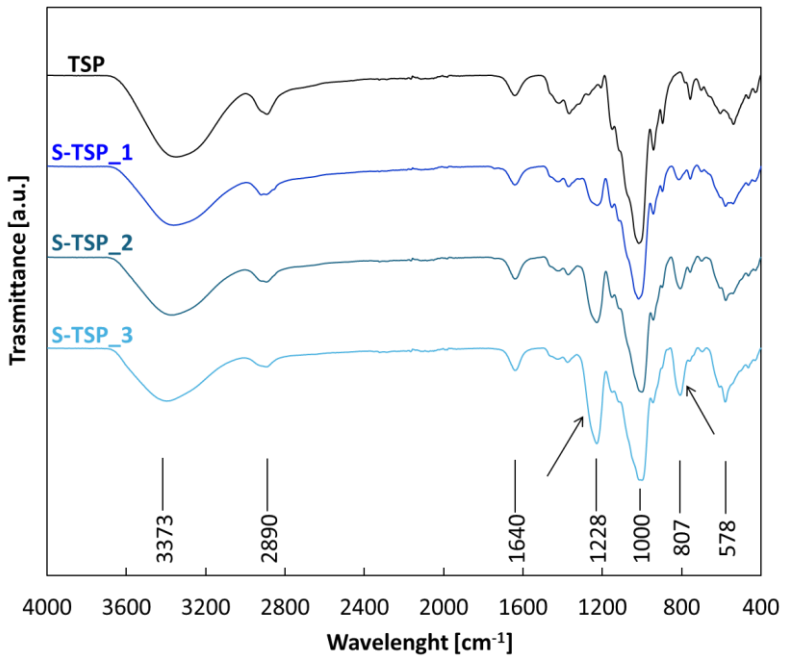

Figure 2-2. *FT-IR spectra of TSP and S-TSP samples.*
TSP is in black, S-TSP_1 in dark blue, S-TSP_2 in blue and S-TSP_3 in light blue. The new bands assigned to S=O and C–O–S stretching vibrations are signed with arrows.

2.2. Physical-chemical characterization of TSP and sulfated products

2.2.1. Molecular weight distribution

Molecular Weight Distribution HP-SEC-TDA with multi-detector systems (Right Angle and Low Angle Light Scattering, Refractive Index and Viscosimeter) was used to determine the molecular weight distribution, intrinsic viscosity, hydrodynamic radius and Mark–Houwink parameters of TSP and S-TSP products. After various preliminary tests using the most common solutions for the elution such as $NaNO_3$ sodium nitrate 0.1M with 0.05% NaN_3, 0.3 M sodium acetate with 0.05% NaN_3 (pH~8.1) was chosen as the mobile phase. The samples had a similar elution volume between 11 and 16 mL with a broad

bell-shaped chromatographic peak, caused by a high polydispersity index (Table 2-2). The chromatograms of TSP and S-TSPs samples are reported in Figure 2-3.

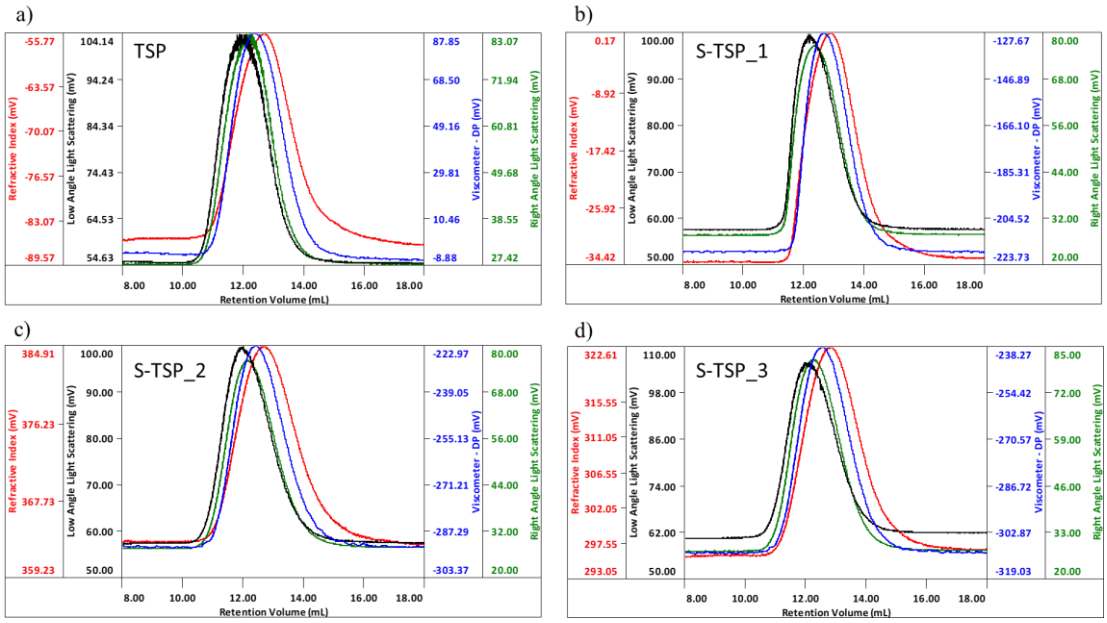

Figure 2-3. *Chromatographic profiles of TSP (a), S-TSP_1 (b), S-TSP_2 (c) and S-TSP_3 (d).*
In red is reported the refractive index, in blue the viscometer, in black the low angle light scattering and in green the right angle light scattering.

Since no published dn/dc values are available for TSP and S-TSP in sodium acetate, they were independently determined under the optimized chromatographic conditions: 0.139 mL/g and 0.125 mL/g were obtained for TSP and S-TSP, respectively. Mw (weight average molecular weight), Mn (number average molecular weight), polydispersion index (expressed as Mw/Mn ratio), [η] (intrinsic viscosity), Rh (hydrodynamic radius) and *a,* corresponding to the slope of Mark-Houwink curve, are reported in Table 2-2. All the results refer to the mean values of duplicate injections.

Table 2-2. *HP-SEC-TDA results for pristine and modified TSP.*
Mw – weight average molecular weight, Mn – number average molecular weight, PDI – Polydispersity index, η – intrinsic viscosity, Rh – hydrodynamic radius, *a* – Mark-Houwink parameter.

Sample	Mw (kDa)	Mn (kDa)	PDI (Mw/Mn)	[η](dl/g)	Rh (nm)	*a*
TSP	620	405	1.5	5.1	35	0.78
S-TSP_1	750	485	1.5	3.8	34	0.82
S-TSP_1a	660	355	1.8	4.0	33	0.70
S-TSP_2	810	540	1.5	4.1	36	0.80
S-TSP_3	1000	730	1.4	4.5	41	0.81

The TSP Mw and Mn were 620 kDa and 405 kDa, respectively; S-TSPs showed higher molecular weight values similar with the theorical Mw values obtained with the presence

of sulfated groups on the polysaccharide chain. The molecular weight increase indicated that the reaction occurred without, or with negligible, sample depolymerization, except for S-TSP_1a, which showed a decreasing of the molecular wight due to the increased temperature (Table 2-2). The Mw/Mn remained constant and similar to the starting TSP, indicating that there was no increase in polydispersity after derivatization. The hydrodynamic radius (Rh) for TSP and S-TSP remain in the same range, except for S-TSP_3, which showed a higher hydrodynamic radius of 41 nm due to higher molecular weight. The intrinsic viscosity, [η], of sulfated products is lower compared to TSP due to the introduction of sulfate groups along the chains that creates a charge density and leads to an increase in structural density, resulting in a decrease in viscosity (Blanco et al., 2013). Comparing the different S-TSP products, the [η] increases with the degree of sulfation, as the effect of increased molecular weight predominates over the increase in density. The Mark–Houwink parameter, *a*, is similar for all the samples and comparable to data reported in the literature (H. Zhang et al., 2020). The values of a are in the range of 0.7–0.9, indicating that, regardless of DS, the molecules remain in a random coil conformation. The weight recovery, determined by the refractive index area, is in a range between 80% and 92% for all the samples, and these values are compatible with the water absorption by dry samples.

2.2.2. Rheological properties

The compound viscosity was also studied using a rheometer; Figure 2-4 shows that TSP and S-TSP behaved like pseudoplastic liquids, with viscosity decreasing for increasing shear rate. S-TSP_1 showed a very similar viscosity with TSP, starting at 165 mPa·s; in contrast, S-TSP_2 and S-TSP_3 had lower viscosity, starting at almost 100 mPa·s, probably due to the presence of the sulfated groups, which changes the conformation of the polysaccharide and decrease the viscosity (Z. Wang et al., 2018). Regarding the trend of viscosity, the more sulfated samples (S-TSP_2 and S-TSP_3) showed lower viscosity compared to TSP, but they were quite similar to each other, unlike the values determined by HP-SEC-TDA, for which the intrinsic viscosity increased from S-TSP_1 to S-TSP_3. It is important to emphasize that intrinsic viscosity, [η], is measured under infinite dilution conditions and is thus influenced by intramolecular rather than in intermolecular interactions. In contrast, viscosity, which provides insights into the behavior of fluid under a variety of conditions, is not measured under infinite dilution, making

intermolecular interactions significant. In this case, the negative charges of the sulfate groups are likely to play a crucial role in the viscous behavior, counteracting the increase in molecular weight, which is not the predominant parameter.

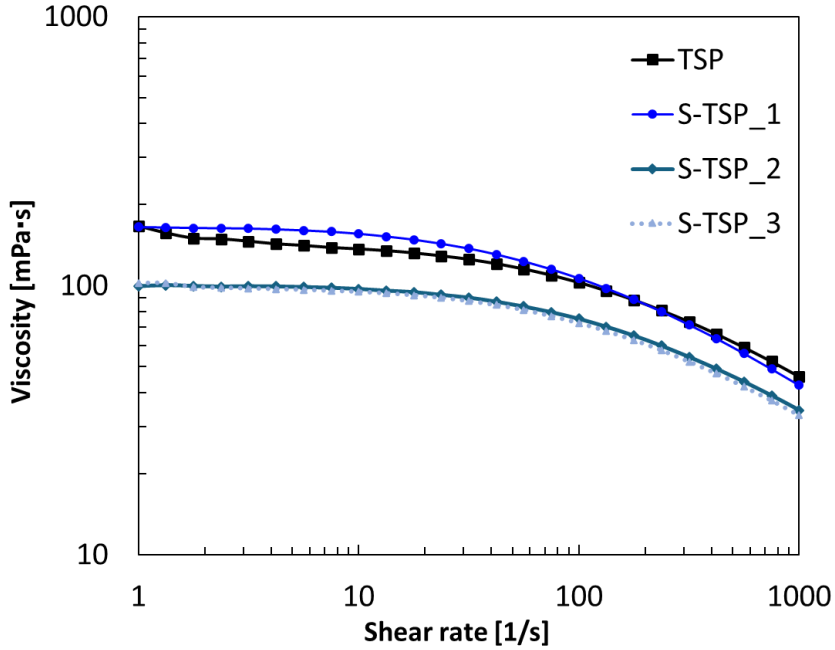

Figure 2-4. *Viscosity curves of TSP and S-TSP samples.*
TSP is in black, S-TSP_1 in dark blue, S-TSP_2 in blue and S-TSP_3 in light blue. The samples were analyzed at 10 mg/mL at 20°C.

2.2.3. Scanning electron microscope (SEM)

The morphology of the samples was analyzed for TSP and S-TSP_3 using SEM, as shown in Figure 2-5, to determine differences in the polysaccharide structure after the sulfation.

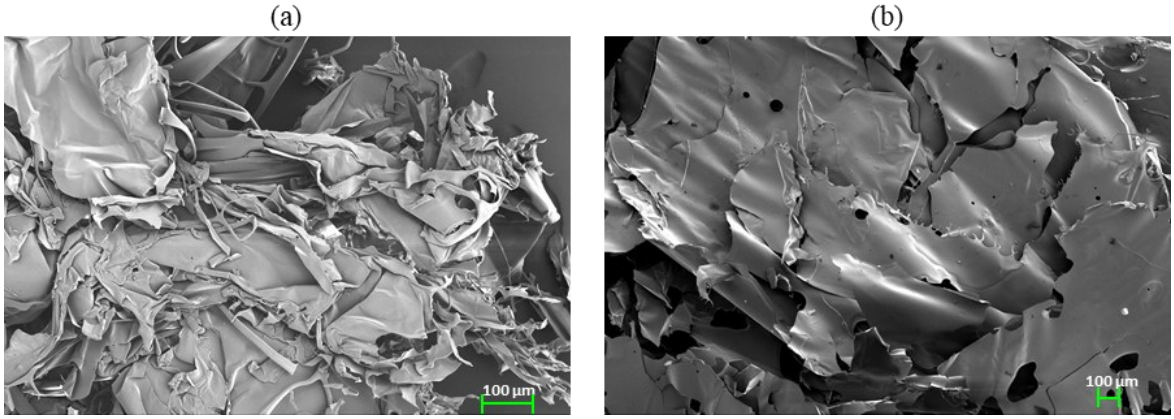

Figure 2-5. *SEM images of TSP (a) and S-TSP_3 (b).*

SEM images, Figure 2-5, revealed a three-dimensional network for both TSP and S-TSP_3, after freeze-drying solutions in the same concentrations. TSP, shown in Figure 2-5 (a), exhibited a compact, rough, and irregular surface, consistent with the previously

reported data (L. Ren et al., 2022). In contrast, the sulfated sample, shown in Figure 2-5 (b), displayed a smoother surface compared to TSP, with some holes visible in the structure. This morphological difference is attributed to the chemical modification, which made the structure less compact (Tu et al., 2016; Z. Wang et al., 2018).

2.3. Structural properties of TSP, S-TSP and their enzymatically hydrolyzed products

TSP and S-TSP products were characterized using monodimensional (1D) and bidimen sional (2D) NMR spectroscopy. In the proton spectra (Figure 2-6), no significant chemical shift changes were observed following functionalization. This is likely to be due to the overlap of broad signals caused by the high viscosity of the samples and the high molecular weight, which reduced the spectral resolution. Consequently, only the well-separated peaks were attributed to those of the anomeric region, specifically to xylose linked to galactose at 5.16 ppm, xylose linked only to glucose at 4.95 ppm, glucose and galactose at approximately 4.55 ppm and the hydrogen at position 2 of glucose at 3.40 ppm.

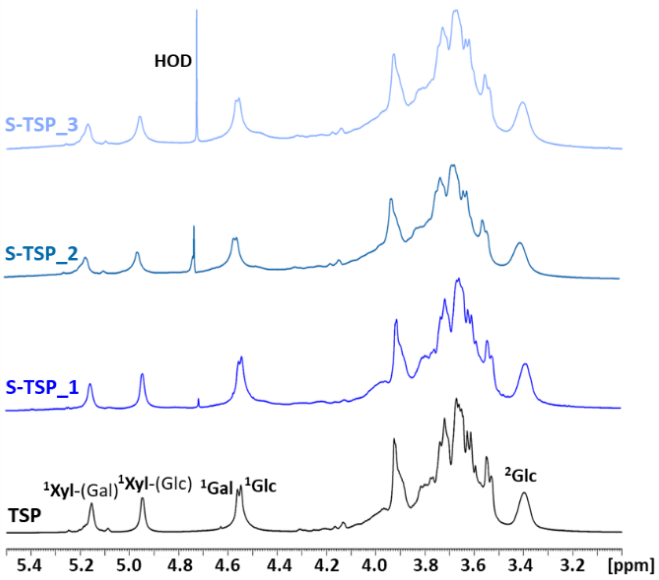

Figure 2-6. *Proton spectra of TSP and S-TSP samples.*
TSP is reported in black, S-TSP_1 in dark blue, S-TSP_2 in blue and S-TSP_3 in light blue. The peaks of the anomeric protons of the residues and the position 2 of glucose are indicated. The superscript corresponds to the carbon number of the observed monosaccharide, labelled in bold, while the monosaccharide linked is in the parentheses. Glc-glucose; Xyl-xylose; Gal-galactose.

2D ^{1}H-^{13}C heteronuclear single quantum correlation (HSQC) NMR allows the resolution of overlapping signals present in ^{1}H NMR and is widely used for characterization of complex neutral (Huang et al., 2022) and charged (Eisele et al., 2023) polysaccharides. The ^{1}H-^{13}C HSQC cross peaks of TSP, attributed in accordance with the literature data (Arruda et al., 2015), are shown in Figure 2-7. In addition to the cross peaks related to glucose, galactose and xylose, signals from arabinose were also observed, likely due to contamination in plant seeds from arabinan or arabinoxylan, as reported in the literature (Tuomivaara et al., 2015; H. Zhang et al., 2020).

In the HSQC NMR spectrum of S-TSP, the CH_2 crosspeaks at about 4.33–4.22/69.9 ppm, which are separated from the other backbone signals (blue circles in Figure 2-7), are consistent with sulfation of the primary alcohol of galactose and/or glucose (D. Zhang, 2014).

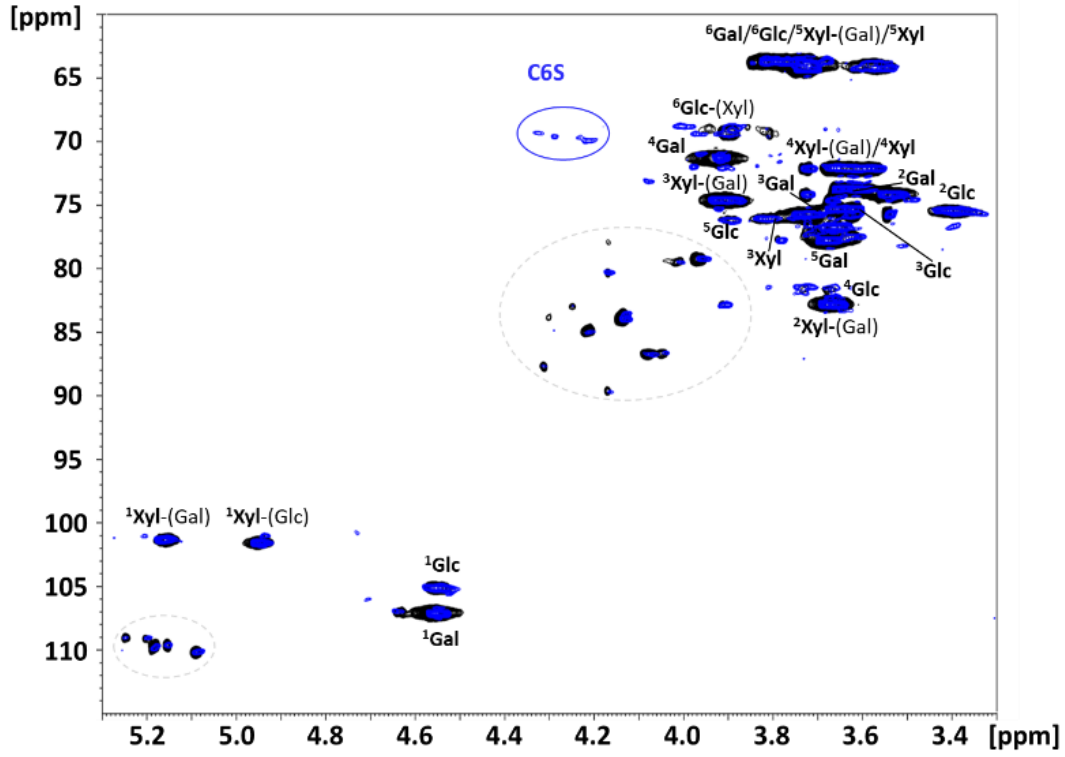

Figure 2-7. *^{1}H-^{13}C HSQC superimposition of TSP in black with partial assignments and S-TSP_1 in blue.* The superscript corresponds to the carbon number of the observed monosaccharide, which is in bold, while the monosaccharide linked is in the parentheses. Signals related to the sulfation were circled in blue. Arabinose signals are circled in grey. Glc-glucose; Xyl-xylose; Gal-galactose.

As with the proton spectra, the resolution remains low because of the high molecular weight, which may prevent the detection of other signals related to sulfation. Moreover, as previously demonstrated with high molecular weight hyaluronic acid (Nizzolo et al., 2024), two dimensional experiments are not quantitative due to the different

conformational mobility of the residues. Indeed, in the anomeric region of the TSP (Figure 2-7), galactose, which has greater conformational mobility compared to the other residues but is present in lower molar ratios (Glc:Gal = 3.1:1) relative to the theoretical unit (Raj & Lee, 2024), displays higher intensity than xylose and glucose.

To address this, enzymatic degradation was performed to reduce the molecular weight of the polysaccharide while maintaining the substitutions, to allow a more effective NMR study. The lower molecular weight of the S-TPS products was expected to make LC-MS analysis feasible. Xyloglucanase and cellulase, enzymes with different specificity towards xyloglucans, were used: xyloglucanase hydrolyses the β-1,4 bond, primarily forming the repeating unit of TSP, Figure 2-8(a), (H. Zhang et al., 2020); cellulase, expected to be less specific and less sensitive to branching, cleaves both the β-1,4 linkage between glucose units and β-1,2-linked xylose and galactose (Ejaz et al., 2021), as shown in Figure 2-8(b).

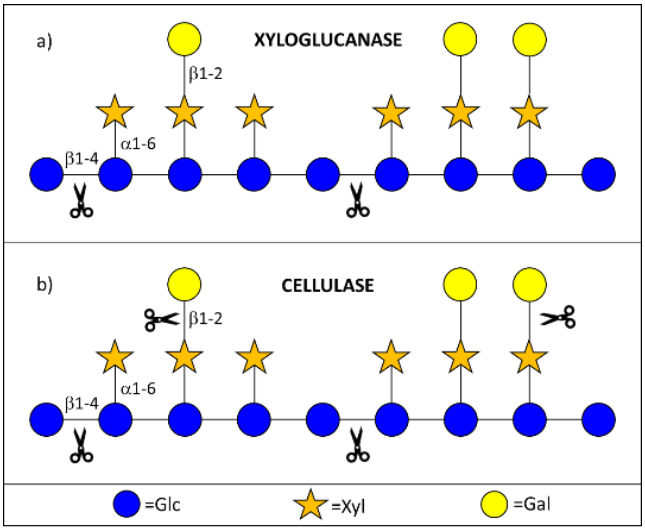

Figure 2-8. *Schematic representation of the mechanism of action of xyloglucanase (a) and cellulase (b).*

After 24 h of depolymerization of TSP with cellulase and xyloglucanase, oligomers with Mw < 2kDa, reported in Table 2-3, similar to the theorical Mw of the repeating unit were obtained, regardless of the enzyme used. For S-TSP, the enzymes were less active due to the presence of sulfate, especially for the cellulase which could not hydrolyzed the TSP, that maintained a Mw of 253 kDa. Instead, oligomers with a Mw similar to the repetitive unit were obtained with xyloglucanase, but a fraction of almost 7 kDa still remained. Consequently, a mixture of both enzymes was used, and the hydrolysis time was extended to 48h compared to that used for TSP.

Table 2-3. *HP-SEC-TDA results for hydrolyzed TSP and S-TSP.*
Mw – weight average molecular weight, Mn – number average molecular weight.

Sample	Enzyme	Mw (kDa)		Mn (kDa)		Recovery (%)	
TSP	Cellulase	1.4		1.2		90	
	Xyloglucanase	1.3		1.3		115	
S-TSP_1	Cellulase	253		117		84	
	Xyloglucanase	7.0	1.5	4.5	1.2	29	71
	Both enzymes	5.1	1.4	4.1	1.2	28	72

2.3.1. NMR hydrolyzed TSP

HSQC spectra of hydrolyzed TSP samples were recorded to verify the cleavage site of the enzymes. As shown in Figure 2-9, xyloglucanase hydrolyzed only the linkage between the backbone glucose units. Indeed, in the anomeric region, the signals of the α/β reducing ends (REs) of the glucose were observed (Figure 2-9).

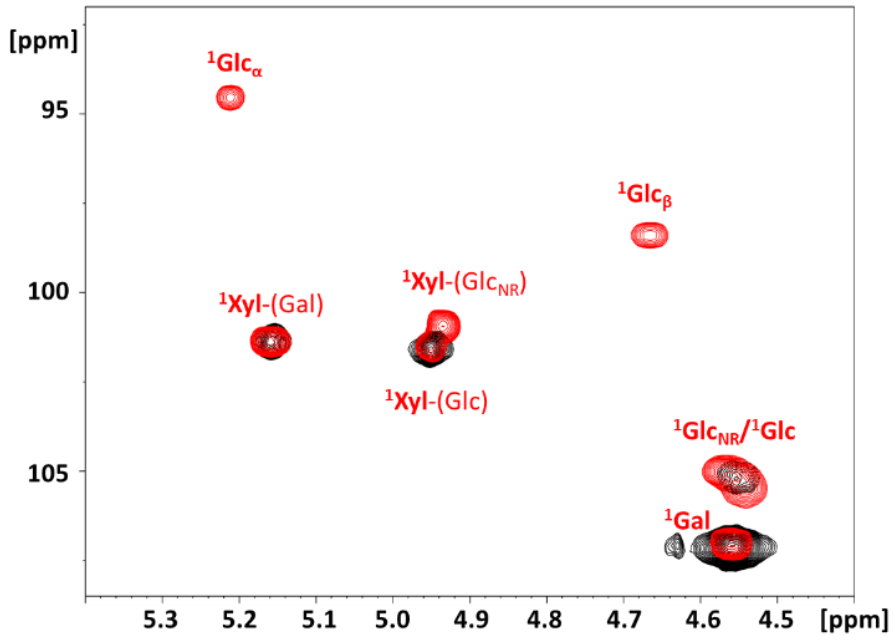

Figure 2-9. *^1H-^{13}C HSQC superimposition of the anomeric region of TSP in black and hydrolyzed TSP, with xyloglucanase in red.*
The superscript corresponds to the carbon number of the observed monosaccharide, which is in bold, while the monosaccharide linked is in parentheses. NR—non reducing end; Glc—glucose; Xyl—xylose; Gal—galactose.

In contrast, cellulase also cleaved the β-1,2 linkage between the xylose and the galactose, as indicated by the signals of the galactose monomeric unit in Figure 2-10.

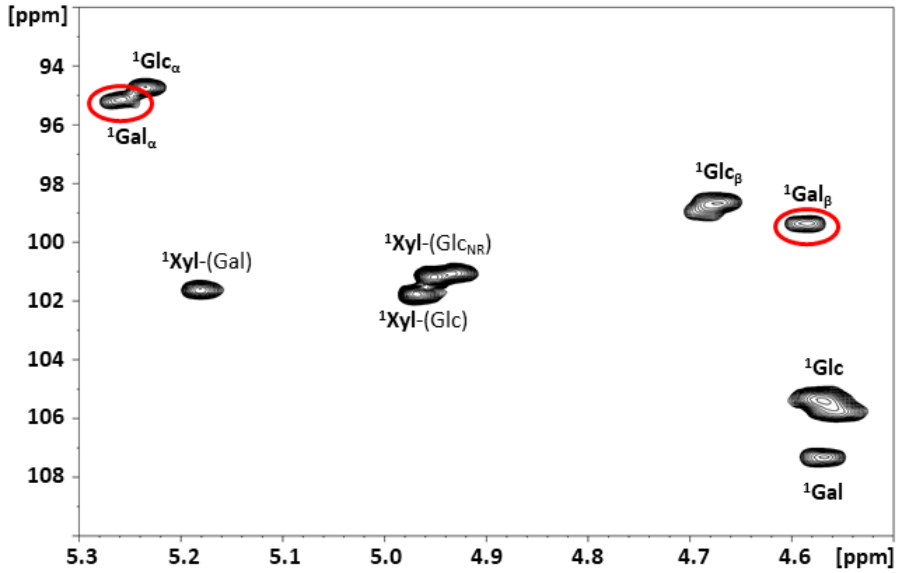

Figure 2-10. *^{1}H-^{13}C HSQC anomeric region of hydrolysed TSP with cellulase.*
Signals related to Galactose anomeric signals, α and β. The superscript corresponds to the carbon number of the observed monosaccharide, which is in bold, while the monosaccharide linked is in the parentheses. Glc-glucose; Glc_{red}-glucose reducing end; Xyl-xylose; Gal-galactose.

With both enzymes, a new signal at 4.93/100.9 ppm, attributed to the xylose linked to the non-reducing (NR) end glucose, was also observed (Figures 2-9/10). Owing to the short oligosaccharides, new signals in the hydrolyzed TSP appeared to the non-hydrolyzed pristine TSP, particularly in the region from 4.10 to 3.20 ppm. The complete attribution of the hydrolyzed TSP obtained by xyloglucanase digestion is reported in Table 2-4 and in Figure 2-11.

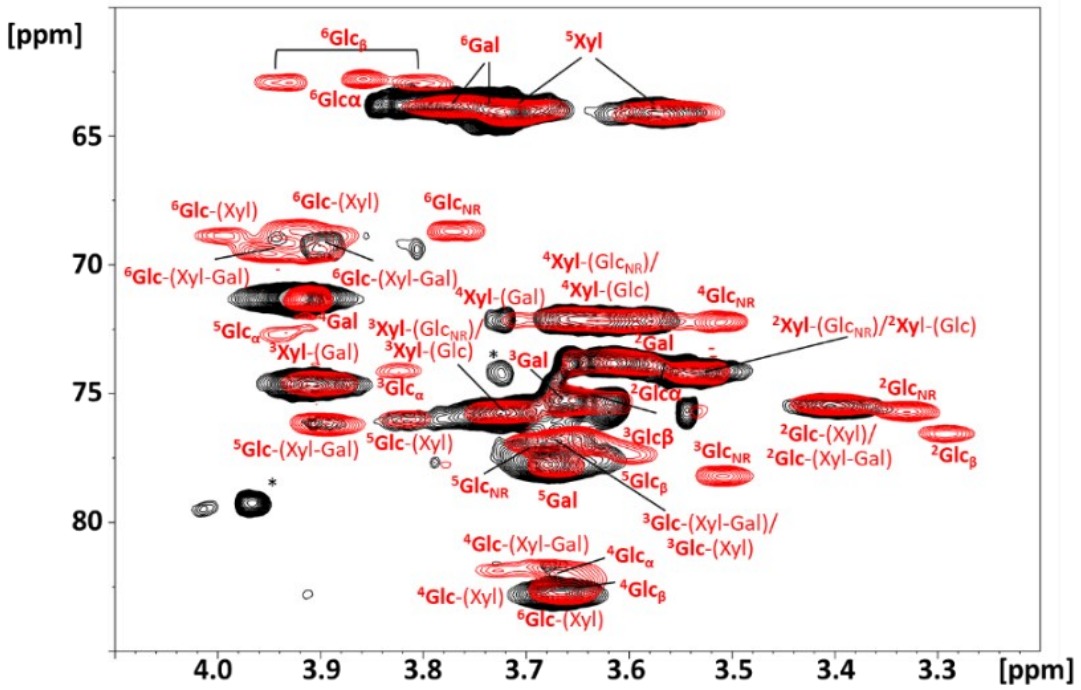

Figure 2-11. *^{1}H-^{13}C HSQC superimposition of TSP in black and hydrolyzed TSP with xyloglucanase in red.*
The superscript corresponds to the carbon number of the observed monosaccharide, which is in bold style, while the monosaccharide linked is in the parentheses. * signals assigned to the arabinose residue. Glc—glucose; Xyl—xylose; Gal—galactose

Table 2-4*. Attribution of the HSQC's signal of hydrolyzed TSP with xyloglucanase.*
The observed monosaccharide is in bold, while the monosaccharide linked is in the parentheses. Glc-glucose; Xyl-xylose; Gal-galactose.

Monosaccharide Residues	**Chemical shift (ppm) H/C**					
	1	**2**	**3**	**4**	**5**	**6**
Glc_{NR}	4.55/105.2	3.33/75.7	3.51/78.2	3.51/72.1	3.69/77.0	3.77/68.5
Glc-(Xyl)	4.55/105.2	3.40/75.4	3.67/76.8	3.67/81.9	3.81/76.0	3.99-3.92/68.7
Glc-(Xyl-Gal)	4.55/105.2	3.40/75.4	3.67/76.8	3.67/82.6	3.89/76.1	3.95-3.91/69.4
Glc_{α}	5.21/94.4	3.62/73.8	3.82/74.1	3.68/81.9	3.93/72.6	3.86/62.6
Glc_{β}	4.65/98.3	3.29/76.5	3.65/77.1	3.68/81.7	3.60/77.2	3.93-3.81/62.7
Xyl-(Gal)	5.16/101.4	3.66/82.7	3.90/74.6	3.71/72.1	3.71-3.56/63.9	-
Xyl-(Glc)	4.95/101.6	3.54/74.1	3.72/75.7	3.59/72.1	3.71-3.56/63.9	-
Xyl-(Glc_{NR})	4.93/100.9	3.54/74.1	3.72/75.7	3.63/72.1	3.71-3.56/63.9	-
Gal	4.55/107.2	3.60/73.8	3.65/75.1	3.91/71.3	3.67/77.7	3.77/63.7

A quantitative HSQC analysis of the samples treated with xyloglucanase was possible due to the reduced molecular weight of the product. The 1:1 ratio between galactose and xylose linked to galactose, which showed the same values of integration, 16 and 17% respectively, along with a Glc:Xyl:Gal of 3.7:3:1.3, confirmed the proposed structure of the repeating unit as shown in Figure 2-12.

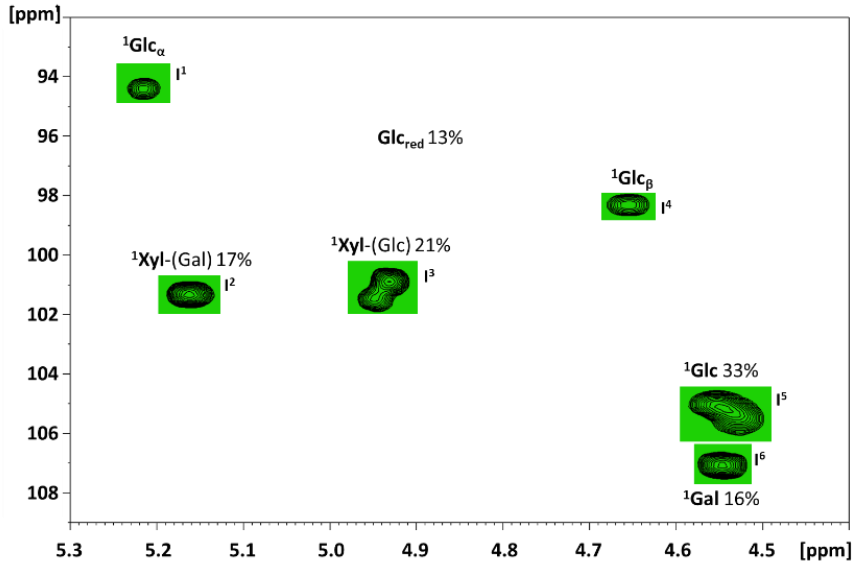

Figure 2-12. *Integration of ^{1}H-^{13}C HSQC anomeric region of hydrolyzed TSP with xyloglucanase.* The superscript corresponds to the carbon number of the observed monosaccharide, which is in bold, while the monosaccharide linked is in the parentheses. The relative molar percentages of the individual monosaccharides are reported. Glc-glucose; Glc_{red}-glucose reducing end; Xyl-xylose; Gal-galactose

2.3.2. LC-MS of enzymatically hydrolyzed TSP and S-TSP

The cellulase and xyloglucanase generated digestion products of TSP were also analyzed by hydrophilic interaction chromatography (HILIC) coupled with an ESI-QTOF mass spectrometer. The LC-MS profile of TSP hydrolyzed by xyloglucanase (Figure 2-13, on the bottom) showed two major peaks attributed to oligomers, the first composed of five hexoses and three pentoses (Hex_5P_3, *m/z* 611.21 at 12.5 min) and the second composed of six hexoses and three pentoses (Hex_6P_3, *m/z* 692.24 at 13.5 min), both corresponding to the main repeating unit of the TSP, compatible with the values obtained by the integration of the NMR bidimensional spectra, Figure 2-12 (H. Zhang et al., 2020). As expected, the less selective cellulase gave rise to shorter oligomers than xyloglucanase (Figure 2-13, on the top). Overall, the shorter oligomers are more abundant in the TSP treated with cellulase. The most intense peak corresponds to the oligomer composed by five hexoses and three pentoses (Hex_5P_3, *m/z* 611.21 at 12.5min), as that previously obtained with xyloglucanase, while Hex_6P_3 was detected only in trace amounts. The

observed differences between the products obtained by two enzymes are in accordance with the known higher specificity of xyloglucanase. It is most likely that the cellulase was able to cut the linkage between the xylose and the galactose, leading to the formation of Hex_5P_3. This hypothesis is in accord with the generation of monosaccharide galactose determined by NMR in cellulase-degraded TSP, shown in Figure 2-10.

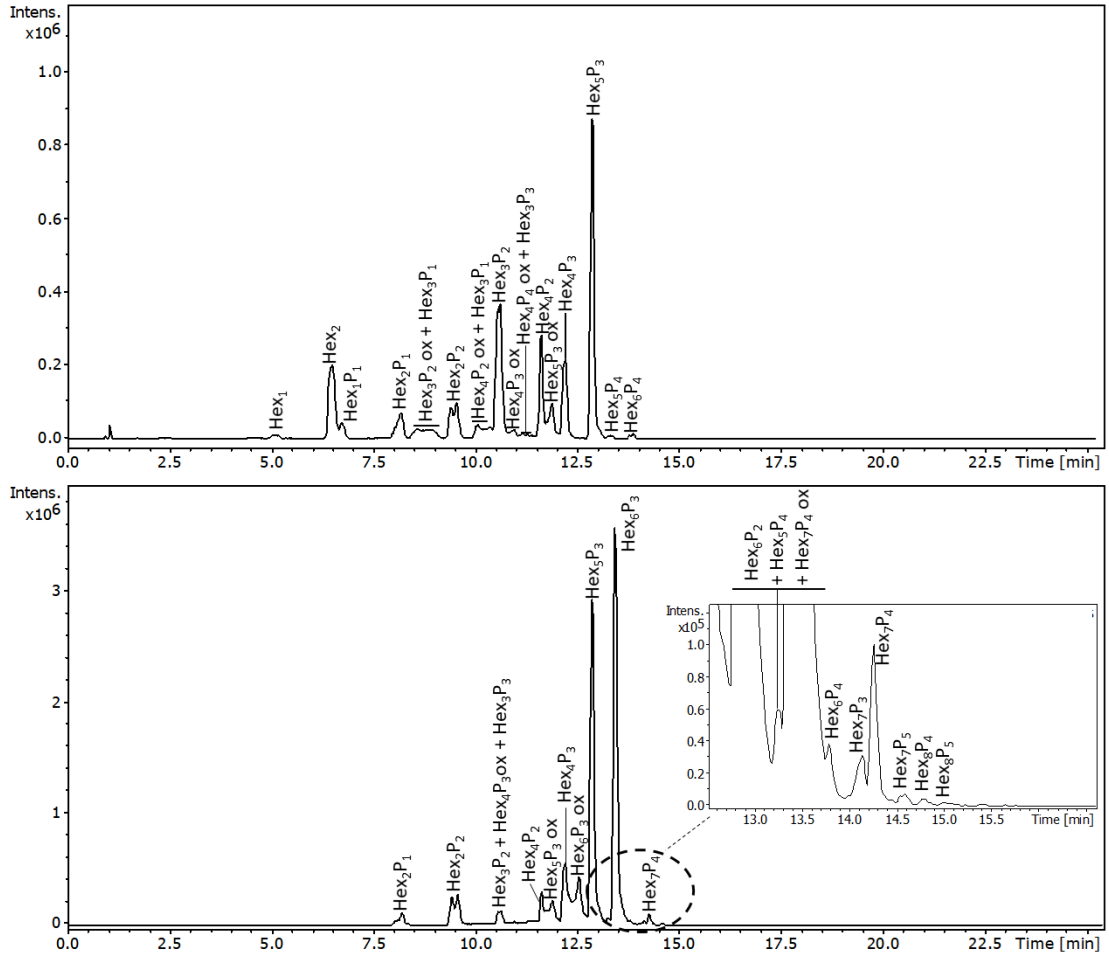

Figure 2-13. *HILIC/ESI-QTOF-MS chromatograms of TSP hydrolyzed by cellulase on the top and TSP hydrolyzed by xyloglucanase on the bottom.*
Hex—hexose (glucose or galactose, 162 Da), P—pentose (xylose, 132 Da); the numbers in subscript indicate the number of hexoses and pentoses with in the detected oligosaccharide: ox indicates the oxidized minor components (−2 Da), most likely related to the C4-oxidized oligomers, as previously reported by P. Sun et al., 2020.

Interestingly, both enzymes generate a short oligomer composed by two hexoses and two pentoses (Hex_2P_2, *m/z* 605.21 at 9.4min, Figure 2-13). This oligomer can be unambiguously attributed to the structure containing two glucoses, both branched with xylose. Probably the enzymes hydrolyzed two glucoses even if they were both linked with the xylose, with this fragment derived from longer oligomers with four or more xylose units near each other. The disaccharide Hex_2 that was detected only in the LC-MS analysis of cellulase degraded TSP was attributed to the sucrose present in the cellulase as a

stabilizer. The LC-MS analyses also showed minor oligomers with a−2Da mass shift compared to the regular TSP oligomers, suggesting possible oxidation of one of the hydroxy-groups to a C=O group. Such a side oxidation degradation of xyloglucans has been previously studied by MALDI-TOF (P. Sun et al., 2020). The authors reported that the C=O may be generated at the NRE of the formed oligosaccharides at the level of enzymatic cleavage of the xyloglucan backbone. The S-TSP_1, with a DS value of two, hydrolyzed with the mixture of cellulase and xyloglucanase, was analyzed by ion-pair reversed phase high performance liquid chromatography (IPRP-HPLC) coupled with ESI-QTOF-MS (Figure 2-14). IPRP-HPLC is widely used for sulfated oligosaccharides due to its compatibility with ESI-MS and selectivity towards sulfated oligomers, including positional isomers (Alekseeva et al., 2020; Gardini et al., 2021; Kang et al., 2022). LC-MS analysis showed well-defined groups of oligomers with different sulfate group numbers (from zero to at least six). Interestingly, only short neutral fragments were detected as minor components, suggesting that sulfation occurs in a random but relatively homogenous way along the polymer, and non-sulfated oligomers longer than Hex_3P_2 were not detected.

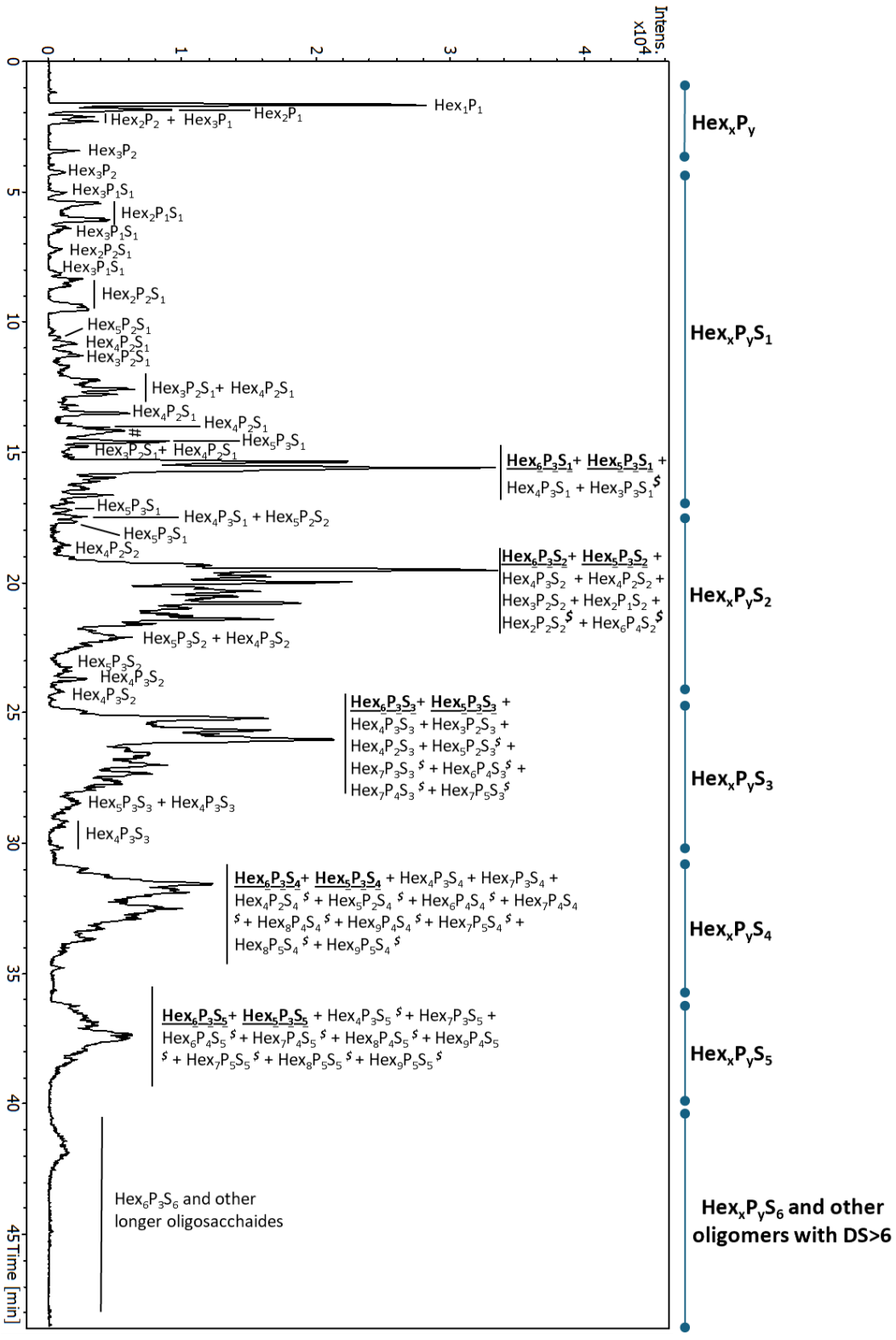

Figure 2-14. *IPRP-HPLC/ESI-QTOF-MS chromatogram of S-TSP hydrolyzed by cellulase and xyloglucanase.*

Hex—hexose (glucose or galactose, 162 Da), P—pentose, (xylose, 132 Da), S—sulfate (SO_3-,80Da); the numbers in subscript indicate the number of hexoses and pentoses within the detected oligosaccharide. The most abundant oligomers $Hex_6P_3S_x$ and $Hex_5P_3S_x$ are underlined and in bold. $—oligomers with the intensity lower than 500 (the intensity of the highest peaks $Hex_6P_3S_1$/$Hex_5P_3S_1$ and $Hex_6P_3S_2$/$Hex_5P_3S_2$ are higher than 1×10^4).

As expected, the profile (Figure 2-14) suggests significantly higher structural heterogeneity of the S-TSP compared to the starting material. The increased complexity of the resulting oligosaccharide mixture is caused by non-specific sulfation reactions, leading to various positional isomers as well as enzymatic specificity of both xyloglucanase and cellulase that probably do not recognize highly sulfated regions.

The extracted ion chromatograms (EICs) for *m/z* 732.19 ($Hex_6P_3S_1$), 651.17 ($Hex_5P_3S_1$), 772.18 ($Hex_6P_3S_2$), 691.15 ($Hex_5P_3S_2$), 876.73 ($Hex_6P_3S_3$), 731.13 ($Hex_5P_3S_3$), 981.28 ($Hex_{56}P_3S_4$) and 900.26 ($Hex_5P_3S_4$) are following reported in Figure 2-15.

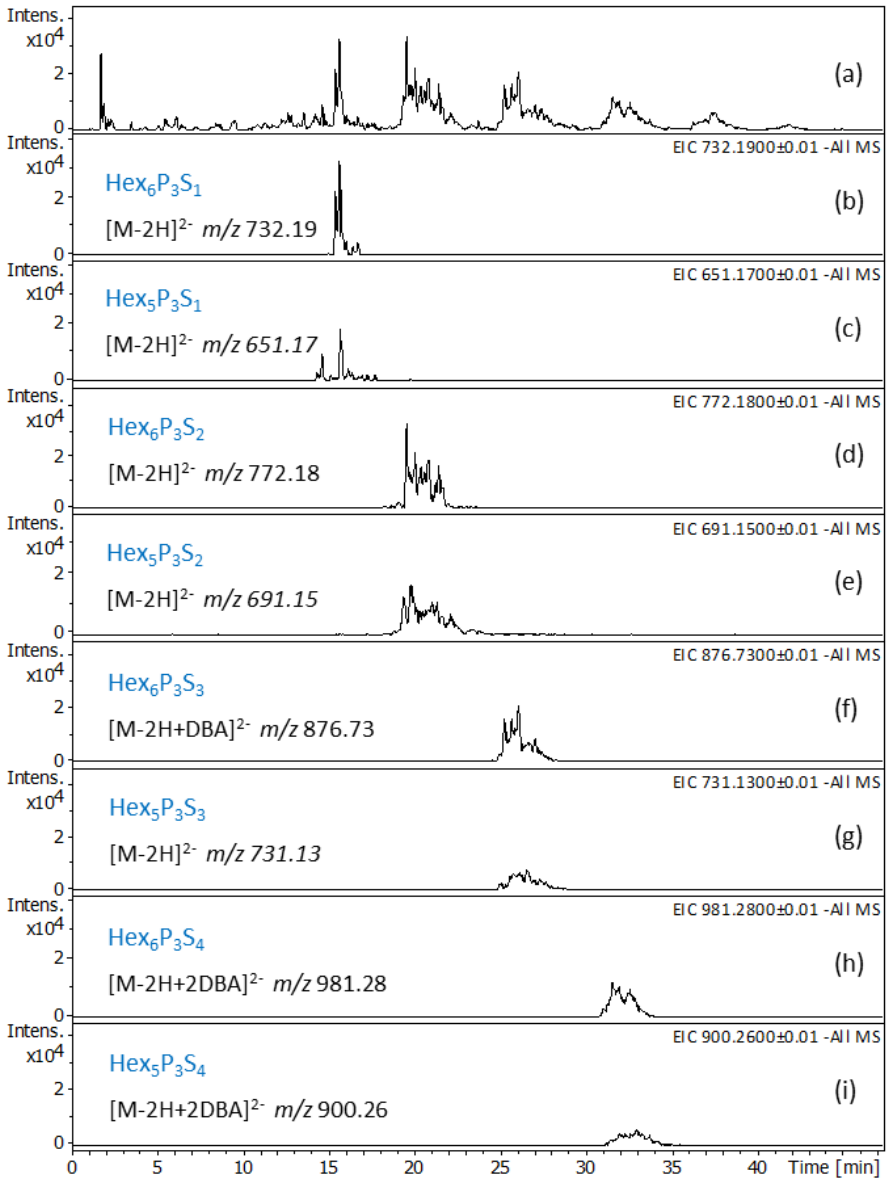

Figure 2-15. *IPRP-HPLC/ESI-QTOF-MS chromatogram of S-TSP hydrolyzed by cellulase and xyloglucanase (**a**) and extracted ion chromatograms (EICs) showing the separation of various positional isomers of the most abundant mono-, di-, tri- and tetrasulfated $Hex_6P_3S_x$ and $Hex_5P_3S_x$ (**b-i**).*
Hex - hexose (glucose or galactose, 162 Da), P – pentose, (xylose, 132 Da), S – sulfate (SO_3^-, 80 Da); DBA – dibutylamine (129 Da); the numbers in subscript indicate the number of hexoses and pentoses within the detected oligosaccharide.

Multiple peaks of each *m/z* confirm the presence of numerous positional isomers. The mass spectra of the most abundant oligomers co-eluted in the regions of mono-, di-, tri-, tetra-, penta- and hexasulfated oligosaccharides are shown in Figure 2-16 and the value *m/z* values and the corresponding ion forms are reported in Table 2-5.

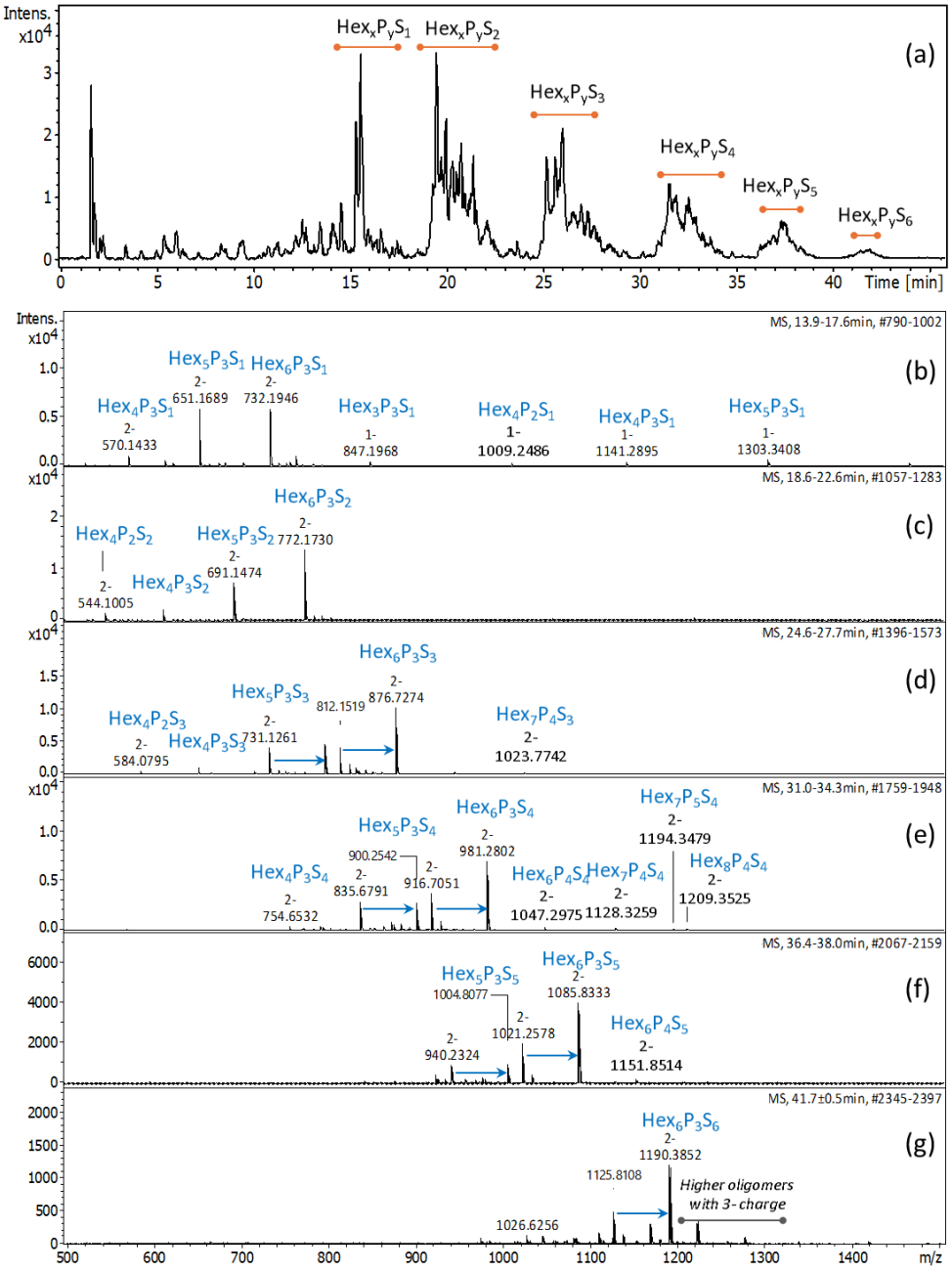

Figure 2-16. *LC-MS chromatogram (a) and MS spectra of the most abundant peaks co-eluted in the regions of mono (b), bi- (c), tri- (d), tetra- (e), penta- (f) and hexasulfated (g) oligomers.*
Because various oligomers with the same sulfation degree, including positional isomers, are co-eluted, the mass spectra were averaged for their retention time range: 13.9–17.6 min ((b), $Hex_xP_yS_1$); 18.6–22.6 min ((c), $Hex_xP_yS_2$); 24.6–27.7 min ((d), $Hex_xP_yS_3$); 31.0–34.3 min ((e), $Hex_xP_yS_4$); 36.4–38.0 min ((f), $Hex_xP_yS_5$); 41.7 ± 0.5 min ((g), $Hex_xP_yS_6$). Hex—hexose (glucose or galactose, 162 Da), P—pentose, (xylose, 132 Da), S—sulfate (SO_3-, 80 Da); DBA—dibutyl amine (129 Da, adducts are indicated with blue arrow); the numbers in subscript indicate the number of hexoses and pentoses within the detected oligosaccharide.

Table 2-5. *MS data of oligosaccharides identified in the S-TSP_1 digested with cellulase and xyloglucanase*

	Oligosaccharide	*Monoisotopic ions observed in ESI-MS*			
		Ion form	*m/z* experimental	*m/z* theoretical	Error, ppm
No sulfated oligomers	Hex_1P_1	$[M-H]^-$	311,0971	311,0984	-4,2
		$[2M-H]^-$	623,2009	623,2040	-5,0
	Hex_2P_1	$[M-H]^-$	473,1497	473,1512	-3,2
	Hex_2P_2	$[M-H]^-$	605,1901	605,1935	-5,6
	Hex_3P_1	$[M-H]^-$	635,1984	635,2040	-8,8
	Hex_3P_2	$[M-H]^-$	767,2415	767,2463	-6,3
Mono-sulfated oligomers	$Hex_2P_1S_1$	$[M-H]^-$	553,1042	553,1080	-6,9
	$Hex_3P_1S_1$	$[M-H]^-$	715,1568	715,1608	-5,6
	$Hex_2P_2S_1$	$[M-H]^-$	685,1459	685,1503	-6,4
	$Hex_3P_2S_1$	$[M-H]^-$	847,1954	847,2031	-9,1
	$Hex_4P_2S_1$	$[M-H]^-$	1009,2486	1009,2559	-7,2
	$Hex_5P_2S_1$	$[M-2H]^{2-}$	585,1488	585,1507	-3,2
	$Hex_3P_3S_1$ $^{\$}$	$[M-2H]^{2-}$	489,1173	489,1190	*-3,5*
	$Hex_4P_3S_1$	$[M-2H]^{2-}$	570,1446	570,1454	-1,4
	$Hex_5P_3S_1$	$[M-2H]^{2-}$	651,1684	651,1719	-5,4
	$Hex_6P_3S_1$	$[M-2H]^{2-}$	732,1945	732,1982	-5,1
Di-sulfated oligomers	$Hex_2P_1S_2$ $^{\$}$	$[M+DBA-H]^{1-}$	762,2108	762,2166	-7,6
	$Hex_2P_2S_2$ $^{\$}$	$[M+DBA-H]^{1-}$	894,2524	894,2513	1,2
	$Hex_3P_2S_2$	$[M+DBA-H]^{1-}$	1056,3050	1056,3117	-6,3
	$Hex_4P_2S_2$	$[M-2H]^{2-}$	544,1005	544,1027	-4,0
	$Hex_5P_2S_2$	$[M-2H]^{2-}$	625,1273	625,1291	-2,9
	$Hex_4P_3S_2$	$[M-2H]^{2-}$	610,1217	610,1239	-3,6
	$Hex_5P_3S_2$	$[M-2H]^{2-}$	691,1475	691,1503	-4,1
	$Hex_6P_3S_2$	$[M-2H]^{2-}$	772,1729	772,1766	-4,8
	$Hex_6P_4S_2$ $^{\$}$	$[M-2H]^{2-}$	838,1935	838,1978	-5,1
Tri-sulfated oligomers	$Hex_3P_2S_3$ $^{\$}$	$[M-2H]^{2-}$	503,0543	503,0547	-0,8
	$Hex_4P_2S_3$	$[M-2H]^{2-}$	584,0795	584,0811	-2,7
	$Hex_5P_2S_3$ $^{\$}$	$[M-2H]^{2-}$	665,1053	665,1075	-3,3
	$Hex_4P_3S_3$	$[M-2H]^{2-}$	650,0981	650,1023	-6,5
	$Hex_5P_3S_3$	$[M-2H]^{2-}$	731,1249	731,1287	-5,2
		$[M+DBA-2H]^{2-}$	795,7010	795,7046	-4,5

	$Hex_6P_3S_3$	$[M-2H]^{2-}$	812,1518	812,1551	-4,1
		$[M+DBA-2H]^{2-}$	876,7303	876,7310	-0,8
	$Hex_7P_3S_3$ $^{\delta}$	$[M+DBA-2H]^{2-}$	957,7494	957,7574	-8,4
	$Hex_6P_4S_3$ $^{\delta}$	$[M+DBA-2H]^{2-}$	942,7545	942,7521	-2,5
	$Hex_7P_4S_3$ $^{\delta}$	$[M+DBA-2H]^{2-}$	1023,7742	1023,7785	-4,2
	$Hex_7P_5S_3$ $^{\delta}$	$[M+DBA-2H]^{2-}$	1089,7941	1089,7996	-5,0
Tetra-sulfated oligomers	$Hex_4P_2S_4$ $^{\delta}$	$[M+DBA-2H]^{2-}$	688,6337	688,6354	-2,5
	$Hex_5P_2S_4$ $^{\delta}$	$[M+DBA-2H]^{2-}$	769,6561	769,6618	-7,6
	$Hex_4P_3S_4$	$[M+DBA-2H]^{2-}$	754,6548	754,6565	-2,3
	$Hex_5P_3S_4$	$[M+DBA-2H]^{2-}$	835,6804	835,6830	-3,1
		$[M+2DBA-2H]^{2-}$	900,2555	900,2588	-3,7
	$Hex_6P_3S_4$	$[M+2DBA-2H]^{2-}$	981,2802	981,2852	-5,1
	$Hex_7P_3S_4$	$[M+2DBA-2H]^{2-}$	1062,3061	1062,3116	-5,2
	$Hex_6P_4S_4$ $^{\delta}$	$[M+2DBA-2H]^{2-}$	1047,2975	1047,3064	-8,5
	$Hex_7P_4S_4$ $^{\delta}$	$[M+2DBA-2H]^{2-}$	1128,3259	1128,3328	-6,1
	$Hex_8P_4S_4$ $^{\delta}$	$[M+2DBA-2H]^{2-}$	1209,3525	1209,3592	-5,5
	$Hex_9P_4S_4$ $^{\delta}$	$[M+2DBA-2H]^{2-}$	1290,3777	1290,3856	-6,1
	$Hex_7P_5S_4$ $^{\delta}$	$[M+2DBA-2H]^{2-}$	1194,3382	1194,3539	-13,1
	$Hex_8P_5S_4$ $^{\delta}$	$[M+2DBA-2H]^{2-}$	1275,3743	1275,3803	-4,7
	$Hex_9P_5S_4$ $^{\delta}$	$[M+2DBA-2H]^{2-}$	1356,4063	1356,4067	-0,3
Penta-sulfated oligomers	$Hex_4P_3S_5$	$[M+2DBA-2H]^{2-}$	859,2096	859,2108	-1,4
	$Hex_5P_3S_5$	$[M+2DBA-2H]^{2-}$	940,2331	940,2372	-4,4
		$[M+3DBA-2H]^{2-}$	1004,8057	1004,8131	-7,4
	$Hex_6P_3S_5$	$[M+2DBA-2H]^{2-}$	1021,2579	1021,2637	-5,7
		$[M-2H+3DBA]^{2-}$	1085,8336	1085,8395	-5,4
	$Hex_7P_3S_5$ $^{\delta}$	$[M-2H+3DBA]^{2-}$	1166,8599	1166,8659	-5,1
	$Hex_6P_4S_5$ $^{\delta}$	$[M+3DBA-2H]^{2-}$	1151,8572	1151,8607	-3,0
	$Hex_7P_4S_5$ $^{\delta}$	$[M+3DBA-2H]^{2-}$	1232,8802	1232,8871	-5,6
	$Hex_8P_4S_5$ $^{\delta}$	$[M+3DBA-2H]^{2-}$	1313,9039	1313,9135	-7,3
	$Hex_9P_4S_5$ $^{\delta}$	$[M+3DBA-2H]^{2-}$	1394,9255	1394,9399	-10,3
	$Hex_7P_5S_5$ $^{\delta}$	$[M+3DBA-2H]^{2-}$	1298,9013	1298,9082	-5,3
	$Hex_8P_5S_5$ $^{\delta}$	$[M+3DBA-2H]^{2-}$	1379,9202	1379,9346	-10,5
	$Hex_9P_5S_5$ $^{\delta}$	$[M+3DBA-2H]^{2-}$	1460,9437	1460,9610	-11,8

Even if the ESI-MS cannot be considered quantitative because the ionization of oligomers of different length and DS may vary, it is evident that the most abundant oligomers have the same backbone ($Hex_6P_3S_x$ and $Hex_5P_3S_x$) as for the digested neutral TSP, suggesting that sulfation did not significantly affect the enzymatic cleavage of the polysaccharide chain. Assuming that the enzymes would not recognize the sulfated glucose backbone, we suppose that sulfation occurred prevalently at the level of external galactose residues. These results are in agreement with the 2D NMR results (discussed below). The presence of oligomers of the same length but with the number of sulfates higher than the theoretical number of primary hydroxy-groups (CH_2OH of non-substituted glucose and galactose) suggests that sulfation may also occur on secondary alcohol of the residues. Additionally, the presence of longer oligomers (Figure 2-16) indicates that sulfation also happened on the backbone of the structure, on the glucose, in the proximity to the enzyme's cleavage site, thus inhibiting the enzymatic cleavage. The presence of trace oligomers such as $Hex_5P_4S_4$ and $Hex_8P_6S_4$ (Table 2-5) suggests that regions poorly substituted with galactoses are present within the TSP chains.

2.3.3. NMR of enzymatically hydrolyzed S-TSP

To confirm the LC-MS results, NMR analysis was also performed. In the HSQC spectra of the hydrolyzed sulfated sample with both enzymes, new signals appeared compared to the spectrum of TSP hydrolyzed with cellulase (Figure 2-17). The presence of CH_2 signals at about 69 ppm for ^{13}C indicated that sulfation mainly occurred on the primary alcohols of glucose and galactose residues, as previously suggested by the NMR and LC-MS results. The signals at 4.22/70.0 and 4.31/69.4 ppm were attributed respectively to the presence of the sulfated group on the position C6 of the galactose and glucose, in accordance with literature (Gardini et al., 2021; Nizzolo et al., 2024). Indeed, the substitution is preferred in the galactose side chain of the polysaccharide due to steric availability of these groups (Raj & Lee, 2024). Moreover, the substitution on galactose led to a shift of the hydrogen in position 1 to lower fields, as shown in the literature (da Silva et al., 2022; London, 2022). Other new signals were present, arising from sequence effects following sulfation or to the presence of sulfated groups on secondary alcohols, in accordance with the LC-MS results, but extensive fractionation steps will be necessary for complete attribution.

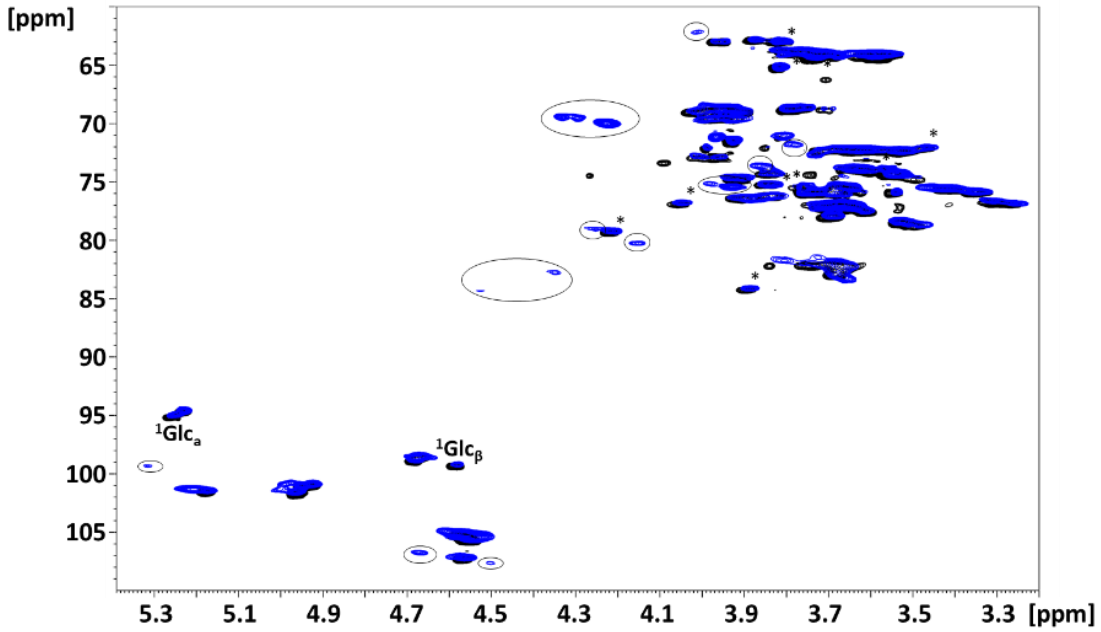

Figure 2-17. *^1H-^{13}C HSQC superimposition of TSP in black hydrolyzed with cellulase and S-TSP_1 hydrolyzed with xyloglucanase and cellulase in blue.*
Circled signals are related to sulfation. Galactose anomeric signals, α and β, are reported in the figure. The superscript corresponds to the carbon number of the observed monosaccharide, which is in bold, while the monosaccharide linked is in parentheses. * signals assigned to the cellulose enzyme; Gal—galactose.

2.4. Mucoadhesion

Mucoadhesion, the ability of the polymer to adhere to the mucus layer due to interactions with mucins (Madsen et al., 1998; de Oliveira Cardoso et al., 2020), is an important property for the application of TSP, especially in the ophthalmic field (Uccello-Barretta et al., 2013). For this reason, mucoadhesion was also studied for the sulfated products. A variety of analytical approaches can be used to evaluate the mucoadhesion properties of the polysaccharide. Here, rheology and the zeta potential were employed, based on Graça et al. (Graça et al., 2018).

2.4.1. Rheology

The viscosities of solutions of TSP and S-TSP_1 at 10 mg/mL with and without mucin (2.5 *w/w*) were measured, and their viscosity curves are reported in Figure 2-18.

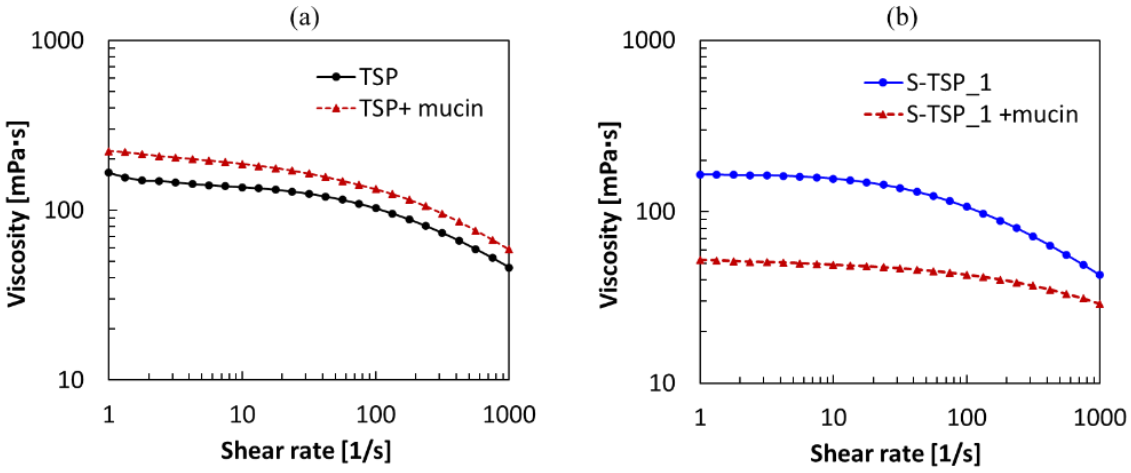

Figure 2-18. *Viscosity curves: (a) TSP (10 mg/mL) in black and TSP with mucin (2.5 w/w) in red; (b) S-TSP_1 (10 mg/mL) in blue and S-TSP_1 with mucin (2.5 w/w) in red.*

Changes in viscosity were observed in the presence of mucin for TSP and S-TSP (Figure 2-18), demonstrating that both TSP and S-TSP interact with the glycoprotein. TSP with mucin showed a higher viscosity than the solution without the glycoprotein, but, surprisingly, the sulfated product, S-TSP, exhibited decreased viscosity in the presence of mucin. These two different behaviors reflect the fundamental structural differences between TSP and S-TSP combined with the different interactions that these result in. Sulfation of a polymer may be expected to stiffen the polymer chains as a consequence of charge repulsion, leading to decreased conformational flexibility, but the appended charged groups also carry increased volumes of associated water molecules, effectively increasing their volume. These effects cannot readily be deconvoluted, and the manner in which these charged groups influences subsequent interactions with mucin is also difficult to predict. For TSP, viscosity increased after cooperative inter/intrapolymer interactions between mucin and the polysaccharide, whereas in the case of S-TSP the interaction with the glycoprotein probably led to a decrease of the hydrodynamic volume, perhaps through tighter association, driven by charge interactions, including cation-mediated interactions, and so to decreased viscosity (Menchicchi et al., 2015).

2.4.2. Zeta potential

The adhesion of the polysaccharide to mucin lead to changes in the surface properties such as the Zp. Table 2-6 shows the Zp of solutions of TSP and S-TSP with and without mucin.

Table 2-6. Zeta potential of solution of mucin 0.5 w/w, TSP and S-TSP_1 at 2 mg/mL without and with mucin.

Sample	Zeta potential (mV)
Mucin	-2.59±0.13
TSP	-0.70±0.16
TSP + mucin	-2.09±0.15
S-TSP_1	-43.0±1.02
S-TSP_1 + mucin	-10.1±0.75

The solution of TSP with mucin showed a similar Zp to the solution of the glycoprotein, showing that the interaction with mucin is not based on electrostatic forces, since TSP is a neutral polysaccharide (Uccello-Barretta et al., 2013). Instead, the presence of mucin led to a significant change of Zp for S-TSP, which demonstrates a probable electrostatic interaction between the protein and the sulfated product. Indeed, S-TSP interacted with the positively charged domain of the mucin, leading to charge compensation and variation in the Zp, as reported in the literature for negatively charged polysaccharides (Yermak et al., 2020). We conclude that the S-TSP samples showed an ability to interact with mucin.

2.5. Ocular Irritation test

As previously reported, TSP is used in the formulation of eye drops. For this reason, an ocular irritation test was performed on the sulfated products to evaluate whether the chemical modification induced eye irritation. A cellular model of transformed human corneal keratinocytes which is structurally, morphologically, and functionally similar to the human cornea was used for the assay. The cells were incubated with PBS, as negative control, and with eye drops formulation based on TSP (0.2%), S-TSP_1 and S-TSP_2 at different concentrations, (0.4%, 0.2% and 0.1%). The cell viability was assessed using an MTT assay, to determine the effects of the samples on the corneal tissue. Specifically, if viability is lower than 50% the products considered capable to induce serious eye damage, (Category 1), or eye irritation, (Category 2); if viability is higher than 50%, the samples are considered non-irritant (No Category) (Alépée et al., 2016). The viabilities of the samples are reported in Figure 2-19.

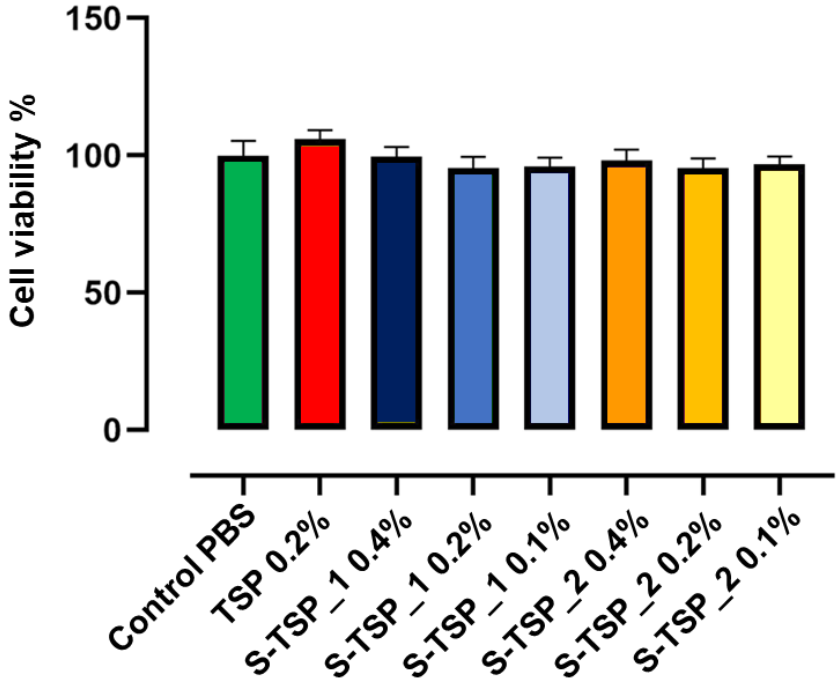

Figure 2-19. *Effect of PBS (negative control), TSP, S-TSP_1 and S-TSP_2 compounds on cell viability after 24-hour treatment.*
Cell viability was assessed and expressed as a percentage relative to the vehicle-treated control. Data are presented as mean ± SEM (n = 6). Statistical analysis was performed using One way ANOVA followed by post-test Bonferroni.

All the modified samples, at the three different concentrations, showed a cell viability of 100% similar to the negative control and the TSP, as represented shown in Figure 2-19. Therefore, the chemical sulfation of TSP can be considered safe, as it did not cause any eye damage or irritation. Moreover, the different degrees of sulfation, 2 for the S-TSP_1 and 3 for S-TSP_2, did not affect tissue viability.

2.6. Conclusion

In this study, synthesis and characterization of sulfated TSP samples were achieved. The sulfated reaction was carried out successfully in organic solvent (in aqueous media it was unsuccessful reproducing the synthesis of Nguyen et al.) at room temperature without depolymerization, providing varied extents of sulfation with different concentrations of reagent. The concentration of TSP and the TSP/sulfation reagent ratio are critical and can be used to control the sulfation reaction. The success of the sulfation reaction was established using three different techniques: conductimetric titration, FT-IR spectroscopy, and analysis of the zeta potential. The first method allowed the calculation of the number of sulfated groups per repeating unit of the TSP and the increase in DS with increasing concentration of reagent. Two new bands in the FT-IR spectra demonstrated the formation of new bonds consistent with sulfated groups, and the negative Zp confirmed the addition of negatively charged groups, whose presence also increased the solubility of the product due to electrostatic repulsions of the charges (Bertini et al., 2017). Moreover, the addition of sulfates bestowed new biological activities on the products, as reported above. The physical properties of the sulfated samples were also studied to verify the maintenance of the properties of TSP, including high molecular weight and pseudoplastic behavior. S-TSPs showed higher molecular weights than TSP, consistent with the DS obtained. The mild conditions of the reaction guarantee the maintenance of polymer chain length and the structure of TSP. The viscosity of S-TSP at low shear is very similar to TSP (Figure 2-4) but is maintained better at higher shear rate, indicating stronger intermolecular interactions. The presence of sulfated groups led to lower viscosity: in general, the sulfation of a polysaccharide tends to reduce the viscosity of the solution, mainly due to the electrostatic repulsion between the polymer chains, which prevents aggregation and favors a more compact conformation. Moreover, S-TSP tends to be more soluble in water than its unsulfated version: increased solubility can reduce the interaction between chains, leading to a decrease in the viscosity of the solution. To study in detail the structure of sulfated products, an enzymatic hydrolysis step was necessary, which allows for the reduction of molecular weight without altering the chemical structure, thereby generating oligosaccharides that can also be characterized using LC-MS techniques (York et al., 1993). The presence of sulfate groups inhibits the action of enzymes specific to TSP, likely due to the steric hindrance of the anionic group, which prevents, or slows down,

cleavage of the β-1,4 glucose-glucose bonds. By studying the hydrolysis products of S-TSP using NMR, partial sulfation of the C6 positions of glucose and galactose was first demonstrated, as evidenced by the presence of signals in the HSQC spectrum corresponding to both the CH_2OH and CH_2OR groups. Indeed, the SO_3·Py reagent induces sulfation at primary hydroxyl group, at the C-6 or C-5 positions of hexose/pentose units, respectively (Jana et al., 2021). Additionally, it was shown that even the secondary alcohols of the monosaccharide subunits can react, since new HSQC correlation peaks appeared in the anomeric region, likely indicating a substitution at position 2 of the sugar. This finding is also supported by the HILIC/ESI QTOF-MS chromatogram of the hydrolyzed sulfated product. As expected, sulfation was not selective, and the preference for primary hydroxyl groups was confirmed. This resulted in the generation of various positional isomers that occur in a random but relatively homogeneous manner along the polymer. The complexity of the LC-MS profiles of the digested S-TSP may also be affected by the α/β-anomers. For precise determination of the sulfation position, size fractionation steps are required prior to NMR and/or LC-MS analyses. The interaction of biomaterials with mucin potentially leads, under physiological conditions, to mucoadhesion, the ability of a polysaccharide to adhere to mucosal surfaces, such as those in the mouth, nose, intestine or genitourinary tract; these phenomena are particularly relevant to fields including pharmacology, medicine and biomedical technologies (Szilágyi et al., 2020). An interesting result was obtained from the study of the interaction between S-TSP and mucin, a glycoprotein involved in the mucus adhesion process. This study highlighted how the presence of negatively charged groups with significant steric hindrance along the TSP chain led to an interaction with mucin, specifically involving these charges, as evidenced by a change in Zp. This interaction differs from the one between TSP and the glycoprotein, which does not involve charges, but is likely to arise from steric interactions. This distinct interaction produces opposing effects in terms of viscosity: in the case of TSP with mucin, there is an increase in viscosity compared to the native TSP, indicating the formation of a complex with lower structural density. Conversely, with S-TSP, the complex that forms is likely to have higher structural density. Indeed, high molecular weight negatively charged samples are more flexible and can link distant domain of mucin, reducing the hydrodynamic volume and, consequently, the viscosity (Yermak et al., 2022; Ferreira et al., 2023). The decrease of viscosity with S-TSP may be advantageous, for example, in formulations for treating eye diseases, where increasing the viscosity can cause irritation to the eye (Lynch et al., 2019).

S-TSP samples showed no irritation effects, making them suitable in the eye drops solution. Formulative tests will be performed to investigate if S-TSP could be used as a replacement of TSP in ophthalmic products.

2.7. Materials and methods

2.7.1. Materials

TSP was provided by FARMIGEA (Pisa, Italy). Sodium azide, trimethylsilyl-3-propionic acid, hydrochloric acid (≥37%), sulfur trioxide pyridine complex, N,N-dimethylformamide, cellulase from *Penicillium funiculosum* (6.7 units/mg), dibutylamine, amberlite® IR-120 H^+, sodium hydroxide, acetic acid glacial, ammonium acetate, 3-(4,5-Dimethylthiazol-2-yl)-2,5-diphenyltetrazolium bromide (MTT), Dulbecco′s Phosphate Buffered Saline (PBS), without calcium chloride and magnesium chloride were purchased from Sigma Aldrich (Milan, Italy); NaOH 0.1 M from Merck (Kenilworth, NJ, USA); dimethyl sulfoxide from Fluka Analytical (Milan, Italy); acetonitrile and methanol from Carlo Erba (Milan, Italy); and xyloglucanase (GH5) (*Paenibacillus* sp.) from Megazyme International (Wicklow, Ireland). Ethanol (96%) was purchased from Girelli Alcool (Milan, Italy), and deuterium oxide (99.9%) from Eurisotop (Saint-Aubin, France). SkinEthic™ HCE (Human Corneal Epithelium) tissue and SkinEthic Maintenance Medium were purchased from Episkin (Lyon, France) Deionized water (conductivity less than 0.1 µS) was prepared with an osmosis inverse system (Culligan, Milan, Italy). PolyCAL-Pullulan Std-102K and PolyCAL-DextranStd-T67K were purchased from Malvern Panalytical (Malvern, UK). When not specified, the reagents were ≥ 98% pure.

2.7.2. Methods

2.7.2.1. Sulfation reaction

1.0 g of dry TSP was suspended in dry dimethyl formamide (DMF, 100 mL or 200 mL), and the mixture was stirred overnight at room temperature. Then, different mole/residue ratios of polysaccharide/ SO_3·Py (1:1 and 1:2) were added: S-TSP_1 was obtained adding 2.74 g of the reagent in 100 mL of DMF, S-TSP_2 using 5.48 of sulfur trioxide-pyridine complex in 100 mL and S-TSP_3 using 5.48 g in 200 mL. The resulting finely dispersed suspension was stirred vigorously for 24 h at room temperature. After dilution with water (20 mL), a homogeneous mixture was obtained and then precipitated with alcohol (EtOH/H_2O 70% *v/v*) to remove DMF, pyridine and salt excess of sulfating agent and potential degradation production of the latter (Na_2SO_4). The S-TSP products were recovered by centrifugation. The solid obtained after centrifugation was dissolved in

water (~150 mL) and precipitated with ethanol 70% *v/v*. This process was repeated for a third time, and lastly the precipitate was solubilized in water and dialyzed in water (c.o. = 6–8 kDa). The pH was also controlled and adjusted to a neutral value.

2.7.2.2. 1D and 2D NMR Analysis

TSP's ^{1}H and ^{1}H-^{13}C HSQC spectra were obtained with a Bruker AVANCE 600 III apparatus (Bruker, Karlsruhe, Germany) at 313 K. About 8 mg of sample was dissolved in 0.6 mL of deuterium oxide (D_2O). The TSP sample was stirred overnight to ensure complete solubilization before transferring to a 5 mm NMR tube for analysis. 1H-NMRspectra were acquired with presaturation of residual HOD, using the Bruker zgcppr pulse program, with the following parameters: number of scans 16, relaxation delay 12 s D1, time domain 32 k points and spectral width of 18 ppm, with transmitter offset 4.7 ppm. ^{1}H-^{13}C HSQC experiments were performed using the Bruker hsqcetgpsisp2.2 pulse program, with GARP4 decoupling. The following acquisition parameters were used: 24 scans, 16 dummy scans, relaxation delay 2 s, time domain 2048 (F2) and 256 (F1), spectral width 8 ppm (F2) and 160 ppm (F1), transmitter offset 4.7 ppm (F2) and 80 ppm (F1), and number of t1 increments 320. The 1 JC–H tune value was set to 150 Hz. S-TSP's ^{1}H-^{13}C HSQC spectra were obtained with a Bruker AVANCE NEO 500 MHz spectrometer (Bruker, Karlsruhe, Germany) equipped with a 5 mm TCI cryoprobe at 303 K. About 8 mg of sample was dissolved in 0.6 mL of deuterium oxide (D_2O) with 0.002% trimethylsilyl-3-propionic acid. The S-TSP samples were stirred overnight to ensure complete solubilization before transferring to a 5 mm NMR tube for analysis. ^{1}H-NMR spectra were acquired with presaturation of residual HOD, using the Bruker zgcppr pulse program, with the following parameters: number of scans 32, relaxation delay 12 s D1, time domain 32 K points and spectral width of 11 ppm, with transmitter offset 4.7 ppm. ^{1}H-^{13}C HSQC scans were acquired using the Bruker hsqcedetgpsisp2.2 pulse program, with the following parameters: number of scans 48, dummy scans 16, relaxation delay 2 s, time domain 2048 (F2) and 256 (F1), spectral width 7.9 ppm (F2) and 80 ppm (F1) and transmitter offset 4.7 ppm (F2) and 80 ppm (F1). The hydrolyzed with cellulase TSP sample's ^{1}H-^{13}C HSQC spectrum was obtained with a Bruker AVANCE IIIHD spectrometer operating at a proton frequency of 500 MHz (Bruker), equipped with a 5 mm BBO probe, at 303 K. About 20 mg of sample was dissolved in 0.6 mL of deuterium oxide (D_2O) with 0.002% trimethylsilyl-3-propionic acid and transferred to a 5 mm NMR

tube for analysis. ^{1}H-^{13}C HSQC scans were acquired using the Bruker hsqcedetgpsisp2.2 pulse program, with the following parameters: number of scans 20, dummy scans 16, relaxation delay 2 s, time domain 2048 (F2) and 320 (F1), spectral width 7.9 ppm (F2) and 120 ppm (F1) and transmitter offset 4.7 ppm (F2) and 70 ppm (F1). The hydrolyzed with xyloglucanase TSP sample's ^{1}H-^{13}C HSQC spectrum was obtained with a Bruker AVANCE III HD spectrometer operating at a proton frequency of 500MHz (Bruker), equipped with a 5 mm BBO probe, at 303K. About20mgofsamplewasdissolvedin0.6 mL of deuterium oxide (D_2O) with 0.002% trimethylsilyl-3-propionic acid and transferred to a 5 mm NMR tube for analysis. ^{1}H-^{13}C HSQC scans were acquired using the Bruker hsqcedetgpsisp2.2 pulse program, with the following parameters: number of scans 64, dummy scans 16, relaxation delay 1.5 s, time domain 1024 (F2) and 320 (F1), spectral width 9.9 ppm (F2) and 160 ppm (F1) and transmitter offset 4.7 ppm (F2) and 85 ppm (F1). The hydrolyzed S-TSP sample's ^{1}H-^{13}C HSQC spectrum was obtained with a Bruker AVANCE NEO500 MHz spectrometer (Bruker, Karlsruhe, Germany) equipped with a 5 mm TCI cryoprobe, at 303 K. About 20 mg of sample was dissolved in 0.6 mL of deuterium oxide (D_2O) with 0.002% trimethylsilyl-3-propionic acid and transferred to a 5 mm NMR tube for analysis. ^{1}H-^{13}C HSQC scans were acquired using the Bruker hsqcedetgpsisp2.2 pulse program, with the following parameters: number of scans 20, dummy scans 16, relaxation delay 2 s, time domain 1024 (F2) and 320 (F1), spectral width 7.9 ppm (F2) and 120 ppm (F1) and transmitter offset 4.7 ppm (F2) and 70 ppm (F1). All spectra were processed with BrukerTopspin software version 4.1.1.

2.7.2.3. FT-IR

The infrared spectra of TSP and S-TSP were recorded using an Alpha spectrometer (Bruker, Bremen, Germany) in the range of 4000 – 400 cm^{-1} at room temperature. An ATR (Attenuated Total Reflection) (Bruker, Bremen, Germany) platinum diamond was used for the measurement. A resolution of 4 cm^{-1} and a phase resolution of 32 were employed. The sample scan time and the background scan time were both 100 scans. The data were analyzed using OPUS software version 7.0 (Bruker, Bremen, Germany)

2.7.2.4. Zeta Potential

The zeta potential was measured using a Zetasizer Nano ZS apparatus (Malvern Panalytica, Malvern, UK) with a fixed scattering angle of 173° and a 633 nm helium–

neon laser. Data were analyzed using Zetasizer software version 7.11 (Malvern Panalytical, UK). TSP and S-TSP were diluted in deionized water to the desired concentration (2.00 mg/L). The measurement was performed at 25°C, five measurements, 10 run, 60 s time delay and general purpose method for the acquisition using disposable folded capillary cells (DTS1070, Malvern Panalytical, UK).

2.7.2.5. Determining Degree of Sulfation using Conductimetric Titration

The sulfation degree of S-TSP was determined by conductimetric titration adapting the method proposed by Alekseeva et al., 2020 (Alekseeva et al., 2020). The analyses were performed with an automatic "Titrando" 888 ("Metrohn", Herisau, Switzerland) titrator coupled with a Metrohm Conductimeter 712 with a conductivity cell characterized by a constant of 0.76 cm^{-1}. An aqueous solution (10 mL) of each sample (120 mg), previously exchanged on an activated Amberlite® IR-120 (H^+) (Sigma Aldrich, Milan, Italy) column (20 mL), was titrated by adding point by point 150 µL of 0.1 M NaOH solution every 200 s to a maximum volume of 6 mL. The number of sulfated groups on the repetitive unit was calculated using the following equation:

$$\text{DS (mole)} = \frac{\text{(mmole NaOH added)}}{\dfrac{\text{mg S TSP-}\left(\text{mmole NaOH added}\times 80\,\frac{\text{g}}{\text{mole}}\right)}{1207\,\frac{\text{g}}{\text{mole}}}} \qquad (9)$$

where "1207 g/mole" is the weight of an average repeating unit of TSP and "80 g/mole" is the weight difference between the group–SO_3H and the group–OH.

2.7.2.6. Molecular Weight Distribution by Size Exclusion Chromatography with Triple Detector Array (HP-SEC-TDA)

Chromatographic acquisitions were performed on a Viscotek system model TDA302 (Malvern Panalytical, UK) equipped with a triple detector array exploiting simultaneous action of a refraction index detector (RI), Right and Low Angle Light Scattering (RALS and LALS) and a Viscometer (DP). Measurements were performed at 40°C using 2× TSKGMPWXL columns, 13µm, 7 mm ID × 30 cm L, in series (Tosoh Bioscience, Tokyo, Japan)). AcONa 0.3 M + NaN_3 0.05% pH~8, prefiltered (0.22 µm mixed cellulose ester filter) was used as mobile phase at a flow rate of 0.6 mL/min. Chromatographic profiles were elaborated using OmniSEC software version 4.6.2. RI increments, referred to as

dn/dc, were determined to enable conversion of RI values into concentrations of TSP and products-TSP. dn/dc values equal to 0.139 and 0.125 were calculated for TSP and S-TSP, respectively. The detectors were calibrated with Pullulan standard, with certified molecular weight, polydispersion index and intrinsic viscosity (PolyCAL-PullulanStd-102K Malvern Panalytical, UK). Samples were analyzed at 1 mg/mL in AcONa 0.3 M + NaN_3 0.05% pH~8.

2.7.2.7. Rheology

The rheological properties were studied using a Modular Compact Rheometer MCR 92 (Anton Paar GmbH, Graz, Austria), with measure system DG26.7 (double gap geometry with a cylinder spindle) at a temperature of 20°C. Viscosity measurements were performed in rotation mode, investigated in the range of 1–1000 s^{-1}, with a logarithmic ramp, and ten points per decade were acquired. Samples were solubilized in deionized water to a concentration of 10 mg/mL; about 60 mg was solubilized in 6 mL of deionized water.

2.7.2.8. Interaction with mucin

The interaction with mucin was evaluated comparing the viscosity of TSP and S-TSP without and with mucin. A solution of mucin 5% (*w/w*) was prepared by solubilizing 1 g of mucin in 20 mL of deionized water. TSP and S-TSP solutions were prepared at 10 mg/mL in deionized water, and the viscosity was measured. For experiments with mucin, 60 mg of TSP or S-TSP were solubilized in 3 mL of deionized water. After complete solubilization, 3 mL of mucin solution was added to obtain a final concentration of 10 mg/mL for the polysaccharide and 2.5% of mucin (*w/w*). Viscosity measurements were performed in rotation mode and investigated in the range of 1–1000 s^{-1}, with a logarithmic ramp, and ten points per decade were acquired. The interaction was also studied measuring Zp. In total, 20 mg of TSP or S-TSP was solubilized in 5 mL of deionized water, and 200 mg of mucin was solubilized in 20 mL of deionized water (1% *w/w*). Then, 1 mL of the solution of TSP or S-TSP was added to 1 mL of mucin 1% (*w/w*) to a final concentration of 2 mg/mL of TSP or S-TSP and 0.5% (*w/w*) of mucin. The measurement was performed at 25°C, five measurements, 10 runs, 60 s time delay and general-purpose method for the acquisition using disposable folded capillary cells (DTS1070, Malvern Panalytical, UK).

2.7.2.9. Enzymatic depolymerization

Enzymatic depolymerizations were carried out using cellulase from *Penicillium funiculosum* and xyloglucanase (GH5) from *Paenibacillus* sp, which is stored in buffer ammonium sulfate 3.2 M. In total, 100 mg of TSP as solubilized in 18 mL of deionized water at 37°C overnight, and 20 mg of cellulase was dissolved in 2 mL of water with low agitation overnight. After complete solubilization, 2 mL of the cellulase solution was added to the TSP solution. A concentration ratio of TSP to enzyme of 5:1 w/w was used for hydrolysis. Then, 24 h after addition of the enzyme, the solution was heated at 100°C for 10 min to denature the enzyme, filtered to remove the precipitated enzyme (LLG-Syringe filter, Meckenheim Germany, CA pore size 0.20 µm, Ø 13 mm) and lyophilized. Depolymerization of TSP with xyloglucanase was performed adapting the method used by Zhang and Ai (H. Zhang et al., 2020). TSP was solubilized at a concentration of 10 mg/mL in deionized water at 40°C, dissolving 40 mg of TSP in 4 mL of deionized water overnight. Then, 20 µL of xyloglucanase (*Paenibacillus* sp., 20 U) was added to the solution. After 24 h, the reaction mixture was heated at 100°C for 10 min to inactivate the enzyme and centrifuged at 8000 rpm for 15 min to remove insoluble materials. The supernatant was also filtered to remove the precipitated enzyme (LLG-Syringe filter, CA pore size 0.20 µm, Ø13 mm) and then lyophilized. For hydrolysis of S-TSP, 40 mg of S-TSP_1 was solubilized in 4 mL of deionized water at 40°C overnight. Then, 40 µL of xyloglucanase (*Paenibacillus* sp., 20 U) and 200 µL of cellulase 10 mg/mL were added to the solution. After 24 h, the reaction mixture was heated at 100°C for 10 min to inactivate the enzyme and centrifuged at 8000 rpm for 15 min to remove insoluble materials. The supernatant was also filtered to remove the precipitated enzyme (LLG-Syringe filter, CA pore size 0.20 µm, Ø 13 mm) and then lyophilized.

2.7.2.10. LC/MS Analyses of Enzymatically Digested TSP and S-TSP

LC/MS analyses of both neutral and sulfated oligomers generated enzymatically were performed on an Elute UHPLC system (Bruker) coupled with an Impact II ESI-Q-TOF mass spectrometer (Bruker). Separation of neutral TSP oligosaccharides generated by cellulase or xyloglucanase was performed by hydrophilic interaction chromatography on a XBridge BEH Amide column (100 × 2.1 mm, 2.5 µm, Waters, Milford, MA, USA) at 40°C. The eluents A (5 mM ammonium acetate in water) and B (acetonitrile) were delivered at a 0.2 mL/min flow rate. Separation was achieved by applying the following

gradient: the solvent composition was held at 20% A for the first 2 min, then increased to 80% A over 23 min, where it was held at 80% A for 5 min and then returned to 20% A over 1 min, where it was held for the last 10 min for equilibrating the chromatographic column before injection of the next sample. The samples were injected at 0.1 mg/mL in 50% acetonitrile. The injected volume was 5 µL. The sulfated S-TSP oligosaccharides generated by cellulase and xyloglucanase were analyzed in an ion pair reversed phase (IPRP) HPLC on a C18 Kinetex column (100 × 2.1 mm, 2.6 µm, Phenomenex, Torrance, CA, USA) using dibutylamine (DBA) acetate as the ion pair reagent. Eluent A (10 mM DBA, 10 mM acetic acid in water) and eluent B (10 mM DBA and 10mM acetic acid in methanol) were delivered at 0.15 mL/min. The separation of oligomers with different lengths and sulfation degrees was performed keeping the column at 35°C and using the following gradient: the solvent composition was held at 7% B for the first 5 min, then increased to 45% B over 35 min, and up to 90% B over another 10 min, where it was held at for 7 min; afterwards, it was returned to 7% B over 3 min, and the column was equilibrated for the last 30 min. Samples were analyzed at a concentration of 1 mg/mL, and the injection volume was 2 µL. The mass spectra were acquired in negative ion mode (capillary voltage 4 kV) in the m/z 140–2500 mass range. Nitrogen was used as a drying (7 L/min) and nebulizing (1.8 bar) gas, and the ion transfer capillary was kept at 200°C.

2.7.2.11. Cell culture

HCE tissues SkinEthic™ were transferred in a 6-well plate with 1 mL of maintenance medium. Cells were incubated at 37°C and 90% of humidity for one night.

2.7.2.12. Treatment protocol

Cells were transferred in a 24-well plate with 300 µL of fresh maintenance medium. The tissues are then treated with 30 µL of: negative control (Phosphate Buffering Saline, PBS), S-TSP_1 at 0.1%, 0.2% and 0.4%, S-TSP_2 at 0.1%, 0.2% and 0.4%, and TSP at 0.2%. Every treatment was made in double, and the tissues were incubated for 30' at 37°C and 90% of humidity. Then, the tissues were rinsed with PBS and transferred in a 24-well plate with 750 µL in apical side and 750 µL in the basal side of fresh maintenance medium. Then, the cells were incubated again for 30' at 37°C and 90% of humidity. The tissues were rinsed with PBS and tested with the cell viability assay.

2.7.2.13. Cell viability assay

Cell viability was assessed using the MTT assay. Cells were transferred in a plate with 300 µL of MTT solution (1 mg/mL in serum-free Dulbecco's Modified Eagle Medium (DMEM) for 3 hours at 37°C. Subsequently, the medium was removed, and the formazan crystals formed were dissolved by adding 600 µL of DMSO to each insert. The solution was transferred to a 96-well plate, and absorbance was measured at 570 nm using a microplate reader. Results were expressed as a percentage of viable cells compared to the untreated control.

CHAPTER 3 - SYNTHESIS AND CHARACTERIZATION OF CROSSLINKED TAMARIND SEED POLYSACCHARIDE

Tamarind seed polysaccharide (TSP) was crosslinked using 1,4-butanediol diglycidyl ether (BDDE) as crosslinked agent, to obtain a biopolymer capable of absorbing liquids, modifying enzymatic activities to improve the permanence in a biological system and with new rheological properties. BDDE is biodegradable crosslinker less toxic than other ether-bond crosslinking agents such as divinyl sulfone and, under alkaline conditions, its epoxides can react with the TSP hydroxyl groups to form derivatives of 1,4-dibutanediol di-(propan-2,3 diolyl) ether (BDPE). The functionalization of the TSP was in order to obtain products with new rheological properties and applications based on a different polysaccharide than other used in literature. Indeed, TSP show different interesting properties which make it a promising alternative to products based on HA. TSP is a bioproduct of the tamarind pulp industry and for this reason it is cheaper than HA which is derived from animals and it is now produced by fermentation with high cost and risk of contamination (Mansingh et al., 2021; Serra et al., 2023). Moreover, the two polysaccharides show similar range of molecular weight but with a different structure: TSP is a branched heteropolysaccharide, instead HA has a linear structure formed by two sugars (La Gatta et al., 2022). In addition, both the biopolymers present high biocompatibility and bioadhesivity, especially for TSP, which present a mucomimetic structure able to adhere to the mucus layer (Uccello-Barretta et al., 2013). TSP is also very stable at different rage of pH and temperature and also in the physiological system, instead HA has high degradability also caused by physiological enzyme like hyaluronidase (Salwowska et al., 2016; Nagar et al., 2022). Moreover, the pharmacological potential of TSP and its derivatives have gained increasing attention, particularly for protecting the intestinal barrier in inflammatory bowel diseases (IBD). Intestinal epithelial barrier dysfunction is a hallmark of IBD, contributing to enhanced permeability, microbial translocation, and sustained inflammation. Recent studies have demonstrated that polysaccharides such as TSP can exert protective effects by multiple mechanisms, including the formation of a mucoadhesive layer that reinforces mucosal integrity, the modulation of tight junction protein expression, and the attenuation of oxidative stress and pro-inflammatory cytokine release (Uccello-Barretta et al., 2013).

TSP has been shown to adhere to the mucus layer due to its mucomimetic branched galactoxyloglucan structure, thereby forming a physical barrier that limits luminal antigen penetration. Furthermore, its antioxidant and anti-inflammatory properties may mitigate epithelial damage and contribute to mucosal healing. The development of TSP-based hydrogels with tailored swelling, viscosity, and bioadhesivity could thus provide innovative therapeutic strategies for restoring barrier function and delivering bioactive compounds directly to inflamed sites in the gastrointestinal tract.

For this reason, in this part of the study TSP is functionalized with BDDE to obtain different hydrogels compared to the ones based on HA in literature. Different concentrations of the reagent were used to obtain both hydrogels and soluble modified samples. Characterizations of the chemical-physical properties of the products were conducted with different analytical approaches for hydrogels and lower viscosity samples, due to their different solubility and viscosity. Morphological, rheological, and spectroscopic studies were conducted for all the samples. Moreover, in gel samples the swelling capacity and elastic moduli were studied, and the molecular weight of the viscous sample was analysed. NMR analyses were also performed, after an enzymatic degradation with xyloglucanase, to study the chemical structure and calculate the degree of crosslinking. The viability and the potential role of the modified products as barrier-like agents in intestinal barrier dysfunction were assessed by *in vitro* tests, using Caco-2 cells. C-TSP samples showed a more compact structure compared to the TSP. In NMR spectra, the new signals attributed to the BDDE confirm the presence of the crosslinker in the samples. The gel-like samples showed a higher viscosity than TSP and a swelling capacity between 60-80 g/g, instead the viscous-like sample exhibited a similar viscosity and molecular weight to TSP. The BDDE content ranged from 2 to 17% and the degree of crosslinking from 1.8 to 2.2%. No cytotoxic effects of C-TSP products were detected, and all the synthesized samples were able to preserve intestinal integrity by reducing intestinal permeability, particularly those with higher degree of crosslinking.

3.1. Chemical crosslinking of TSP

C-TSP samples preparation was conducted utilizing BDDE as a reagent, which is already known for crosslinking HA to produce gels, as reported in literature (Fallacara et al., 2017). For the activation of the BDDE, to open the epoxide groups, a basic environment is necessary. Indeed, a sodium hydroxide solution 1M was used as solvent. In the literature, BDDE cross-linking of HA is often performed under milder alkaline conditions, typically using 0.25-0.3 M NaOH (Fidalgo et al., 2018), however, these methods generally used longer reaction times, from 4 to 24 hours, to achieve sufficient cross-linking (T. Zhang et al., 2023). In contrast, the cross-linking of TSP in this work was performed in 2 hours using stronger alkaline conditions, in order to accelerate epoxide activation and crosslinking formation while limiting prolonged exposure of TSP to a basic environment. To further enhance reaction kinetics and improve TSP solubility, the reaction was conducted at 50°C. This temperature is higher than those commonly reported for HA-based systems, 30–40°C, and was used to promote a higher degree of cross-linking and a shorter reaction time (Al-Sibani et al., 2016; T. Zhang et al., 2023).
In TSP, the deprotonated hydroxyl groups, formed due to the basic environment, react with the epoxide groups of BDDE to form stable covalent ether bonds between the polysaccharide and the cross-linkers, as is the case for HA hydrogel (Kenne et al., 2013). The ring opening BDDE epoxide groups produces derivatives of 1,4-butanediol di-(propan-2,3 diolyl) ether (BDPE), which can be linked at the both side with TSP formed a crosslinked structure, or react with the polysaccharide on one side resulting in “mono-linked” BDPE (La Gatta et al., 2022), as showed in the following Figure 3-1.

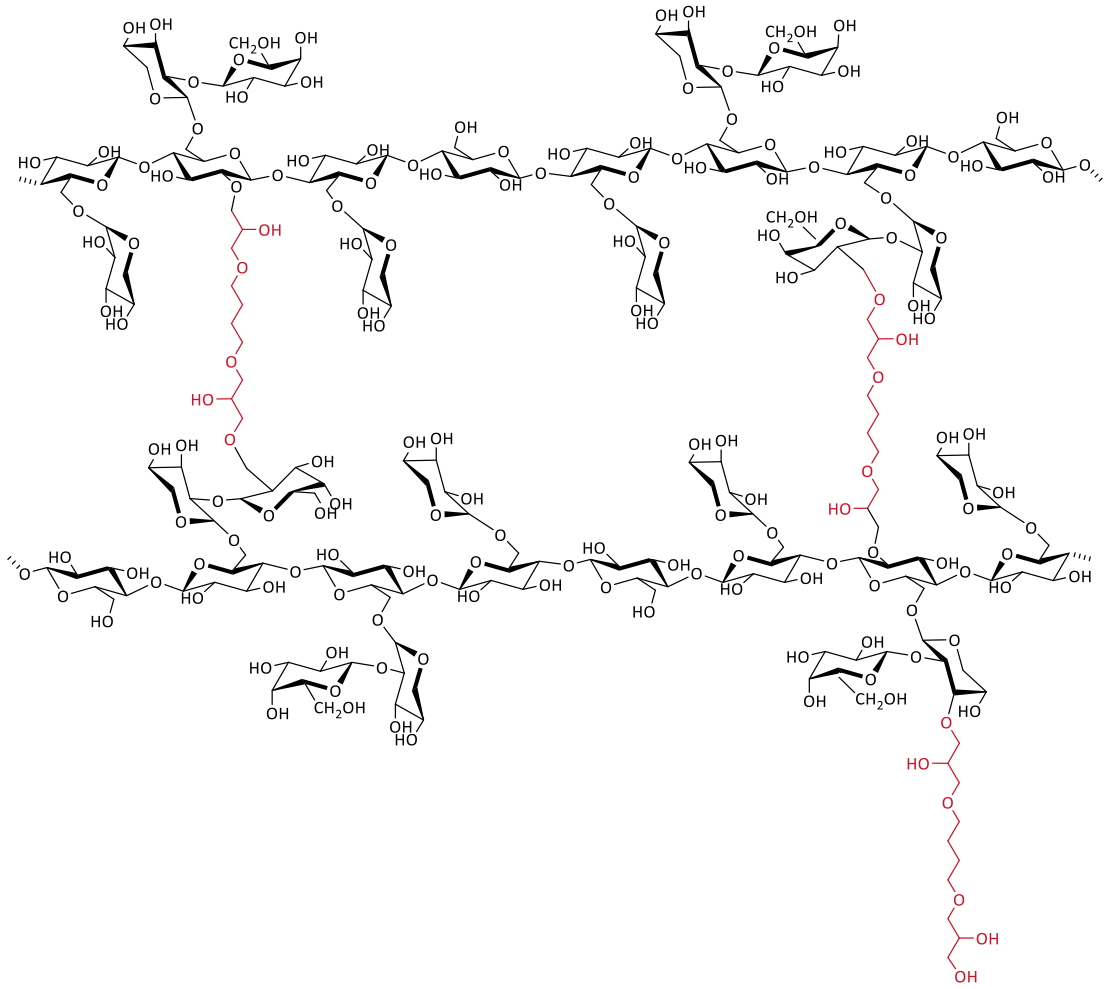

Figure 3-1. *Example of structure of TSP crosslinked with BDDE.*
The BDDE is represented in red in a crosslinked and mono-linked form.

Several syntheses were performed using various concentrations of BDDE, with a molar ratio TSP/BDDE in a range of 1:0.1-2, were used as reported in Table 3-1. The molar ratio was calculated using for the TSP the molecular weight of the repetitive unit, 1207 g/mol, and for the BDDE the molecular weight of 202 g/mol and density of 1.1 g/mL. Sodium hydroxide and the unreacted BDDE, in the open form with the hydroxyl groups or in the form with the epoxide groups, were eliminated by a dialysis step in deionized water as they can be toxic for their reactivity (De Boulle et al., 2013).

Table 3-1. *Molar ratio TSP/BDDE used for the syntheses of crosslinked samples.*

Samples	**Molar ratio (TSP/BDDE)**
C-TSP_A	1:0.1
C-TSP_B	1:0.8
C-TSP_C	1:2

3.2. Scanning Electron Microscopy (SEM)

The morphology of lyophilized samples was studied using a Scanning Electron Microscope and the images are reported in Figure 3-2.

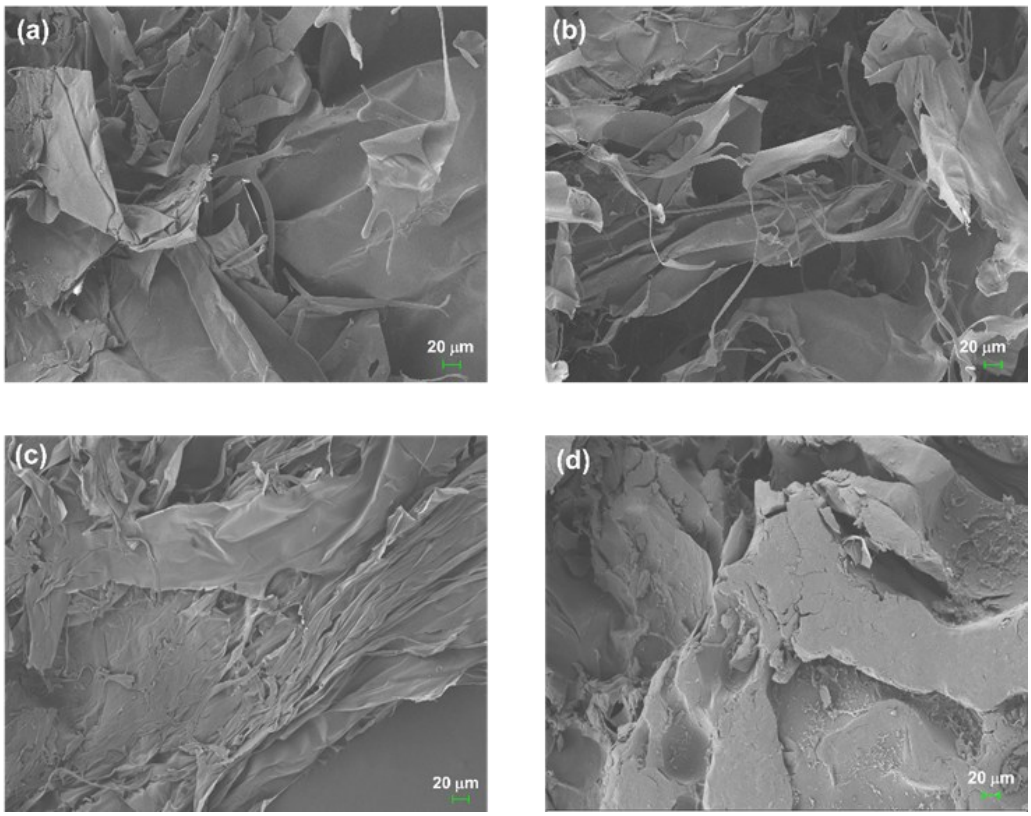

***Figure 3-2**. SEM images of freeze-dried samples: (a) TSP, (b) C-TSP_A, low degree of crosslinking, (c) C-TSP_B, medium degree of crosslinking, (d) and C-TSP_C, high degree of crosslinking.*

All the samples exhibited three-dimensional network structures. With increasing BDDE concentration, a more compact structure was observed, compatible with a higher degree of cross-linking degree. Sample C-TSP_C exhibited a denser structure compared to the other products and the TSP. C-TSP-A showed more fraying than the TSP probably due to the lower concentration of BDDE employed and to the basic treatment required during the synthesis which can lead to depolymerization of the sugar chain.

3.3. FTIR

FTIR spectra of TSP and C-TSP samples are reported in Figure 3-3.

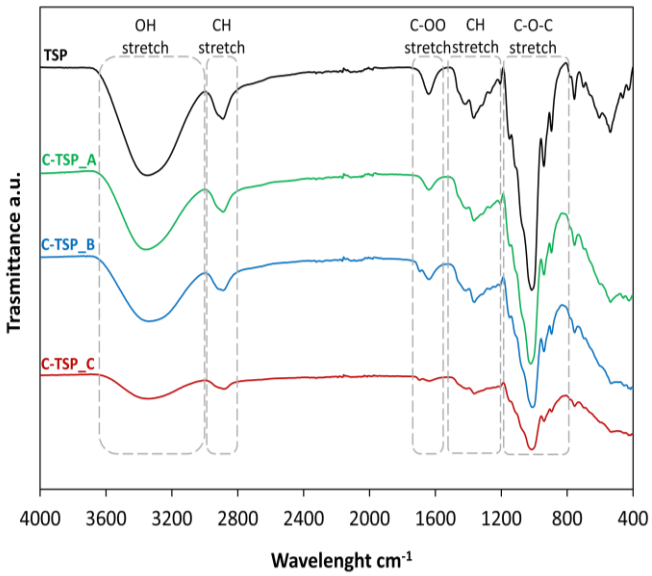

Figure 3-3. *FT-IR spectra of TSP in black, C-TSP_A in green, C-TSP_B in blue and C-TSP_C in red with bands partial assignation of the functional groups.*

The spectra of crosslinked samples showed no significant differences to TSP, suggesting that no major functional group alterations occurred during crosslinking. The other observed corresponded to the characteristic structure of TSP. Indeed, the broad absorption peak from about 3600 cm^{-1} to 3000 cm^{-1} was attributed to the stretching vibration of hydroxyl groups (O–H) induced by inter- or intramolecular interactions. The peak at 2900 cm^{-1} corresponded to C–H stretching and bending vibrations including CH, CH_2 and CH_3 (Y. Liu et al., 2024). Additionally, peaks from 1500 cm^{-1} to 1200 cm^{-1} were also related to C–H bands, while the peak from 1150 to 800 cm^{-1} was attributed to C–O–C stretches The band at 1635 cm^{-1} was due to the small traces of uronic acid in the TSP (L. Ren et al., 2022a). Only a small new peak around 1700 cm^{-1} was observed in the more crosslinked samples, C-TSP_B and C-TSP_C, which can be attributed to the ketone group of acetone, used to precipitate the products (Ngohang et al., 2015), as traces may have remained even after purification. Additionally, in the crosslinked samples, there was no increase in the intensity of the peak at around 900 cm^{-1}, attributed to the epoxide group (Osborne-Richards et al., 2025; Privar et al., 2024), suggesting that the epoxide groups of BDDE open during the reaction and the unreacted crosslinker was removed. The lower intensity of spectra for the crosslinked samples compared to TSP was likely due to the different physical aspects of the products, which showed grainy compared to the powdered form of TSP, as observed in SEM images.

3.4. *Rheological properties*

3.4.1. *Viscosity curves*

The rheological properties of TSP and C-TSPs samples were studied at 10 mg/mL and 37°C, the physiological temperature. The viscosity curves of the modified samples and TSP are shown in Figure 3-4.

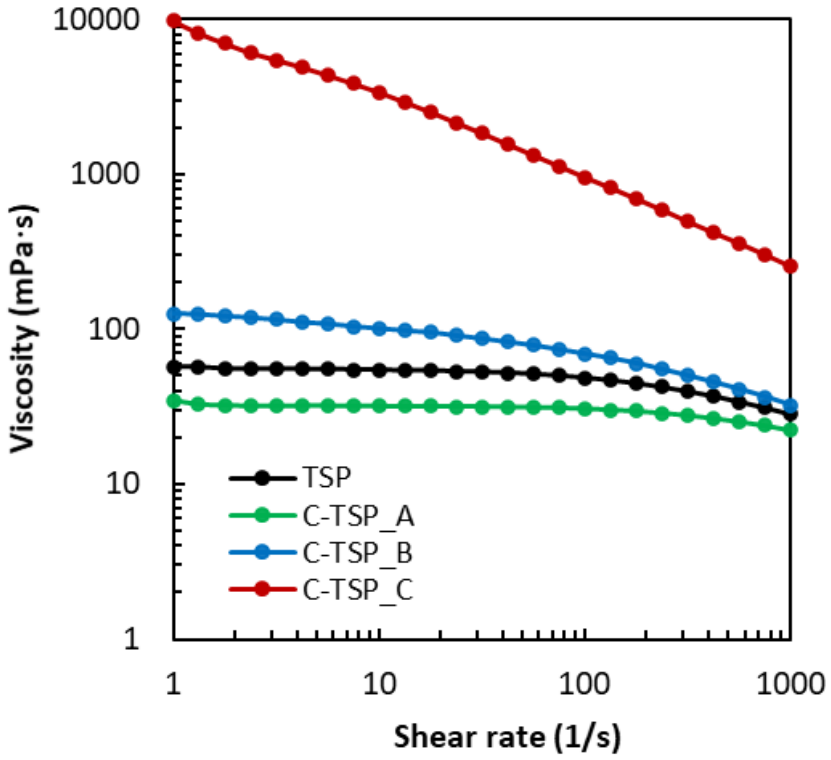

Figure 3-4. *The viscosity curves of TSP are in black, C-TSP_A in green, C-TSP_B in blue and C-TSP_C in red at 37°C and 10 mg/mL.*

All samples exhibited pseudoplastic behavior; with viscosity decreasing as the shear rate increased (Figure 3-4). As expected, the sample with the highest BDDE concentration, C-TSP_C, showed the greatest viscosities. C-TSP_B also displayed higher viscosity than TSP, whereas C-TSP_A exhibited the lowest viscosity due to the lowest concentration of BDDE and probably to depolymerization during the basic treatment. Depolymerization probably occurred also for C-TSP_B and C-TSP_C, but the higher concentration of the BDDE used increased the viscosity forming a crosslinked structure.

3.4.2. *Amplitude sweeps*

The storage modulus G', and loss modulus, G", were also determined for the TSP and the functionalized samples. Samples with G' lower than G" show a fluid structure while, when G' is greater than G'', the structure is solid. Through this analysis it is possible to identify the shear rate range in which the sample exhibits linear viscoelastic behaviour, so, where no material damage is observed (La Gatta et al., 2022). Figure 3-5 showed the elastic moduli obtained with the amplitude sweep analysis of TSP and crosslinked products at 37°C and 10 mg/mL.

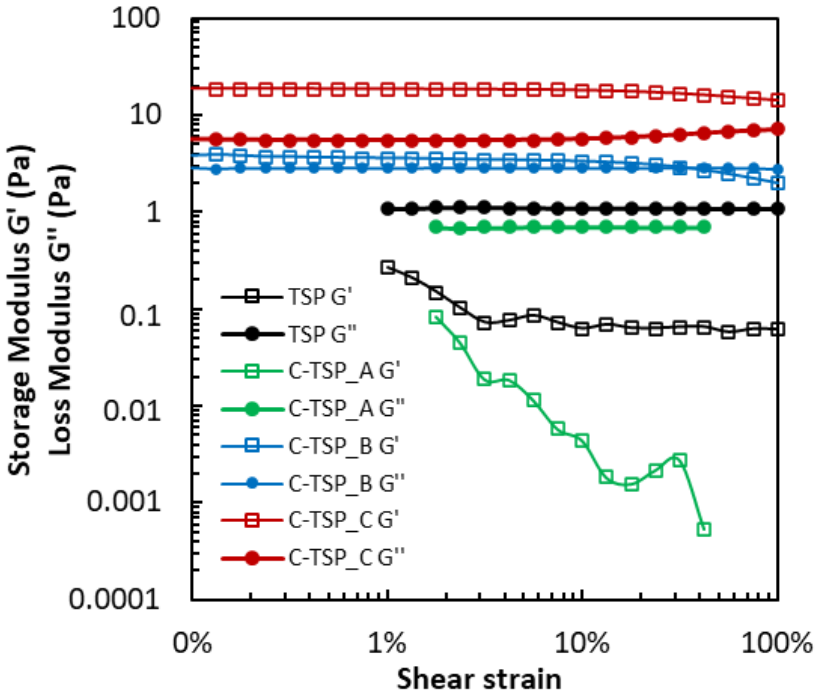

***Figure 3-5**. The elastic moduli G' (empty square sign) and G" (full round sign) of TSP in black, C-TSP_A in green, C-TSP_B in blue and C-TSP_C in red obtained after the amplitude sweep tests at 37°C and 10 mg/mL.*

TSP and the low crosslinked product, C-TSP_A, presented a viscous-like behaviour with G' lower than G". In contrast, C-TSP_C exhibited gel-like structure with G' higher than G". Specifically, C-TSP_C showed values of the storage modulus almost six times greater than that of C-TSP_B, demonstrating a gel-like structure resulting from the higher concentration of BDDE. Values of the elastic moduli for C-TSP_B were very similar and a flow point, where the values of G' and G" are equal, was also detected. Beyond this point, an inversion of the moduli occurs, indicating that the sample has been damaged due to a change in its physical nature (Øvrebø et al., 2024).

With the study of the elastic moduli, we determined the sample mechanical behaviour, viscous-like for the C-TSP_A and gel-like for C-TSP- B and C-TSP_C. For this reason, distinct analytical methods were used for the characterization of C-TSP_A, which is soluble in water (HP-SEC-TDA and solution NMR were used), and C-TSP_B and C-TSP_C, which are hydrogel (frequency sweep, swelling degree, and solid state NMR were employed); results are presented and discussed below.

3.5. Characterization of water-soluble liquid-like sample

As a viscous-like water soluble product, C-TSP_A was characterized by high performance size exclusion chromatography equipped with a triple detector array (HP-SEC-TDA) to determine the molecular weight distribution and NMR spectroscopy to investigate its chemical structure.

3.5.1. High Performance Size Exclusion Chromatography

HP-SEC-TDA with multi-detector system (Right and Low Angle Light Scattering, Refractive Index and Viscosimeter) was used to determine the molecular weight distribution, intrinsic viscosity and hydrodynamic radius of TSP and C-TSP_A, which were the only samples which could be solubilized in the mobile phase ($NaNO_3$ 0.1M / NaN_3 0.05%). In Table 3-2 HP-SEC-TDA results are reported.

***Table 3-2**. HP-SEC-TDA of TSP and C-TSP_1: Mw-weight average molecular weight, Mn-number average molecular weight, PDI-Polydispersity Index, η-intrinsic viscosity, Rh -hydrodynamic radius, a-Mark-Houwink parameters.*

Sample	Mw (kDa)	Mn (kDa)	PDI (Mw/Mn)	[η](dl/g)	Rh (nm)	*a*
TSP	720	380	1.9	6.0	39	0.70
C-TSP_A	580	300	1.9	5.1	34	0.67

TSP exhibited a molecular weight of 720 kDa, in accordance with the data in the literature (Chawananorasest et al., 2016; Ziliani et al., 2024). C-TSP_A showed a decreasing of the molecular weight to 580 kDa, suggesting that depolymerization occurred during the reaction, as a result of the basic environment and the elevated temperature (50°C). Moreover, the hydrodynamic radius and the intrinsic viscosity, as for the dynamic viscosity measured with the rheometer, also decreased compared to TSP, as a result of decreasing molecular weight.

3.5.2. NMR

3.5.2.1. NMR attributions of BDDE

Monodimensional (1D) and bidimensional (2D) NMR spectroscopy were used to verify the signals of the BDDE, in order to perform NMR study on the crosslinked samples. In the following Figure 3-6, the superimposition of ^{13}C and ^{1}H-^{13}C HSQC of the BDDE is reported.

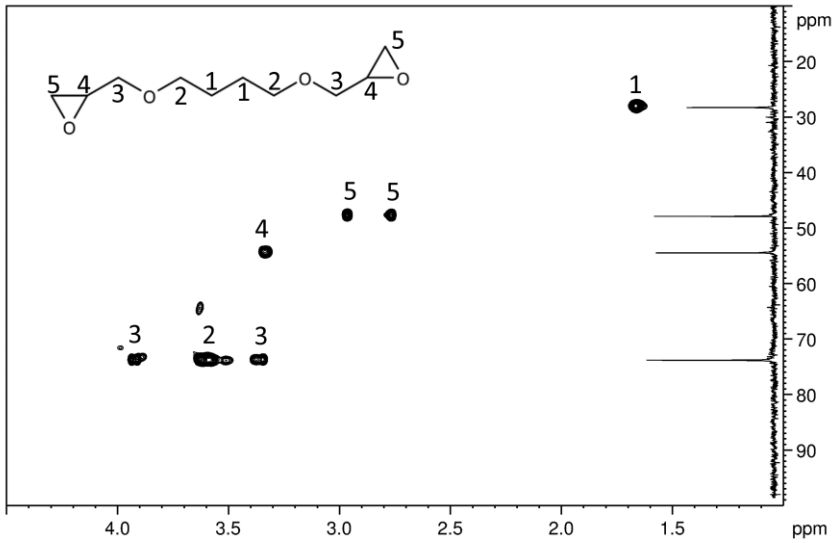

Figure 3-6. *^{13}C and ^{1}H-^{13}C HSQC superimposition of BDDE.*
The crosslinker structure is reported with assignations of the signals.

Each NMR assignment of BDDE corresponds to two equivalent positions, owing to the molecular symmetry, which can be observed from the crosslinker's structure in Figure 3-6. The cross-peak (signal 1 in Figure 3-6) at 1.65/28 ppm was attributed to the aliphatic CH_2CH_2 in the internal position of BDDE, in accordance with the data in literature (Wende et al., 2017). The adjacent CH_2 (signals 2 in Figure 3-6) and the CH_2 near the epoxide ring (signal 3 in Figure 3-6) corresponded respectively to the cross-peaks 3.60/73.9 ppm and 3.91-3.35/73.9 ppm. Finally, the cross-peaks at 3.32/54.4 ppm and 2.95-2.75/47.8 ppm were attributed to the epoxide ring (respectively signal 4 and 5 in Figure 3-6), as reported in literature (Øvrebø et al., 2024).

The BDDE structure was also studied in its open form (BDPE), adding a small volume of concentrated sodium deuteroxide NaOD to the BDDE. The superimposition of ^{13}C, and ^{1}H-^{13}C HSQC of the BDPE is reported in Figure 3-7.

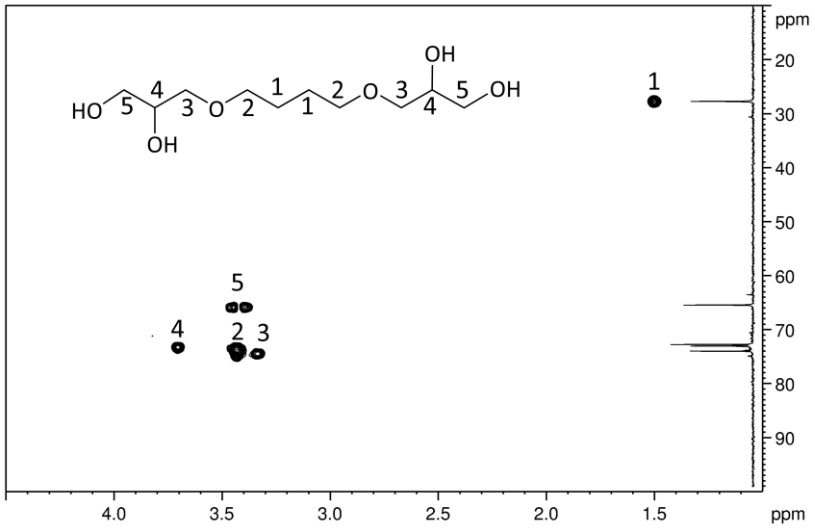

***Figure 3-7**. ^{13}C, and ^{1}H-^{13}C HSQC superimposition of BDPE.*
The open crosslinker structure is reported with assignations of the signals.

As can be observed in the spectrum, the aliphatic CH_2CH_2 (signal 1 in Figure 3-7) remained in the same position at 1.65/28 ppm. Also, the adjacent CH_2 (signal 2 in Figure 3-7) corresponded to the same cross-peak in the BDDE at 3.58/73.9 ppm. Instead, a shift in the signal 3 (Figure 3-7) is observed at 3.48/74.8, since it is near to the hydroxyl group in the open conformation. Moreover, the signal 4 (Figure 3-7), which is a CH, is attributed to the cross-peak at 3.85/73.6 ppm. Finally, signals related to the epoxide groups disappeared due to the opening of the ring, caused by the basic conditions. Indeed, the formation of the primary alcohol is verified by the presence of the cross-peak at 3.59-3.54/66.2 ppm, as reported in literature (Wende et al., 2017).

3.5.2.2. NMR attribution of C-TSP_A

After the attribution of the BDDE's signals, the chemical structures of TSP and C-TSP_A were characterized using NMR spectroscopy. The proton spectra are reported in Figure 3-8.

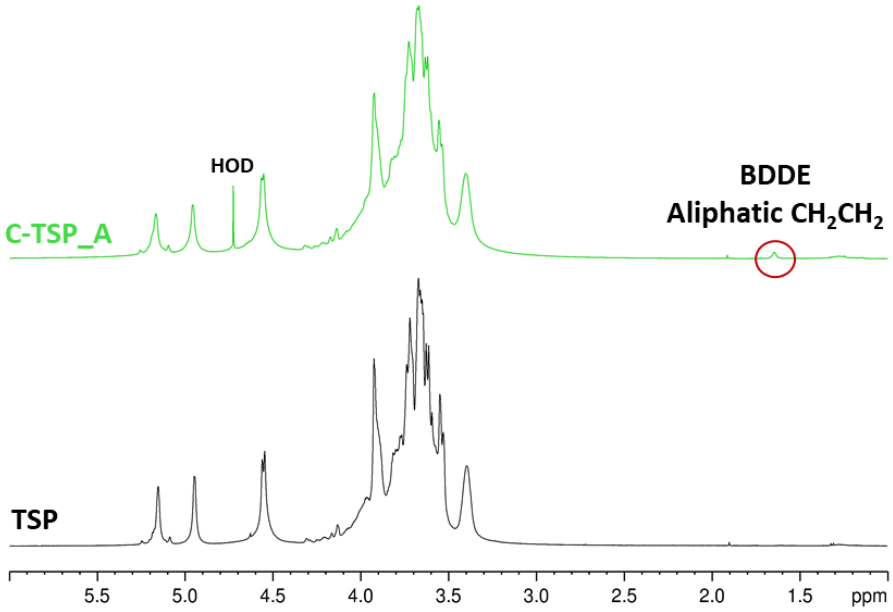

Figure 3-8. *NMR proton spectra of TSP, in black, and C-TSP_A in green.*
The aliphatic CH_2CH_2 signal of the BDDE is indicated in the C-TSP_A spectrum (upper) with a red circle.

In proton spectrum, Figure 3-8, no significant chemical shift changes were observed following functionalization except for the peaks at 1.65 ppm attributed to the aliphatic CH_2CH_2 protons in the internal position of BDDE, as previously reported (Figure 3-6 and 3-7). Moreover, in the C-TSP_A spectrum no signals ppm related to the epoxide groups of the BDDE (Figure 3-6) were detected as a result of the successful removal of the unreacted crosslinker and the opening of the epoxide groups due to the NaOH solution. In both samples, the high molecular weight and high viscosity result in proton signal broadening with a loss of resolution, indeed peaks from 4 to 3.5 ppm are not well defined. For this reason, only the well-separated peaks were attributed: in the anomeric region xylose linked to the galactose at 5.16 ppm and linked only with the glucose at 4.95 ppm, glucose and galactose at 4.55 ppm and the hydrogen in position 2 of glucose at 3.40 ppm. TSP and C-TSP_A were also characterized using the ^{1}H-^{13}C HSQC, reported in the following Figure 3-9.

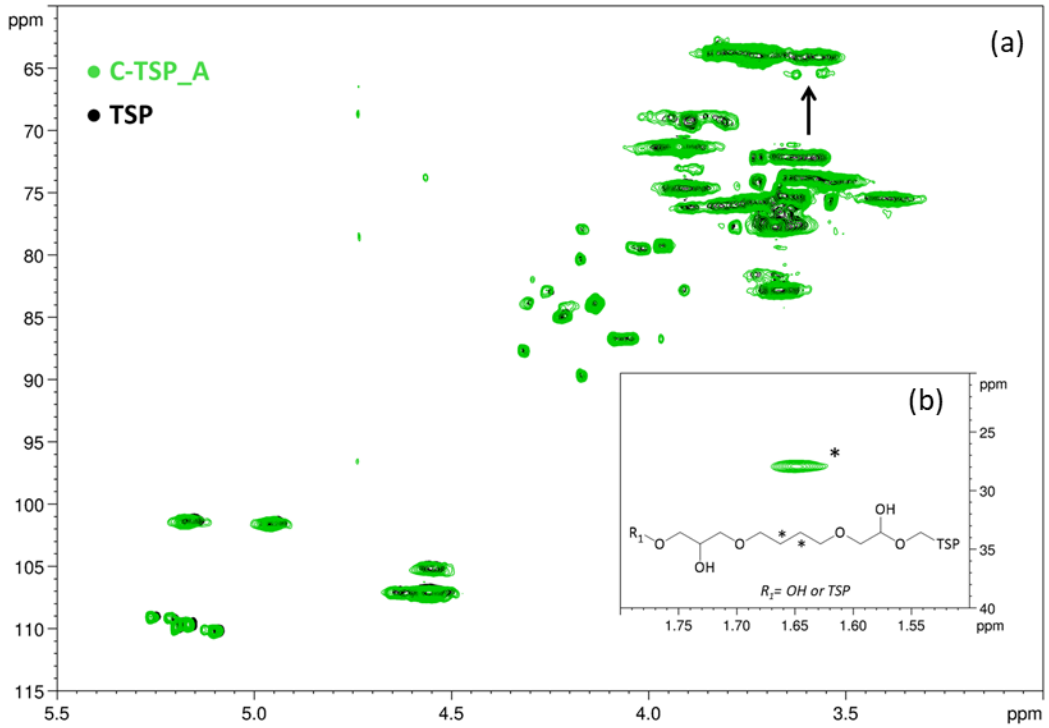

Figure 3-9. *^{1}H-^{13}C HSQC superimposition of TSP and C-TSP_A.*
The signals of the BDDE are signed with black arrow in (a). Inset (b), the zoomed region showing the aliphatic CH_2CH_2 protons of BDDE, indicated with *.

In HSQC of C-TSP_A of Figure 3-9, aliphatic CH_2CH_2 signals are observed arising from the presence of the BDDE. As in proton spectrum, Figure 3-8, the cross peak at 1.65/28 ppm attributed to the CH_2 protons in the internal position of BDDE was present, but also new signals were observed. The cross peaks at 3.63-3.56/65.5 were attributed to the hydroxyl groups formed after the opening of the BDDE epoxide rings during the reaction, as reported in Figure 3-9. The signal at 3.70/73.5 ppm was also related to the presence of the crosslinker, while the new cross peak at 3.84/71.8 ppm could be attributed to the formation of a link between the TSP and the BDDE.

As in proton spectra, the resolution is low due to the high viscosity and molecular weight of the samples, so, the exact position of the link could not be detected and a quantitative analysis could not be performed due to the different mobility of the residues, as previously demonstrated with high molecular weight hyaluronic acid (Nizzolo et al., 2024). For this reason, an enzymatic degradation was performed to reduce the molecular weight of the polysaccharide, while maintaining the functionalization, to enable a more effective NMR study (H. Zhang et al., 2020), as following reported in Paragraph 3.7.

3.6. *Characterization of hydrogel samples*

For samples showed a gel-like behaviour, C-TSP_B and C-TSP_C, product stability was studied by frequency sweep analysis, solution absorption capacity by swelling tests, and the chemical structure by solid state NMR.

3.6.1. *Frequency sweep*

Once the linear viscoelastic region (1% of shear strain) has been determined by amplitude test, it was possible to perform the frequency sweep test on the gel-like products, during which the samples are subjected to an oscillatory stress with varying angular frequency. In this way, the viscoelasticity of the material can be measured and information on the internal structure of the polymers and the long-term stability of the dispersions can be obtained, evaluating the behaviour of the sample over time. Indeed, with high frequencies, rapid movement on a short-term scale is simulated, while with low frequencies, slow movement on a long-term or resting scale is simulated (Ramli et al., 2022). In Figure 3-10 the elastic moduli obtained after the frequency sweep test of C-TSP_B and C-TSP_C are reported.

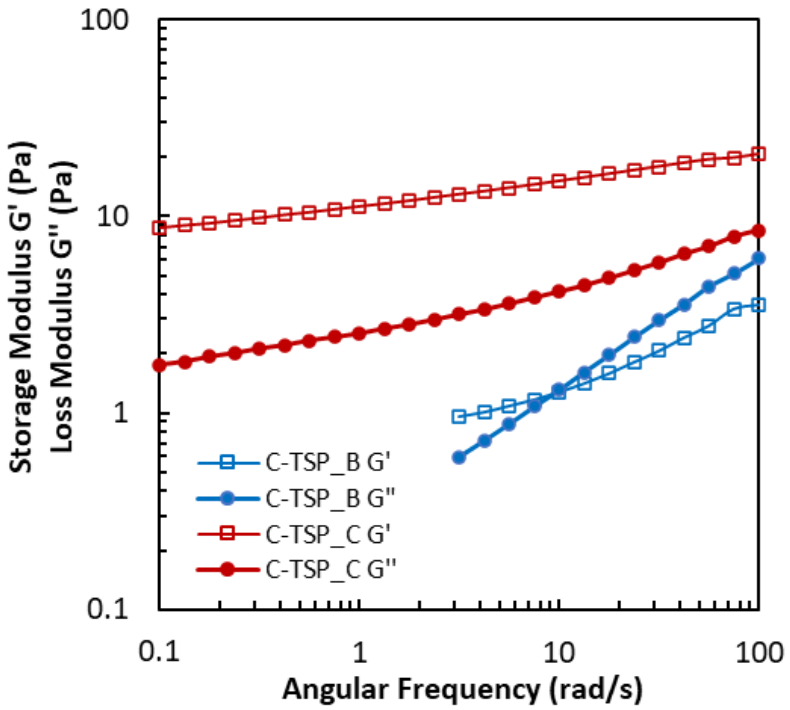

Figure 3-10. *The elastic moduli G' (empty square sign) and G" (full round sign) of C-TSP_B in blue and C-TSP_C in red obtained after the frequency sweep test.*

Frequency sweep test on the gel-like products within the linear viscoelastic region (1% of shear strain), see Figure 3-5, was determined at high frequencies, rapid movement on a short-term scale is simulated, while at low frequencies, slow movement on a long-term or resting scale is simulated (Ramli et al., 2022), thereby providing indirect information on the hydrogel structure and stability. In Figure 3-10 the elastic moduli obtained after the frequency sweep test of C-TSP_B and C-TSP_C are reported.

The results confirmed that C-TSP_C showed predominantly gel-like behaviour (G'>G") over the entire angular frequency range: this behaviour suggests that the material as a long-term shape stability (Stojkov et al., 2021). In contrast, C-TSP_B exhibited two regimes: at low angular frequencies ($\omega < 10$ rad/s), $G' > G''$, whereas at high angular frequencies ($\omega > 10$ rad/s), $G' < G''$. This samples can be defined as a viscoelastic solid material (Ramli et al., 2022).

3.6.2. Swelling capacity

Swelling capability refers to the ability of a material to absorb a solvent and expand in volume or mass without dissolving. This property is particularly important for the performance and functionality of cross-linked samples in various applications (S. Tang et al., 2021). The swelling ratio of C-TSP_B and C-TSP_C are reported in Figure 3-11.

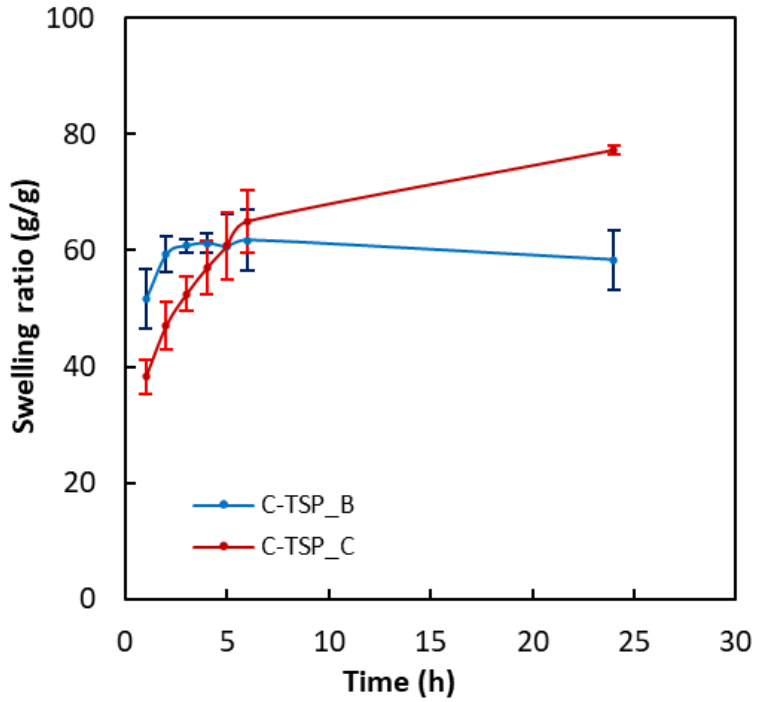

Figure 3-11. *Swelling capacity in water of C-TSP_B in blue and C-TSP_C in red with deviation standard signed with bars.*

The two samples showed different swelling behaviour: C-TSP_C presented a slower swelling kinetics, reaching the maximum swelling capacity of almost 80 g/g after 24 hours compared to C-TSP_B that achieved the maximum of 60 g/g after three hours. Moreover, the C-TSP_B showed a decreasing of the weight and a higher deviation standard due probably to its low gel-like structure, as seen from the results of the amplitude and frequency sweep, which led to a solubilization of part of the sample.

3.6.3. NMR Solid State

Solid-state NMR spectroscopy is a useful technique for determining the chemical structure of polysaccharides, and it is able to distinguish between the crystalline and amorphous components. This method has, however, yielded limited results due to broad NMR resonances and the absence of detailed spectral assignments. In fact, cross-polarization magic-angle spinning (CP-MAS) solid-state ^{13}C NMR spectra resemble those obtained in solution, though with lower resolution (Bai et al., 2010). Nevertheless, assigning resonances in the solid state based on solution-state spectra carries risks, because substantial shifts in chemical resonance can occur due to conformational changes or packing effects. This is particularly evident in the case of cellulose: its various solid forms display markedly different CP-MAS spectra, both from each other and from the ^{13}C NMR spectrum of cellulose in solution, largely due to differences in molecular conformation (Foston, 2014). NMR solid state was performed for gels (C-TSP_B and C-TSP_C) due to the high viscosity and highly crosslinked structure, which did not allow the solubilization of the products. ^{13}C cross polarization with magic angle spinning, CP-MAS's spectra of TSP and C-TSP_B and C-TSP_C is reported in Figure 3-12.

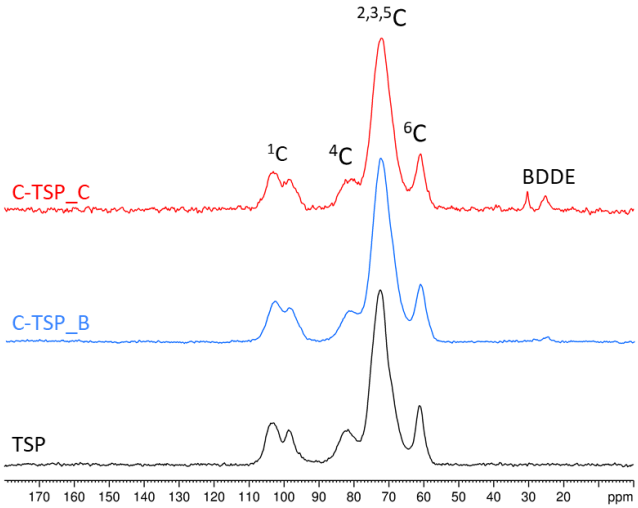

Figure 3-12. *^{13}C CP-MAS spectra of TSP in black, C-TSP_B in blue and C-TSP_C in red.*

As shown, the C-TSP samples presented a similar profile to that of TSP; so, after the reaction, the products maintain the structure of TSP. Moreover, in C-TSP_C, the BDDE peaks appeared, demonstrating the presence of the crosslinker in the product, but no further deduction concerning the position of the crosslinking could be made. The broad peaks indicate that the samples have an amorphous structure.

The spin-lattice relaxation time ^{1}H T1ρ values were also measured for these samples (Table 3-3). This parameter provides information about the populations of nuclei in phase, related to the structure of the samples: crystalline samples show high values of T1ρ (100 ms), instead amorphous samples lower values of T1ρ (10 ms) (Madsen et al., 1998).

Table 3-3*. ^{1}H T1ρ values of TSP and C-TSP_C.*

Peaks (ppm)	TSP	C-TSP_B	C-TSP_C
103 (^{1}C)	8.17	7.65	6.72
99 (^{1}C)	8.04	7.53	6.63
82 (^{4}C)	8.36	7.22	6.64
73 (^{2,3,5}C)	8.20	7.75	6.76
61 (^{6}C)	8.19	7.60	6.66
32 (BDDE)	-	-	4.36

T1ρ values less than 10 ms indicate an amorphous structure and the similar values for every peak denote homogeneity. BDDE derivatized sample have slightly inferior values, indicating lower values due probably to the functionalization. Even for these samples, a quantitative analysis could not be performed and also no information about the position of the crosslinker on the sugar chain were obtained. For this reason, an enzymatic hydrolysis was conducted on all crosslinked samples.

3.7. *Enzymatic hydrolysis*

3.7.1. *NMR*

Xyloglucanase, an enzyme able to hydrolyse the β-1,4 bond, to generate TSP repeating unit (Zhang, et al., 2020), as reported in previous Chapter 2 (Paragraph 2-3), was used. Enzymatic degradation was performed to reduce the molecular weight of the samples without affecting the chemical modification to perform quantitative NMR analysis. The ^{1}H-^{13}C HSQC spectrum of C-TSP_C is reported with partial assignation (Figure 3-13), obtained in a previous work (Ziliani et al., 2024).

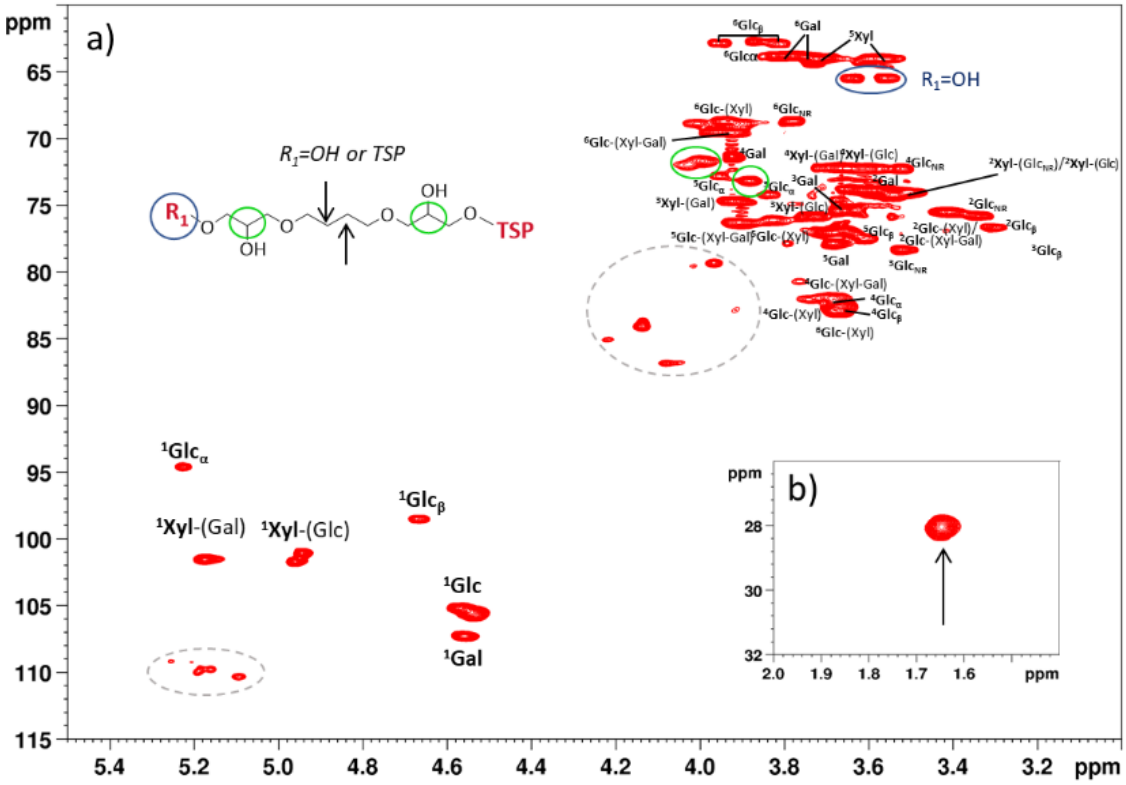

Figure 3-13. *^{1}H-^{13}C HSQC spectrum of C-TSP_C hydrolyzed with xyloglucanase.*
(a) partial assignation of the cross-peaks is shown. The new signals attributed to the presence of the BDDE are indicated (green and blue circles) and the impurities (grey). (b) the zoomed region where aliphatic CH_2CH_2 of BDDE (arrow). The superscript corresponds to the carbon number of the observed monosaccharide, which is in bold style, while the monosaccharide linked is in the parentheses. Glc—glucose; Xyl—xylose; Gal—galactose.

New cross-peaks related to the presence of the BDDE are shown in Figure 3-13. The signal attributed to the internal protons of the BDDE is shown at 1.65/28 ppm, as previously observed in HSQC spectrum in Figure 3-9b. The cross-peaks at 3.63-3.56/65.5 ppm are related to the opening of the epoxide ring of the crosslinker without the linking with the TSP. The new signals at 3.99/71.7 and 3.88/73.2 were attributed to the secondary

alcohol formed after the opening of the BDDE, using a ^{1}H-^{13}C HSQC-DEPT, reported in Figure 3-14, where a distinction between the signal of the CH_2 (blue in Figure 3-14) and the CH or CH_3 (red in Figure 3-14) is possible due to the different colour of the cross-peaks.

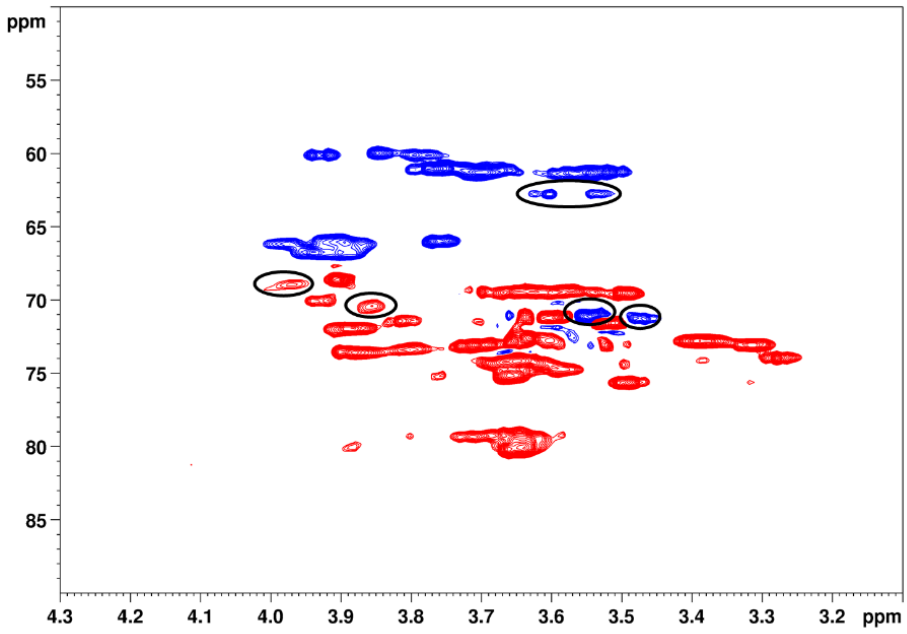

Figure 3-14. *^{1}H-^{13}C HSQC-DEPT spectrum of C-TSP_C hydrolyzed with xyloglucanase from 4.3 to 3.1 ppm.*
In blue the signals related to the CH_2 are colored in blue and the cross-peaks related to CH or CH_3 are shown in red. The signals related to the presence of the BDDE are circled in black.

The degree of modification (MoD), which is the stoichiometric ratio between the BDDE (mono and crosslinked) and the moles of TSP repeating unit, the effective crosslinker ratio (CrR), that described the stoichiometric ratio between the BDDE crosslinked and the moles of TSP repeating unit and the degree of crosslinking (CrD), can be calculated from the integration of NMR spectra adapting the equation (Wende et al., 2017).
The MoD was obtained by quantification of the anomeric region (between 5.25 and 4.45 for the proton and between 93.5 and 108.2 ppm for the carbon), which composed the TSP repeating unit, and the signal of the internal aliphatic signals CH_2CH_2 at 1.65/28.0 ppm of the cross linker. This quantification could not be made by integration of the cross-peaks in the HSQC spectrum, because the comparison between the secondary alcohol of the anomeric region and the primary alcohol in the internal chain of the BDDE is not correct due to the different molecular size and mobility between the backbone of polysaccharide and the crosslinker chain (Nizzolo et al., 2024). For this reason, we decided to perform the quantitative analysis on the proton spectra, integrating the anomeric region and the

signal at 1.65 ppm of the BDDE, as shown in Figure 3-15. However, signals of impurities, in the region between 5.3-5.1 ppm are observed (circled in Figure 3-13a), which contribute to the value of the integration in the proton spectra. Therefore, the values of the impurities were calculated by the integration of the cross-peaks in HSQC (area B in Figure 3-15) and compared to the anomeric region (area A in Figure 3-15). The values of the integrals are reported in Table 3-4.

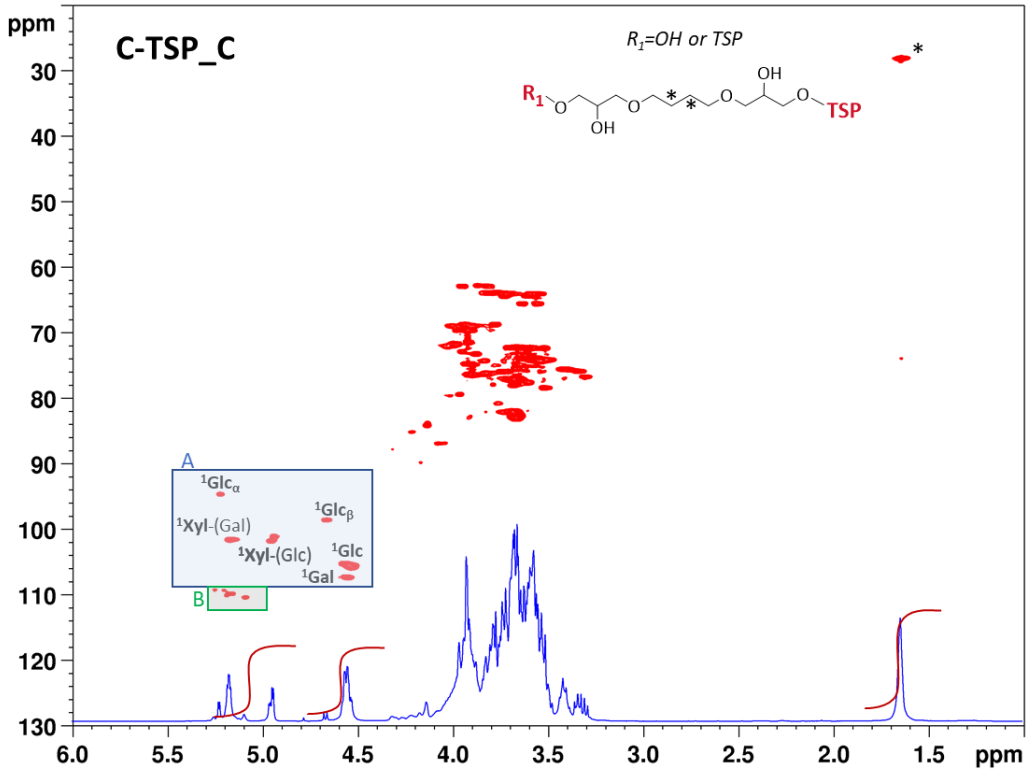

Figure 3-15. *Superimposition of ^{1}H-^{13}C HSQC in red and ^{1}H spectrum in blue of C-TSP_C hydrolyzed with xyloglucanase.*

The assignments of the anomeric cross-peaks are shown which are delimitated by a blue rectangle (A). The signals related to the impurities are shown by a green rectangle (B). The superscript corresponds to the carbon number of the observed monosaccharide, which is bold, while the monosaccharide linked is in parentheses. Glc—glucose; Xyl—xylose; Gal—galactose.

Table 3-4. *Integral values from ^{1}H-^{13}C HSQC of the impurities compared to the anomeric region of the crosslinked samples.*

Samples	Integral region A	Integral region B
C-TSP_A	1.0000	0.3514
C-TSP_B	1.0000	0.3289
C-TSP_C	1.0000	0.0825

Then, the percentage of the impurities obtained in the HSQC (Table 3-4) was subtracted from the integration of the anomeric region in the proton spectra to calculate the MoD (%) with the following equation (10):

$$\text{MoD (\%)} = 100 \times \frac{I_{\delta\ 1.65}\ /4}{(I_{\delta\ 5.4\text{-}4.4}\ \text{-Area B (\%)})} \qquad (10)$$

Where $I_{\delta\ 1.65}$ is the integral of the aliphatic CH_2CH_2 of the BDDE, divided by four (the number of the protons in that position). $I_{\delta\ 5.4–4.4}$ is the integral of the anomeric proton of TSP repeating, composed by Glc:Xyl:Gal with a ratio of 4:3:1. From this integral, the values of the impurities calculated from the HSQC (Table 3-4) are subtracted (Area B). The integration values of the aliphatic CH_2CH_2 of the BDDE and the anomeric region are reported in Table 3-5 and the MoD calculated are showed in Table 3-7.

Table 3-5. *Integral values from ^1H of the aliphatic CH_2CH_2 of the BDDE compared to the anomeric region of the crosslinked samples.*

Samples	**Integral CH_2CH_2 BDDE ($I_{\delta\ 1.65}$)**	**Integral anomeric region ($I_{\delta\ 5.4\text{-}4.4}$)**
C-TSP_A	0.0878	1.5977
C-TSP_B	0.5929	1.6184
C-TSP_C	1.1616	1.9246

The MoD indicated the total amount of the BDDE linked to sugar chain but not the percentage of the crosslinked or monolinked crosslinker.

For this reason, the effective cross-linker ratio (CrR) was calculated (Table 3-7) in order to define the moles of BDDE which were double linked, by the integration of the HSQC spectra of the hydrolysed products using the following equation (Wende et al., 2017):

$$\text{CrR} = 1 - \frac{I_{\delta\ 3.63\text{-}3.56/65.5}}{(I_{\delta\ 1.65\ /28.0}/2)} \qquad (11)$$

Where $I_{\delta\ 3.63–3.56/65.5}$ is the signals of CH_2OH of the opening ring of the BDDE, $I_{\delta\ 1.65/28.0}$ is the aliphatic CH_2CH_2 of the BDDE, divided by two which is the number of the carbons in that position. The values of the integration from the HSQC are reported in Table 3-6.

Table 3-6. *Integral values from ^{1}H-^{13}C HSQC of the aliphatic CH_2CH_2 of the BDDE compared to the CH_2OH of the crosslinker opening ring.*

Samples	Integral CH_2CH_2 BDDE ($I_{\delta\ 1.65/28.0}$)	Integral CH_2OH BDDE ($I_{\delta\ 3.63\text{-}3.56/65.5}$)
C-TSP_A	1.0000	< LOQ*
C-TSP_B	1.0000	0.4589
C-TSP_C	1.0000	0.4532

*Limit Of Quantitation

Finally, the degree of modification (CrD) was calculated by the product between MoD and CrR (Kenne et al., 2013) and reported in Table 3-7.

Table 3-7. *Degree of modification (MoD), effective crosslinking ratio (CrR) and degree of crosslinking (CrD) of C-TSP samples.*

Samples	MoD%	CrR	CrD %
C-TSP_A	2.1	< LOQ*	-
C-TSP_B	13.6	0.08	1.09
C-TSP_C	16.4	0.09	1.48

*Limit Of Quantitation

The MoD values obtained for C-TSP_A, C-TSP_B and C_TSP_C were 2.1, 13.6 and 16.4% respectively (Table 3-7), due to the different BDDE concentrations used for the crosslinking synthesis.

The CrR was calculated only for C-TSP_B and _C, because the signals in the HSQC of the sample C-TSP_A were under the limit of quantitation. The CrR value (Table 3-7) was 0.08 and 0.09 for C-TSP_B and C-TSP _C respectively, showing that the amount of double linked BDDE was very similar for the two products. However, CrD value (Table 3-7) is 1.48 for C-TSP_C and 1.09 for C-TSP_B, showing that the degree of crosslinking is higher for the C-TSP_C due to the higher concentration of monolinked BDDE.

3.7.2. MALDI-TOF

MALDI-TOF analyses were conducted at KU Leuven University on hydrolyzed by xyloglucanase TSP and C-TSPs samples. The MALDI-TOF spectrum of TSP is shown in Figure 3-16 and Table 3-8 compares the experimental and theorical *m/z* values.

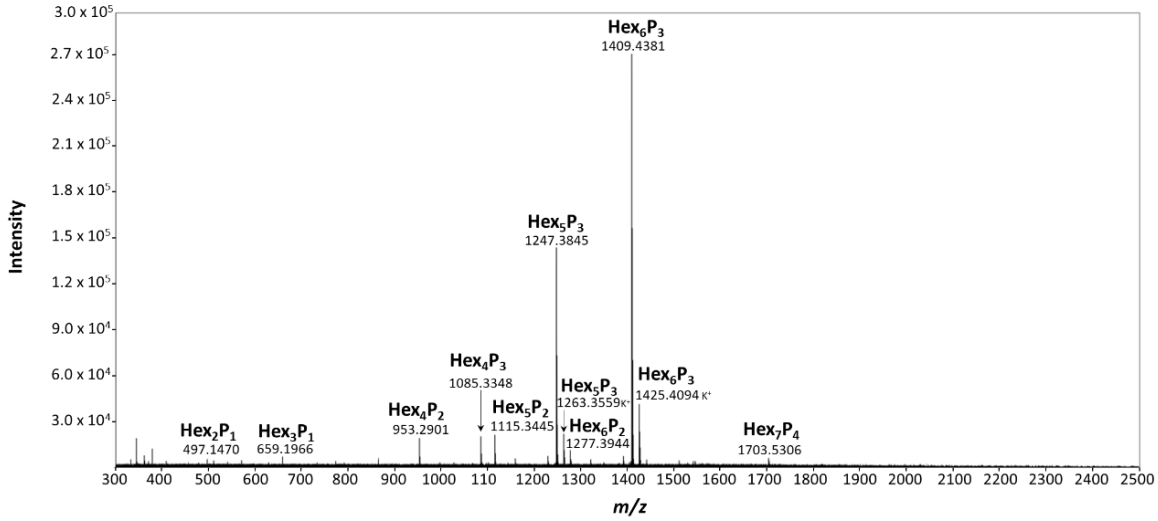

Figure 3-16. *MALDI-TOF spectrum of TSP hydrolyzed by xyloglucanase.*
Hex—hexose (glucose or galactose, 162 Da), P—pentose (xylose, 132 Da); the numbers in subscript indicate the number of hexoses and pentoses with in the detected oligosaccharide. *m/z* values of the attributed peaks are also shown.

The MALDI-TOF profile of hydrolyzed TSP (Figure 3-16) showed two most intense peaks corresponding to oligomers composed of five hexoses and three pentoses (Hex_5P_3, *m/z* 1247.3845), and six hexoses and three pentoses (Hex_6P_3, *m/z* 1409.4381), which represent the repetitive unit structure of TSP, in agreement with the LC-MS results (Paragraph 2.3.2.) and in literature data (H. Zhang et al., 2020). Shorter oligomers composed by three or four sugars (Hex_2P_1, *m/z* 497.1470 and Hex_3P_1, *m/z* 659.1966) were also observed, indicating the enzyme hydrolyzed beyond the repetitive unit, as also seen in LC-MS results (Paragraph 2.3.2.). Longer structures were detected as well, such as the oligomer composed by seven hexoses and four pentoses (Hex_7P_4, *m/z* 1703.5306); longer fragments with more than thirteen sugars (Hex_8P_5, *m/z* 1997.6455) were not observed.

Table 3-8. *MS data of oligosaccharides identified in TSP digested with xyloglucanase.*

Oligosaccharide	*Monoisotopic ions observed in MALDI-TOF-MS*			
	Ion form	*m/z* experimental	*m/z* theoretical	Error, ppm
Hex_1P_1	$[M + Na]^+$	335.0949	335.0949	0
	$[M + K]^+$	-	-	-
Hex_2P_1	$[M + Na]^+$	497.1470	497.1477	-1.4
	$[M + K]^+$	513.1141	513.1216	-14.6
Hex_2P_2	$[M + Na]^+$	629.1880	629.1899	-3.0
	$[M + K]^+$	645.1583	645.1639	-8.7
Hex_3P_1	$[M + Na]^+$	659.1966	659.2005	-5.9
	$[M + K]^+$	675.1673	675.1745	-10.7
Hex_3P_2	$[M + Na]^+$	791.2378	791.2428	-6.3
	$[M + K]^+$	807.2118	807.2167	-6.1
Hex_3P_3	$[M + Na]^+$	923.2789	923.2850	-6.6
	$[M + K]^+$	939.2536	939.2590	-5.7

Hex_4P_1	$[M + Na]^+$ $[M + K]^+$	821.2515 837.2269	821.2533 837.2273	-2.2 -0.5
Hex_4P_2	$[M + Na]^+$ $[M + K]^+$	953.2901 969.2654	953.2956 969.2695	-5.8 -4.2
Hex_4P_3	$[M + Na]^+$ $[M + K]^+$	1085.3348 1101.3058	1085.3379 1101.3118	-2.8 -5.4
Hex_4P_4	$[M + Na]^+$ $[M + K]^+$	1217.3728 -	1217.3801 1233.3541	-6.0 -
Hex_5P_1	$[M + Na]^+$ $[M + K]^+$	983.3005 -	983.3062 999.2801	-5.8 -
Hex_5P_2	$[M + Na]^+$ $[M + K]^+$	1115.3445 1131.3161	1115.3484 1131.3224	-3.5 -5.6
Hex_5P_3	$[M + Na]^+$ $[M + K]^+$	1247.3845 1263.3559	1247.3907 1263.3646	-5.0 -6.9
Hex_5P_4	$[M + Na]^+$ $[M + K]^+$	1379.4263 1395.4101	1379.4329 1395.4069	-4.8 2.3
Hex_6P_2	$[M + Na]^+$ $[M + K]^+$	1277.3944 1293.3742	1277.4012 1293.3752	-5.3 -0.8
Hex_6P_3	$[M + Na]^+$ $[M + K]^+$	1409.4381 1425.4094	1409.4435 1425.4174	-3.8 -5.6
Hex_6P_4	$[M + Na]^+$ $[M + K]^+$	1541.4771 1557.4478	1541.4858 1557.4597	-5.6 -7.6
Hex_6P_5	$[M + Na]^+$ $[M + K]^+$	1673.5381 -	1673.5280 1689.5020	6.0 -
Hex_7P_2	$[M + Na]^+$ $[M + K]^+$	1439.4490 -	1439.4541 1455.4280	-3.5 -
Hex_7P_3	$[M + Na]^+$ $[M + K]^+$	1571.4952 1587.4754	1571.4963 1587.4703	-0.7 3.2
Hex_7P_4	$[M + Na]^+$ $[M + K]^+$	1703.5306 1719.5114	1703.5386 1719.5125	-4.7 0.6
Hex_7P_5	$[M + Na]^+$ $[M + K]^+$	1835.5785 1851.5603	1835.5808 1851.5548	-1.2 3.0
Hex_8P_5	$[M + Na]^+$ $[M + K]^+$	1997.6455 -	1997.6337 2013.6076	5.9 -

As observed in LC-MS results (Paragraph 2.3.2.), oligomers composed of the same number of hexoses and pentoses (Hex_2P_2, *m/z* 629.1880; Hex_3P_3, *m/z* 923.2789; Hex_4P_4, *m/z* 1217.3728) were detected (Table 3-8). Those fragments can be confidently attributed to glucose units all branched with xyloses. The enzyme was able to hydrolyze the bond between two glucoses, even when both were linked to a xylose, as the TSP sugar chain contained regions with more than three xyloses in close proximity.

The MALDI-TOF spectra of hydrolyzed C-TSPs are reported in Figures 3-17, 3-18 and 3-19.

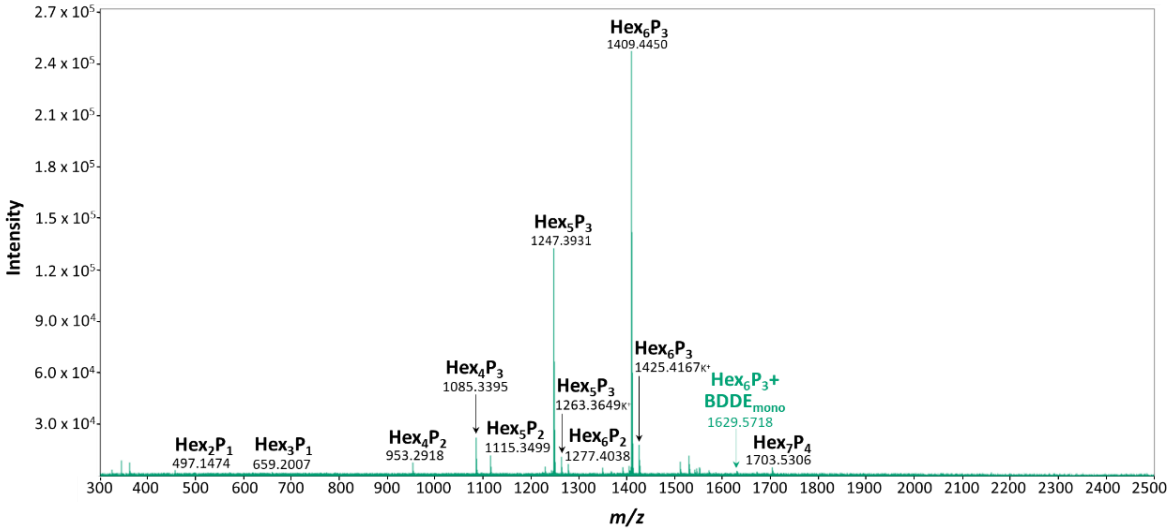

Figure 3-17. *MALDI-TOF spectrum of C-TSP_A hydrolyzed by xyloglucanase.*
Hex—hexose (glucose or galactose, 162 Da), P—pentose (xylose, 132 Da), $BDDE_{mono}$—BDDE linked only on one side (220 Da); the numbers in subscript indicate the number of hexoses and pentoses with in the detected oligosaccharide. m/z values of the attributed peaks are also shown.

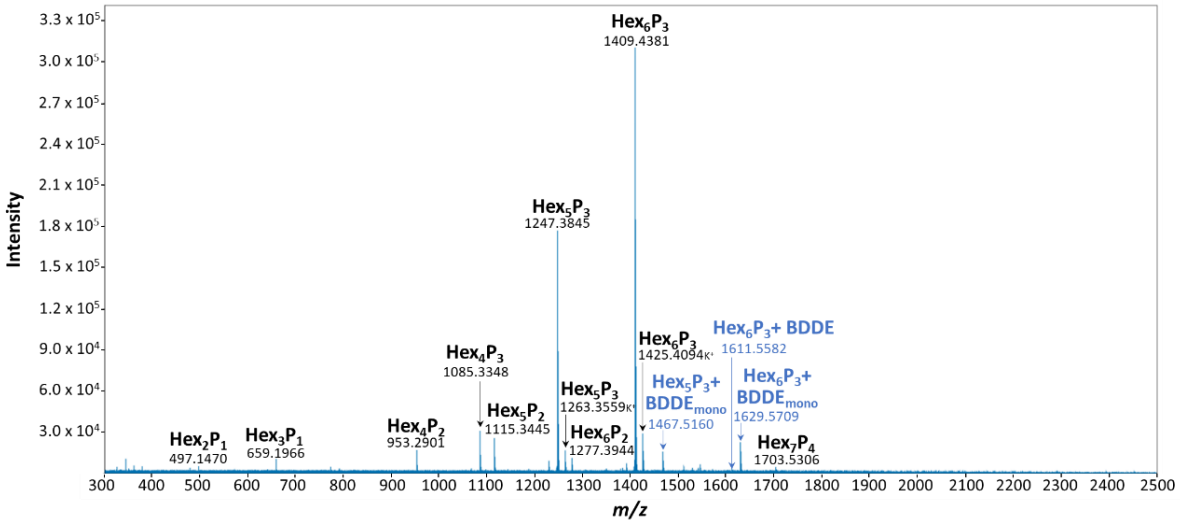

Figure 3-18. *MALDI-TOF spectrum of C-TSP_B hydrolyzed by xyloglucanase.*
Hex—hexose (glucose or galactose, 162 Da), P—pentose (xylose, 132 Da), $BDDE_{mono}$—BDDE linked only on one side (220 Da) BDDE —BDDE crosslinked (202 Da); the numbers in subscript indicate the number of hexoses and pentoses with in the detected oligosaccharide. m/z values of the attributed peaks are also shown.

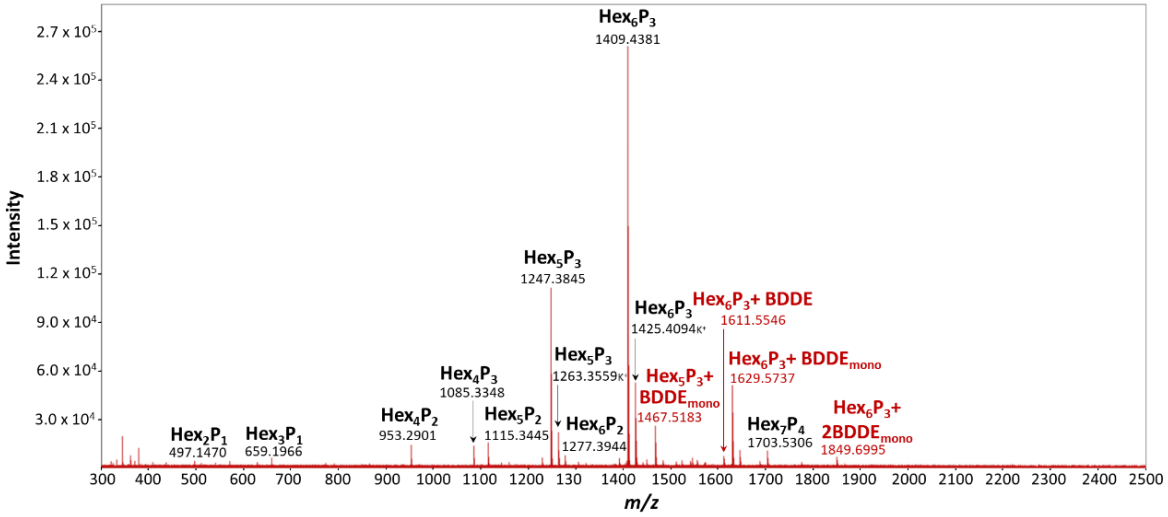

Figure 3-19. *MALDI-TOF spectrum of C-TSP_C hydrolyzed by xyloglucanase.*
Hex—hexose (glucose or galactose, 162 Da), P—pentose (xylose, 132 Da), $BDDE_{mono}$—BDDE linked only on one side (220 Da), BDDE —BDDE crosslinked (202 Da); the numbers in subscript indicate the number of hexoses and pentoses with in the detected oligosaccharide. m/z values of the attributed peaks are also shown.

In all the spectra, the most intense peaks were attributed to the oligomers composing the repetitive unit (Hex_5P_3 and Hex_6P_3), as observed in the TSP spectrum (Figure 3-16), indicating that the xyloglucanase activity was not affected by the presence of BDDE in the samples. However, new peaks compared to the TSP spectrum (Figure 3-16) were observed in the C-TSPs spectra. In C-TSP_A spectrum (Figure 3-17), an oligomer composed by six hexoses and three pentoses linked with the BDDE at one side (Hex_6P_3+$BDDE_{mono}$, *m/z* 1629.5718) was detected. This oligomeric structure was also detected in C-TSP_B and C-TSP_C spectra, at *m/z* values of 1629.5709 and 1629.5737, respectively, and with greater intensity compared to C-TSP_A due to the higher BDDE concentration used. Moreover, in C-TSP_B and C-TSP_C spectra (Figure 3-18 and 3-19), other oligomer structure with monolinked BDDE was detected, composed by five hexoses and three pentoses (Hex_5P_3+$BDDE_{mono}$, *m/z* 1467.5160 for C-TSP_B and 1467.5183 for C-TSP_C). In the C-TSP_C spectrum (Figure 3-19) an oligomeric structure composed of six hexoses and three pentoses with two monolinked BDDE (Hex_6P_3+$2BDDE_{mono}$, *m/z* 1849.6995) was also observed. This result aligns with NMR data (Paragraph 3.7.1.), where the CrD value of C-TSP_C is higher than C-TSP_B. Additionally, in both C-TSP_B and C-TSP_C an oligomeric structure with crosslinked BDDE, composed by six hexoses and three pentoses (Hex_6P_3+BDDE *m/z* 1611.5546 for C-TSP_B and 1611.5546 for C-TSP_C) was observed. In this case, probably, the crosslinker was attached to the same oligomeric fragment, as it is improbable that xyloglucanase can hydrolyze two separate small fragments linked together by BDDE. Nonetheless, structures formed by

oligomers of four hexoses and two or three pentoses crosslinked with BDDE (Hex_4P_2+Hex_4P_2+BDDE, *m/z* theoretical 2085.7225; Hex_4P_3+Hex_4P_2+BDDE, *m/z* theoretical 2217.7647) were detected in all C-TSPs samples, as reported in Table 3-9. Therefore, even in C-TSP_A some crosslinked structures were presented, but at such low concentration that they could not be detected in NMR. Moreover, in C-TSP_B and C-TSP_C, which were analyzed up to *m/z* value of 6000 due to NMR evidence, of crosslinked BDDE, longer oligomers formed by different combinations of Hex_5P_3, Hex_6P_3, and Hex_7P_4 linked with the crosslinker were observed, as shown in Table 3-9. Interestingly, these fragments were also observed linked each other with two BDDE crosslinks or with one crosslinked BDDE and one monolinked BDDE.

In conclusion, different structures of hydrolyzed C-TSPs were observed including oligomers with monolinked BDDE and crosslinked BDDE on the same oligosaccharide. Additionally, oligomers linked to each other with the crosslinker were also detected, especially in C-TSP_B and C-TSP_C samples, where the BDDE concentration was higher compared to C-TSP_A.

Table 3-9. *MS data of oligosaccharides identified in C-TSPs samples digested with xyloglucanase.*

Oligosaccharide	*Monoisotopic ions observed in MALDI-TOF-MS*							
	Ion form	*m/z* theoretical	**C-TSP_A**		**C-TSP_B**		**C-TSP_C**	
			m/z experimental	Error, ppm	*m/z* experimental	Error, ppm	*m/z* experimental	Error, ppm
Hex_1P_1	$[M + Na]^+$ $[M + K]^+$	335.0949 351.0688	335.0951 -	0.6 -	335.0948 351.1226	-0.3 -	335.0951 -	0.6 -
Hex_2P_1	$[M + Na]^+$ $[M + K]^+$	497.1477 513.1216	497.1474 -	-0.6 -	497.1466 513.1209	-2.2 -1.4	497.1472 -	-1.0 -
Hex_2P_2	$[M + Na]^+$ $[M + K]^+$	629.1899 645.1639	629.1874 645.1621	-4.0 -2.8	629.1876 -	-3.6 -	629.1883 645.1627	-2.5 -1.8
Hex_3P_1	$[M + Na]^+$ $[M + K]^+$	659.2005 675.1745	659.2007 675.1758	0.3 1.9	659.1962 675.1709	-6.5 -5.3	659.1970 675.1800	-5.3 8.1
Hex_3P_2	$[M + Na]^+$ $[M + K]^+$	791.2428 807.2167	791.2406 807.2195	-2.8 3.5	791.2373 807.2023	-6.9 -17.3	791.2383 807.2078	-5.7 -11.0
Hex_3P_3	$[M + Na]^+$ $[M + K]^+$	923.2850 939.2590	923.2799 939.2598	-5.5 0.8	923.2832 939.2531	-1.9 -6.3	923.2796 939.2543	-5.8 -5.0
Hex_4P_1	$[M + Na]^+$ $[M + K]^+$	821.2533 837.2273	821.2550 837.2307	2.1 4.1	821.2510 837.2264	-2.8 -1.1	821.2520 837.2274	-1.6 0.1
Hex_4P_2	$[M + Na]^+$ $[M + K]^+$	953.2956 969.2695	953.2918 969.2723	-4.0 2.9	953.2896 969.2649	-6.3 -4.7	953.2908 969.2654	-5.0 -4.2
Hex_4P_2+ $BDDE_{mono}$	$[M + Na]^+$ $[M + K]^+$	1173.4267 1189.4006	1085.3395 1101.3109	1.5 -0.8	1173.4216 -	-4.3 -	1173.4233 1189.4005	-2.9 -0.1
Hex_4P_3	$[M + Na]^+$ $[M + K]^+$	1085.3379 1101.3118	1217.3862 -	5.0 -	1085.3342 1101.3053	-3.4 -5.9	1085.3357 1101.3120	-2.0 0.2
Hex_4P_4	$[M + Na]^+$ $[M + K]^+$	1217.3801 1233.3541	983.3079 -	1.7 -	1305.4636 -	-4.1 -	1217.3629 1233.3580	-14.1 3.2

Hex_5P_1	$[M + Na]^+$ $[M + K]^+$	983.3062 999.2801	1115.3499 1131.3218	1.3 -0.5	1217.3777 -	-2.0 -	983.3013 -	-5.0 -
Hex_5P_2	$[M + Na]^+$ $[M + K]^+$	1115.3484 1131.3224	1335.4900 -	7.9 -	983.3000 -	-6.3 -	1115.3455 1131.3170	-2.6 -4.8
Hex_5P_2+ BDDE	$[M + Na]^+$ $[M + K]^+$	1317.4686 1333.4429	1247.3931 1263.3649	1.9 0.2	1115.3439 1131.3155	-4.0 -6.1	1317.4569 1333.4538	-8.9 8.2
Hex_5P_2+ $BDDE_{mono}$	$[M + Na]^+$ $[M + K]^+$	1335.4795 1351.4334	1449.5128 -	1.1 -	1317.4550 1333.4633	-10.3 15.3	1335.4746 1351.4349	-3.7 1.1
Hex_5P_2+ $2BDDE_{mono}$	$[M + Na]^+$ $[M + K]^+$	1555.6106 1571.5845	1467.5192 1483.4869	-1.8 -5.9	1335.4784 -	-0.8 -	1555.5289 1571.4969	-52.5 -55.7
Hex_5P_3	$[M + Na]^+$ $[M + K]^+$	1247.3907 1263.3646	1379.4325 -	-0.3 -	1247.3839 1263.3608	-5.4 -3.0	1247.3856 1263.3627	-4.1 -1.5
Hex_5P_3+ BDDE	$[M + Na]^+$ $[M + K]^+$	1449.5112 1465.4851	1145.3523 -	*-5.8* -	1449.5041 -	-4.9 -	1449.5064 1465.5028	-3.3 12.1
Hex_5P_3+ $BDDE_{mono}$	$[M + Na]^+$ $[M + K]^+$	1467.5218 1483.4957	1277.4038 1293.3840	2.0 6.8	1467.5160 1483.4955	-3.9 -0.1	1467.5183 1483.4918	-2.4 -2.6
Hex_5P_3+ $2BDDE_{mono}$	$[M + Na]^+$ $[M + K]^+$	1687.6528 1703.6268	1409.4450 1425.4167	1.1 -0.5	1687.6493 -	-2.1 -	1687.6458 -	-4.1 -
Hex_5P_3+BDDE+ $BDDE_{mono}$	$[M + Na]^+$ $[M + K]^+$	1669.6423 1685.6162	1611.5650 -	0.6 -	1379.4314 1395.4153	-1.1 6.0	1669.6369 1685.6076	-3.2 -5.1
Hex_5P_4	$[M + Na]^+$ $[M + K]^+$	1379.4329 1395.4069	1629.5718 1645.5429	-1.7 -3.4	1145.3510 -	-7.0 -	1379.4276 1395.4174	-3.8 7.5
Hex_5P_5	$[M + Na]^+$ $[M + K]^+$	1511.4752 1527.4491	1541.4937 1557.4586	5.1 -0.7	1277.3937↓ 1293.3736	-5.9 -1.2	1511.3815 -	-62.0 -
Hex_6P_2	$[M + Na]^+$ $[M + K]^+$	1277.4012 1293.3752	1673.5261 -	-1.1 -	1497.5180 -	-9.5 -	1277.4012 1293.3698	0 -4.2
Hex_6P_2+ $BDDE_{mono}$	$[M + Na]^+$ $[M + K]^+$	1497.5323 1513.5063	1439.4507 1455.4222	-2.4 -4.0	1409.4373 1425.4086	-4.4 -6.2	1497.5265 1513.5021	-3.9 -2.8
Hex_6P_3	$[M + Na]^+$ $[M + K]^+$	1409.4435 1425.4174	1571.4938 -	-1.6 -	1611.5582 1627.5554	-3.6 10.7	1409.4395 1425.4108	-2.8 -4.6
Hex_6P_3+ BDDE	$[M + Na]^+$ $[M + K]^+$	1611.5640 1627.5379	1703.5388 1719.5135	0.1 0.6	1629.5709 1645.5352	-2.3 -8.1	1611.5546 1627.5390	-5.8 0.7
Hex_6P_3+ $BDDE_{mono}$	$[M + Na]^+$ $[M + K]^+$	1629.5746 1645.5485	1923.6743 -	2.4 -	1849.6960 -	-5.2 -	1629.5737 1645.5444	-0.5 -2.5
Hex_6P_3+ $2BDDE_{mono}$	$[M + Na]^+$ $[M + K]^+$	1849.7056 1865.6796	1835.5767 -	-2.2 -	2069.8385 -	0.9 -	1849.6995 1865.6812	-3.3 -0.8
Hex_6P_3+ $3BDDE_{mono}$	$[M + Na]^+$ $[M + K]^+$	2069.8367 2085.8107	1733.5484 -	*-0.4* -	1831.7059 -	5.9 -	2069.8213 -	-7.4 -
Hex_6P_3+BDDE+ $BDDE_{mono}$	$[M + Na]^+$ $[M + K]^+$	1831.6951 1847.6690	1865.5892 -	-1.2 -	2051.8076 -	-9.1 -	1831.6890 1847.6812	-3.3 6.6
Hex_6P_3+BDDE+ $2BDDE_{mono}$	$[M + Na]^+$ $[M + K]^+$	2051.8262 2067.8001	1997.6407 -	3.5 -	1541.4825 -	-2.1 -	2051.8405 -	7.0 -
Hex_6P_4	$[M + Na]^+$ $[M + K]^+$	1541.4858 1557.4597	2085.7236 -	*0.5* -	1673.5241 -	-2.3 -	1541.4788 1557.4557	-4.5 -2.6
Hex_6P_5	$[M + Na]^+$ $[M + K]^+$	1673.5280 1689.5020	2217.7696 -	*2.2* -	1439.4483 1455.4193	-4.0 -6.0	1673.5270 -	-0.6 -
Hex_7P_2	$[M + Na]^+$ $[M + K]^+$	1439.4541 1455.4280	-	-	1571.4943 1587.4807	-1.3 6.5	1439.4505 1455.4397	-2.5 8.0
Hex_7P_3	$[M + Na]^+$ $[M + K]^+$	1571.4963 1587.4703	-	-	1773.6070 1789.5848	-5.5 -3.3	1571.4969 1587.4645	0.4 -3.6
Hex_7P_3+ BDDE	$[M + Na]^+$ $[M + K]^+$	1773.6168 1789.5908	-	-	1791.6180 1807.5892	-5.2 -6.7	1773.6236 -	3.8 -

Hex_7P_3+ $BDDE_{mono}$	$[M + Na]^+$ $[M + K]^+$	1791.6274 1807.6013	-	-	1703.5361 1719.5104	-1.5 -1.2	1791.6280 1807.5858	0.3 -8.6
Hex_7P_3+ $2BDDE_{mono}$	$[M + Na]^+$ $[M + K]^+$	2011.7585 2027.7324	-	-	1905.6496 -	-5.0 -	2011.7590 -	0.2 -
Hex_7P_4	$[M + Na]^+$ $[M + K]^+$	1703.5386 1719.5125	-	-	1923.6656 -	-2.1 -	1703.5326 1719.5134	-3.5 0.5
Hex_7P_4+ BDDE	$[M + Na]^+$ $[M + K]^+$	1905.6591 1921.6330	-	-	2125.8036 -	6.3 -	1905.6602 1921.6249	0.6 -4.2
Hex_7P_4+ $BDDE_{mono}$	$[M + Na]^+$ $[M + K]^+$	1923.6697 1939.6436	-	-	1835.5772 -	-2.0 -	1923.6694 1939.640	-0.2 -1.8
Hex_7P_3+ $2BDDE_{mono}$	$[M + Na]^+$ $[M + K]^+$	2143.8007 2159.7747	-	-	2055.7113 -	-0.3 -	2143.8022 -	0.7 -
Hex_7P_4+BDDE+ $BDDE_{mono}$	$[M + Na]^+$ $[M + K]^+$	2125.7902 2141.7641	-	-	2037.7278 -	12.9 -	2125.7937 -	1.6 -
Hex_7P_5	$[M + Na]^+$ $[M + K]^+$	1835.5808 1851.5548	-	-	1601.4981 -	-5.5 -	1835.5874 -	3.6 -
Hex_7P_5+ $BDDE_{mono}$	$[M + Na]^+$ $[M + K]^+$	2055.7119 2071.6859	-	-	1733.5383 1749.5267	-6.2 2.0	2055.7084 -	-1.7 -
Hex_7P_5+ BDDE	$[M + Na]^+$ $[M + K]^+$	2037.7014 2053.6753	-	-	1865.5889 -	-1.3 -	2037.6964 -	-2.4 -
Hex_8P_3	$[M + Na]^+$ $[M + K]^+$	1733.5491 1749.5231	-	-	1997.6510 -	8.7 -	1733.5480 1749.5101	-0.6 -7.4
Hex_8P_4	$[M + Na]^+$ $[M + K]^+$	1865.5914 1881.5653	-	-	2217.782 -	7.8 -	1865.5788 1882.5545	-6.7 -
Hex_8P_4+ $BDDE_{mono}$	$[M + Na]^+$ $[M + K]^+$	2085.7225 2101.6964	-	-	2159.6778 -	-4.0 -	2085.7218 2101.7193	-0.3 10.9
Hex_9P_4	$[M + Na]^+$ $[M + K]^+$	2027.6442 2043.6182	-	-	2453.7822 -	0.2 -	2027.6346 2043.6225	-4.7 2.1
Hex_9P_5	$[M + Na]^+$ $[M + K]^+$	2159.6865 2175.6604	-	-	2085.7173 -	-2.5 -	2159.6753 2175.6732	-5.2 5.9
Hex_9P_5+ $BDDE_{mono}$	$[M + Na]^+$ $[M + K]^+$	2379.8176 2395.7915	-	-	2217.7676 -	1.3 -	2379.8188 -	0.5
Hex_4P_2+ Hex_4P_2+BDDE	$[M + Na]^+$ $[M + K]^+$	2085.7225 2101.6964	-	-	2379.8116 -	-2.5 -	2085.7218 -	-0.3 -
Hex_4P_2+ Hex_4P_3+BDDE	$[M + Na]^+$ $[M + K]^+$	2217.7647 2233.7387	-	-	2542.8720 -	-0.7 -	2217.7675 -	1.3 -
Hex_4P_2+ Hex_5P_3+BDDE	$[M + Na]^+$ $[M + K]^+$	2379.8176 2395.7915	-	-	2674.9077 -	-3.1 -	2379.8188 -	0.5 -
Hex_4P_2+ Hex_6P_3+BDDE	$[M + Na]^+$ $[M + K]^+$	2542.8737 2557.8443	-	-	2895.0407 -	-2.1 -	2542.8718 -	-0.7 -
Hex_5P_3+ Hex_5P_3+BDDE	$[M + Na]^+$ $[M + K]^+$	2674.9160 2690.8899	-	-	2877.0477 -	3.9	2674.9076 -	-3.1 -
Hex_5P_3+ Hex_5P_3+BDDE +$BDDE_{mono}$	$[M + Na]^+$ $[M + K]^+$	2895.0471 2690.8899	-	-	2836.9685 -	-0.1 -	2895.0405 -	-2.1 -
Hex_5P_3+ Hex_5P_3+2BDDE	$[M + Na]^+$ $[M + K]^+$	2877.0365 2893.0104	-	-	3057.0977 -	-0.7 -	2877.0391 -	0.9
Hex_5P_3+ Hex_6P_3+BDDE	$[M + Na]^+$ $[M + K]^+$	2836.9688 2852.9428	-	-	3039.0864 -	-0.9 -	2836.9684 -	-0.1 -
Hex_5P_3+ Hex_6P_3+BDDE+ $BDDE_{mono}$	$[M + Na]^+$ $[M + K]^+$	3057.0999 3073.0738	-	-	3131.0634 -	-0.2 -	3057.0976 -	-0.7 -

Hex_5P_3+ Hex_6P_3+2BDDE	$[M + Na]^+$ $[M + K]^+$	3039.0893 3055.0633	-	-	2999.0240 -	0.8 -	3039.0950 -	1.9 -
Hex_5P_3+ Hex_7P_4+BDDE	$[M + Na]^+$ $[M + K]^+$	3131.0639 3147.0378	-	-	3219.1541 -	0.4 -	3131.0632 -	-0.2 -
Hex_6P_3+ Hex_6P_3+BDDE	$[M + Na]^+$ $[M + K]^+$	2999.0216 3014.9956	-	-	3201.1359 -	-2.0 -	2999.0065 -	-5.0 -
Hex_6P_3+ Hex_6P_3+BDDE+ $BDDE_{mono}$	$[M + Na]^+$ $[M + K]^+$	3219.1527 3235.1267	-	-	3293.1201 -	1.0 -	3219.1539 -	0.4 -
Hex_6P_3+ Hex_6P_3+2BDDE	$[M + Na]^+$ $[M + K]^+$	3201.1422 3217.1161	-	-	3201.1359 -	-2.0 -	3201.1358 -	-2.0 -
Hex_6P_3+ Hex_7P_4+BDDE	$[M + Na]^+$ $[M + K]^+$	3293.1167 3309.0907	-	-	3293.1201 -	1.0 -	3293.1200 -	1.0 -

3.8. Pharmacological tests

3.8.1. Cell viability

Cell viability was assessed after 24 hours of treatment with lipopolysaccharide (LPS) (10 µg/ml) alone or in combination with 1% C-TSP_A, C-TSP_B, or C-TSP_C. The results are reported in the following Figure 3-20.

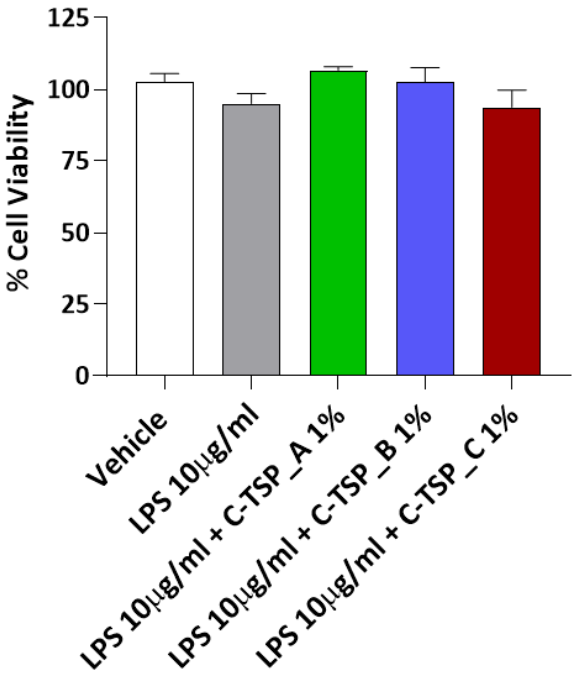

Figure 3-20. *Effect of LPS and C-TSP compounds on cell viability after 24-hour treatment.* Cell viability was assessed and expressed as a percentage relative to the vehicle-treated control. Data are presented as mean ± SEM (n = 6). Statistical analysis was performed using One way ANOVA followed by post-test Bonferroni.

As shown in Figure 3-20, exposure to LPS alone resulted in a slight, non-significant reduction in cell viability compared to the vehicle control, indicating limited cytotoxicity under these conditions. Co-treatment with C-TSP_A and C-TSP_B appeared to restore cell viability to levels similar to the vehicle, while C-TSP_C gave similar relative to pure LPS. However, none of these effects reached statistical significance.

3.8.2. Permeability assessment

3.8.2.1. TEER measurement

The effect of LPS 10 µg/mL and LPS in combination of the C-TSPs on transendothelial electrical resistance (TEER), a measure of intestinal barrier integrity, is showed in Figure 3-21.

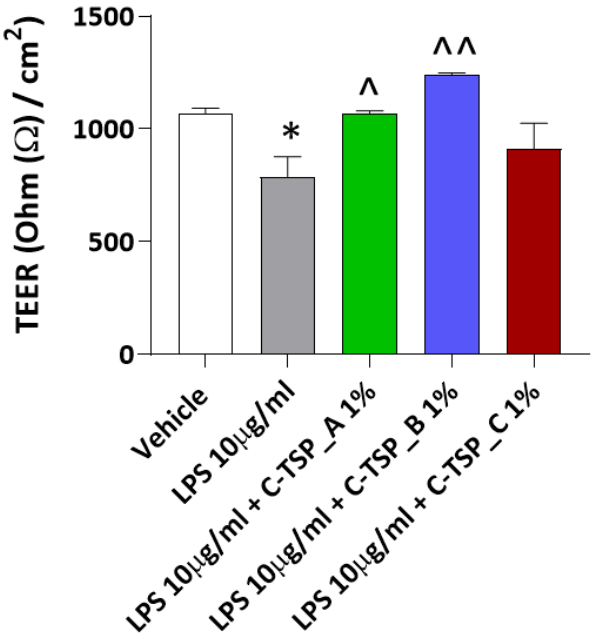

***Figure 3-21**. Effect of LPS and C-TSP compounds on intestinal barrier integrity.*
TEER values (Ohm·cm²) were measured to assess the integrity of the endothelial monolayer. Data are expressed as mean ± SEM (n = 6). Statistical analysis was performed using One way ANOVA followed by Bonferroni post-test. *statistical significance vs vehicle (* $p < 0.05$); ^ statistical significance vs LPS (^ $p < 0.05$; ^^ $p < 0.01$).

The graph in Figure 3-21 showed that the exposure to LPS (10 µg/ml) for 24 hours led to a significant reduction in TEER compared to the Caco-2 cells vehicle, indicating a compromise in intestinal barrier function. Co-treatment with C-TSP_A (1%) significantly restored TEER, suggesting a protective effect against LPS-induced barrier disruption. Notably, C-TSP_B (1%) not only reversed the LPS-induced decrease but also increased

TEER above the baseline level observed in the vehicle group, indicating a strong barrier-enhancing activity. In contrast, C-TSP_C (1%) did not significantly improve TEER compared to LPS alone, showing limited efficacy in maintaining or restoring barrier integrity under inflammatory conditions.

3.8.2.2. FITC 4kDa-dextran permeability test

To assess the impact of LPS and C-TSP compounds on intestinal permeability, a FITC-dextran (4 kDa) flux assay was performed over a 4-hour period. The results are reported in Figure 3-22.

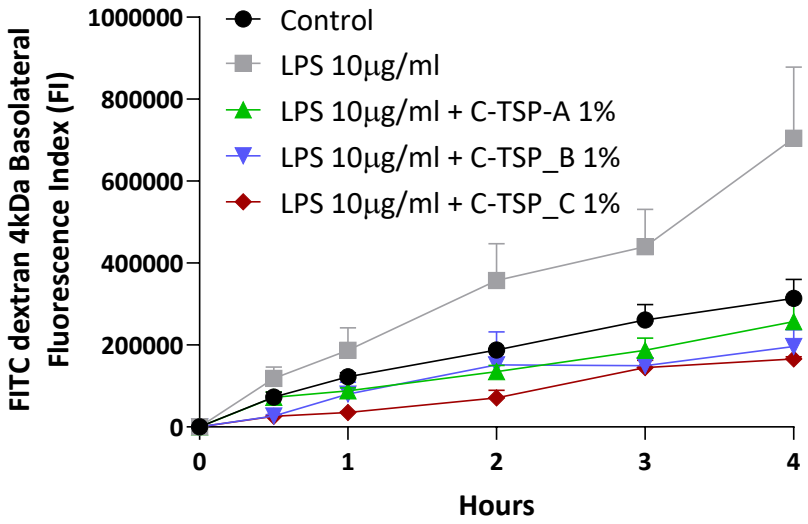

***Figure 3-22**. Effect of LPS and C-TSP derivatives on intestinal permeability assessed by FITC-dextran flux.*
Effect of LPS and C-TSP derivatives on intestinal permeability assessed by FITC-dextran flux.

As shown in Figure 3-22, LPS treatment 10 µg/ml markedly increased paracellular permeability compared to the untreated control, as indicated by a progressive rise in basolateral fluorescence intensity over time. This increase reflects a significant disruption of intestinal barrier function. In contrast, co-treatment with 1% C-TSP_A, C-TSP_B, or C-TSP_C effectively attenuated the LPS-induced permeability, with all three compounds substantially reducing FITC-dextran passage across the monolayer. These findings suggest that C-TSP derivatives, can mitigate LPS-induced barrier dysfunction and preserve intestinal integrity. The protective effects of C-TSP derivatives observed in Caco-2 monolayers under inflammatory conditions suggest potential therapeutic relevance in the context of IBD. IBD is characterized by chronic intestinal inflammation

and impaired epithelial barrier function, leading to increased intestinal permeability and sustained immune activation. In this study, LPS exposure disrupted barrier integrity, as evidenced by a reduction in TEER and an increase in FITC-dextran flux, mimicking the epithelial dysfunction observed in IBD. Co-treatment with C-TSPs, effectively restored barrier properties, reducing paracellular permeability and enhancing monolayer resistance. Given the central role of epithelial barrier dysfunction in IBD pathogenesis, the ability of C-TSP derivatives to preserve or restore barrier integrity under pro-inflammatory conditions positions them as promising candidates for further investigation in preclinical models of colitis.

3.9. Conclusions

This work presents a comprehensive physiochemical and pharmacological characterization of novel hydrogels obtained by functionalizing tamarind seed polysaccharide (TSP) with 1,4-Butanediol diglycidyl ether. Chemical modification enabled the formation of crosslinked networks with BDDE, ranging from viscous-like (C-TSP_A) to fully gel-like (C-TSP_C) behavior. The degree of crosslinking, confirmed by NMR spectroscopy following enzymatic depolymerization, correlated with significant changes in rheological behavior, microstructure, and hydrogel stability. Importantly, pharmacological assays in an *in vitro* model of intestinal inflammation revealed that the C-TSP derivatives were able to mitigate LPS-induced epithelial damage. Specifically, C-TSP_B emerged as the most balanced formulation, showing enhanced transepithelial electrical resistance (TEER), reduced paracellular permeability, and preservation of cell viability—likely due to its optimal viscoelastic properties and ability to interact with the mucosal interface.

These results suggest that BDDE-crosslinked TSP hydrogels possess promising biofunctional properties for use in barrier-protective therapies, such as in the treatment of IBD. Their intrinsic mucoadhesivity, combined with improved mechanical resilience and biocompatibility, positions them as viable candidates for localized drug delivery or mucosal protection. However, some limitations must be acknowledged. Native TSP was not included in the pharmacological assays due to its known properties and distinct physical behavior. C-TSP samples were tested at 1% (w/v), forming semi-solid or gel-like matrices suitable for direct contact with cellular monolayers. In contrast, TSP at 1% remains a low-viscosity solution, which may not remain stable in place on the monolayer, potentially leading to inconsistent exposure.

3.10. Materials and methods

3.10.1. Materials

TSP was provided by FARMIGEA (Pisa, Italy). Sodium azide, Sodium nitrate, sodium hydroxide, acetone, 1,4-Butanediol diglycidyl ether (BDDE), Sodium deuteroxide solution NaOD from Sigma Aldrich (Milan, Italy); Xyloglucanase (GH5) (*Paenibacillus* sp.) was purchased from Megazyme International (Ireland); deuterium oxide (99.9%) from Euriso-top (Saint-Aubin, France). Deionized water (conductivity less than 0.1 μS) was prepared with an osmosis inverse system (Culligan, Milan, Italy). PolyCAL-Pullulan Std-102K and PolyCAL-DextranStd-T67K (Malvern Panalytical, UK). When not specified, the reagents are ≥98%.

3.10.2. Methods

3.10.2.1. Synthesis of crosslinked TSP

Tamarind seed polysaccharide (TSP- 400 mg) was suspended in a solution (8 mL) of sodium hydroxide (NaOH) 1M at the concentration of 50 mg/mL and stirred until complete solubilization at room temperature. Then, the solution was heated to 50°C and BDDE at different mole/residue ratios of polysaccharide/BDDE (5-120 μL) were added. After 2 hours, the resulting products were dialyzed in water (c.o.=6-8 kDa) to remove NaOH and residual BDDE. The samples were then dried using acetone and lyophilization. In Table 3-1, the product obtained are reported. The molar ratio was calculated using for the TSP the molecular weight of the repetitive unit, 1207 g/mol, and for the BDDE the molecular weight of 202.25 g/mol and density of 1.1 g/mL.

3.10.2.2. SEM

SEM analyses were performed with a Zeiss FEG Gemini 500 electronic microscope. The microscope can operate with accelerating voltages of 0.5–30 kV, beam currents of 3 pA-20 nA, with a nominal resolution of 0.6 nm at 15 kV. For the analysis reported in this study, the system was operating at 5 kV. Prior to SEM analysis, samples are gold-sputtered. TSP and C-TSPs samples were analyzed after freeze-drying process.

3.10.2.3. FTIR

The infrared spectra of TSP and C-TSP were recorded using an Alpha spectrometer (Bruker, Bremen, Germany), in the range of 4,000-400 cm^{-1} at room temperature. An ATR (attenuated total reflection) (Bruker, Bremen, Germany), platinum diamond was used for the measurement. A resolution of 4 cm^{-1} and a phase resolution of 32 were employed. The sample scan time was 100 and the background scan time was 50. The data were analysed using OPUS software version 7.0 (Bruker, Bremen, Germany). TSP and C-TSPs samples were analyzed after freeze-drying process. C-TSP-B and C-TSP_C were also grinded to obtain powder.

3.10.2.4. Rheological properties

The rheological properties of soluble resulting products were studied using a Modular Compact Rheometer MCR 92 (Anton Paar GmbH, Graz, Austria), with measure system DG26.7 (double gap geometry) at of 37°C.

Viscosity measurements were performed in rotation mode, they were investigated in the range of 1-1000 s^{-1}, with a logarithmic ramp, and ten points per decade were acquired. Samples were solubilized in deionized water to a concentration of 10 mg/mL, about 100 mg were solubilized in 10 mL of deionized water.

The sample viscoelastic behaviour was investigated in the oscillation mode, to determine the storage modulus G'(ω) and the loss modulus G" (ω) at 37°C at 10 mg/mL. First, preliminary tests were conducted to determine the upper amplitude limit of the linear viscoelastic region (LVE), testing the samples over an extended strain field (0.1-100%), at constant angular frequency (10 rad/s).

Second, after the determination of the LVE (1%) the samples were tested by performing a frequency sweep test over the 100 rad/s-0,1 rad/s frequencies, at a constant strain.

3.10.2.5. HP-SEC-TDA

Chromatographic acquisitions were performed on OmniSEC Multi-detector System (Malvern Panalytical, UK) equipped both systems with a triple detector array exploiting simultaneous action of refraction index detector (RI), Right and Low Angle Light Scattering (RALS and LALS) and Viscometer (DP).

Measurements were performed at 40°C using 2 x TSKGMPWXL colums,13 µm, 7.8 mm ID x 30 cm L, in series (Tosoh Bioscience, Tokyo, Japan). $NaNO_3$ 0.1M+NaN_3 0.05%, prefiltered (0.22 µm Mixed cellulose Ester filter), was used as mobile phase at a flow rate of 0.6 mL/min. Chromatographic profiles were elaborated using OMNISEC software version 11.40 for OmniSEC Multi-detector System.

RI increments, referred to as dn/dc, equal to 0.164 cm^3/g was used.

The detectors were calibrated with Pullulan standard, with certified molecular weight, polydispersion index and intrinsic viscosity (PolyCAL-PullulanStd-102K Malvern Panalytical, UK).

Samples were solubilized at about 1 mg/mL in 0.1M $NaNO_3$ +NaN_3 0.05%.

3.10.2.6. 1D and 2D NMR analysis

TSP and C-TSPs' ^{13}C cross polarization with magic angle spinning (CP-MAS) spectra and the measurement of the spin lattice relaxation time, T1ρ, were performed on AVANCE IIIHD 500MHz spectrometer (Bruker, Karlsruhe, Germany), equipped with 4 mm for solid state probe, at room temperature. About 50 mg of the powder samples were placed directly in the rotor.

^{13}C CP-MAS spectra were acquired using the Bruker cp pulse program, with the following parameters: contact time (P15) 1.4 ms, Irradiation frequency (O1) 78.258 ppm, spectral width of 301.2410 ppm, time domain (TD) 3026, relaxation delay (D1) 8s, 2048 number of scans (NS).

^1H T1ρ were acquired using Bruker cpht1rho pulse program, with the following parameters: contact time (P15) 1.4 ms, Irradiation frequency (O1) 78.258 ppm (F2) and 6.2 (F1), spectral width of 301.2410 ppm (F2) and 10 ppm (F1), time domain (TD) 3026 (F2) and 12 (F1), relaxation delay (D1) 8s, 512 number of scans (NS).

TSP's ^1H and ^1H-^{1}3C HSQC spectra were obtained with a Bruker AVANCE 600 III (Bruker, Karlsruhe, Germany) at 313 K. About 8 mg of sample were dissolved in 0.6 mL of deuterium oxide (D_2O). TSP sample was stirred overnight to ensure a complete solubilization before transfer in a 5 mm NMR tube for the analysis.

^1H-NMR were acquired with pre-saturation of residual HOD, using the Bruker zgcppr pulse program, with the following parameters: number of scans 16, relaxation delay 12 s D1, time domain 32 k points and a spectral width of 18 ppm with transmitter offset 4.7 ppm.

^{1}H-^{13}C HSQC experiments were acquired using the Bruker hsqcetgpsisp2.2 pulse program, with GARP4 decoupling. The following acquisition parameters were set: 24 number of scans, 16 dummy scans, relaxation delay 2 s, time domain 2048 (F2) and 256 (F1), spectral width 8 ppm (F2) and 160 ppm (F1), transmitter offset 4.7 ppm (F2) and 80 ppm (F1), and number of t1 increments equal to 320. The 1 JC–H tune value was set to 150 Hz.

C-TSP_A ^{1}H-^{13}C HSQC spectra were obtained with a Bruker AVANCE NEO 500MHz spectrometer (Bruker, Karlsruhe, Germany) equipped with 5 mm TCI cryoprobe, at 303 K. About 8 mg of sample were dissolved in 0.6 mL of deuterium oxide (D_2O). C-TSP samples was stirred overnight to ensure a complete solubilization before transfer in a 5 mm NMR tube for the analysis.

^{1}H NMR were acquired with pre-saturation of residual HOD, using the Bruker zgcppr pulse program, with the following parameters: number of scans 16, relaxation delay 12 s D1, time domain 32 k points and a spectral width of 18 ppm with transmitter offset 4.7 ppm.

^{1}H-^{13}C HSQC were acquired using Bruker hsqcedetgpsisp2.2 pulse program, with the following parameters: number of scans 32, dummy scan 16, relaxation delay 2 s, time domain 2048 (F2) and 256 (F1), spectral width 9.9 ppm (F2) and 160 ppm (F1), transmitter offset 4.7 ppm (F2) and 80 ppm (F1).

Hydrolyzed with xyloglucanase C-TSPs samples ^{1}H and ^{1}H-^{13}C HSQC spectra were obtained with a Bruker AVANCE NEO 500MHz spectrometer (Bruker, Karlsruhe, Germany) equipped with 5 mm TCI cryoprobe, at 298 K. About 20 mg of sample were dissolved in 0.6 mL of deuterium oxide (D_2O) and transferred in a 5 mm NMR tube for the analysis.

^{1}H NMR was acquired with presaturation of residual HOD, using the Bruker noesypr1d pulse program, with the following parameters: number of scans 16-32, relaxation delay 20 s D1, time domain 32-65 k points and a spectral width of 16-23 ppm with transmitter offset 4.7 ppm.

^{1}H-^{13}C HSQC were acquired using Bruker hsqcedetgpsisp2.2 pulse program, with the following parameters: number of scans 24, dummy scan 16, relaxation delay 2 s, time domain 1024 (F2) and 320 (F1), spectral width 7.9 ppm (F2) and 120 ppm (F1), transmitter offset 4.7 ppm (F2) and 75 ppm (F1).

^{1}H-^{13}C HSQC-DEPT of hydrolyzed C-TSP_C were acquired using Bruker hsqcedetgpsisp2.2 pulse program, with the following parameters: number of scans 16,

dummy scan 16, relaxation delay 2 s, time domain 1024 (F2) and 1024 (F1), spectral width 7.9 ppm (F2) and 140 ppm (F1), transmitter offset 4.7 ppm (F2) and 70 ppm (F1). BDDE and BDPE ^{13}C and ^{1}H-^{13}C HSQC spectra were obtained with a AVANCE IIIHD 500MHz spectrometer (Bruker, Karlsruhe, Germany) equipped with a 5 mm BBO probe, at 303 K. About 15 μL of BDDE were dissolved in 0.6 mL of deuterium oxide (D_2O) and transferred in a 5 mm NMR tube for the analysis. To obtain BDPE 50 μL of NaOD were added to the tube contained the BDDE and left for 30' under agitation before the measurement.

^{13}C NMR was acquired using the Bruker zgig pulse program, with the following parameters: number of scans 32-512, relaxation delay 3 s D1, time domain 32 k points and a spectral width of 301 ppm with transmitter offset 90 ppm.

^{1}H-^{13}C HSQC were acquired using Bruker hsqcedetgpsisp2.2 pulse program, with the following parameters: number of scans 4, dummy scan 16, relaxation delay 3 s, time domain 1024 (F2) and 128 (F1), spectral width 7.9 ppm (F2) and 160 ppm (F1), transmitter offset 4.7 ppm (F2) and 70 ppm (F1).

All the spectra were processed with BrukerTopspin software version 4.1.1.

3.10.2.7. Swelling rate

The powdered samples (50-100 mg) are placed into a metallic filter, with fine meshes, with a known weight, and the filter is dipped in about 450 mL of deionized water for a prescribed period of 24 hours. Then the filter is dripped for two minutes to remove excessive fluid and weighted. The swelling ratio (SR) at time *t* is calculated using the following equation (12):

$$SR\ (g/g) = \frac{W_s}{W_d} \qquad (12)$$

where W_s is the weight of the swollen sample, W_d is the weight of the dry sample. The measurements were made in triplicate.

3.10.2.8. Enzymatic depolymerization

Enzymatic depolymerizations were carried out using Xyloglucanase (GH5) form *Paenibacillus* sp. The depolymerization of TSP and C-TSP was performed adapting the method used by Zhang and Ai (Zhang, et al., 2020). C-TSPs were solubilized at the

concentration of 10 mg/mL in deionized water at 40°C, dissolving 50 mg of C-TSP in 5 mL of deionized water overnight. Then, 25 µL of xyloglucanase (*Paenibacillus* sp., 20 U) were added to the solution for TSP and 50 µL. After 24 h, the reaction mixture was heated at 100°C for 10 min to inactivate the enzyme, centrifugated at 8000 rpm for 15' to precipitate the enzyme, and then the supernatant collected was lyophilized.

3.10.2.9. MALDI-TOF analysis

The MALDI-MS analysis of polysaccharides was performed on a timsTOF MALDI-2 fleX mass spectrometer (Bruker Daltonik, Bremen, Germany). Polysaccharide fractions were dissolved in methanol:water (1:1, v/v), premixed 1:1 (v/v) with a 10 mg/ml solution of dihydroxybenzoic acid (DHB) in methanol:water (1:1, v/v), and spotted on the MALDI target plate. Ionization was achieved using a Bruker SmartBeam 3D laser system, applying a 26 × 26 µm beam scan range and operated at 10 kHz with 200 shots, and 55% laser power. The analysis of the samples was conducted using the following parameters reported in Table 3-10:

Table 3-10. *Parameters for the analysis MALDI-TOF of TSP, C-TSP_A, C-TSP_B and C-TSP_C.*

Parameter	TSP	C_TSP_A	C_TSP_B	C_TSP_C
Spot location	A6	A3	A5	A2
Ion mode	POS	POS	POS	POS
m/z range	100-2500	100-2500	100-6000	100-6000
MALDI plate offset (V)	50	50	50	50
Deflection 1 Delta (V)	70	70	70	70
Funnel 1 RF (Vpp)	300	300	300	300
Funnel 2 RF (Vpp)	350	350	350	350
Multipole RF (Vpp)	400	350	400	400
Collision cell energy (eV)	10	10	10	10
Collision cell RF (Vpp)	2000	1500	2000	2000
Quad energy (eV)	5	5	5	5
Lowest quad mass	100	100	100	100
Transfer time (µs)	80	80	80	100
Pre-pulse storage (µs)	10	10	10	10

All the spectra were processed with mzmine software version 4.7.8. (Heuckeroth et al., 2024).

3.10.2.10. Cell culture

Caco-2 cells (ATCC HTB-37) were cultured in Dulbecco's Modified Eagle Medium (DMEM) supplemented with 10% fetal bovine serum (FBS), 1% non-essential amino acids, 2 mM L-glutamine, and 1% penicillin-streptomycin. Cells were maintained at 37°C in a humidified atmosphere containing 5% CO_2. The culture medium was renewed every 2–3 days.

3.10.2.11. Monolayer formation

For permeability assays, Caco-2 cells were seeded onto Transwell® inserts (polycarbonate membrane, pore size 0.4 µm, 24-well format) at a density of 1×10^5 cells per insert. Cells were cultured for 21 days to allow differentiation and the formation of tight junctions. Monolayer integrity was monitored by measuring transepithelial electrical resistance (TEER) using an epithelial voltohmmeter. Only monolayers with TEER values ≥500 Ω·cm² were used for experiments.

3.10.2.12. Treatment Protocol

After the differentiation period, monolayers were treated for 24 hours with lipopolysaccharide (LPS, 10 µg/mL; Sigma-Aldrich), either alone or in combination with test substances C-TSP_A, C-TSP_B, and C-TSP_C, each applied at a final concentration of 1% (v/v). The TSP compounds were previously solubilized overnight in complete culture medium under constant agitation at room temperature to ensure complete dissolution. Control wells received vehicle treatment.

3.10.2.13. Measurement of Transepithelial Electrical Resistance (TEER)

At the end of the 24-hour treatment, TEER was measured again to assess the impact on epithelial barrier integrity. Values were corrected for blank insert resistance and expressed as Ω·cm².

3.10.2.14. FITC-Dextran Permeability Assay

Paracellular permeability was evaluated using fluorescein isothiocyanate-labeled dextran (FITC-dextran, 4 kDa; Sigma-Aldrich). Monolayers were washed twice with pre-warmed Hank's Balanced Salt Solution (HBSS) and equilibrated for 30 minutes at 37°C. FITC-dextran was added to the apical compartment at a final concentration of 1 mg/mL in HBSS, while the basolateral compartment received fresh HBSS. After incubation (30, 60, 120, 180, 240 minutes), 100 µL samples were collected from the basolateral side and replaced with fresh buffer. Fluorescence intensity was measured using a microplate reader (excitation 485 nm, emission 530 nm).

3.10.2.15. Cell Viability Assay (MTT)

Cell viability was assessed using the MTT assay. After the 24-hour treatment, Caco-2 cells in Transwell inserts were incubated with MTT solution (0.5 mg/mL in serum-free DMEM) for 3 hours at 37°C. Subsequently, the medium was removed, and the formazan crystals formed were dissolved by adding 600 µL of DMSO to each insert. The solution was transferred to a 96-well plate, and absorbance was measured at 570 nm using a microplate reader. Results were expressed as a percentage of viable cells compared to the untreated control.

3.10.2.16. Data analysis

Statistical analyses were performed using one-way ANOVA, followed by Bonferroni post-test. Data are presented as mean ± standard error of the mean (SEM), and statistical significance was defined as $p < 0.05$.

CHAPTER 4 – CONCLUSION AND FUTURE PERSPECTIVE

During this PhD project, chemical modifications of TSP were performed to enhance physical, chemical and biological properties of this polysaccharide and expand its potential applications. Sulfation was carried out to improve the solubility of TSP by introducing negatively charged groups, and to increase its antibacterial, antiviral and anti-inflammatory properties, which are typical characteristics of sulfated polysaccharides.

Sulfated samples with different degrees of sulfation were obtained. These samples exhibited higher solubility compared to native TSP, with a higher molecular weight proportional to the degree of sulfation, a decrease in dynamic viscosity with increasing sulfation of the repetitive unit, and no ocular irritation. The sulfated samples also maintained the mucoadhesive properties of TSP, due to electrostatic interactions between the charged domains of the glycoprotein mucin and the sulfated groups.

Furthermore, TSP was crosslinked using BDDE, a biodegradable and safe crosslinker, to improve the rheological properties and the residence time in biological systems. Both viscous-like and gel-like samples were synthetized. The viscous-like samples displayed similar physical properties similar to TSP, while gel-like samples exhibited higher viscosity, greater swelling capability and a potential barrier-like role in intestinal under inflammatory conditions.

In conclusion, the main goal of this PhD project, to synthetize and characterize TSP modified samples with properties different from the native polysaccharide, was successfully achieved.

In the future, these products will be tested in different eye drops formulations to investigate whether they offer improved effects for treatment of Dry Eye Disease compared to native TSP.

Moreover, the combination of the two chemical modifications, sulfation and crosslinking, will be investigated. Specifically, soluble, viscous-like crosslinked samples will be sulfated with the same method applied to TSP and sulfated samples will be further crosslinked with the BDDE. Their physico-chemical properties and biological activity will be studied to determine whether the combined modifications result in enhanced properties and synergistic improvements compared to individual modification.

Finally, an industrial scale up of the production of the modified samples will be investigated to evaluate process stability, scalability and cost-effectiveness for potential industrial production.

CHAPTER 5 – BIBLIOGRAPHY

Adler, S., Basketter, D., Creton, S., Pelkonen, O., van Benthem, J., Zuang, V., Andersen, K. E., Angers-Loustau, A., Aptula, A., Bal-Price, A., Benfenati, E., Bernauer, U., Bessems, J., Bois, F. Y., Boobis, A., Brandon, E., Bremer, S., Broschard, T., Casati, S., … Zaldivar, J.-M. (2011). Alternative (non-animal) methods for cosmetics testing: Current status and future prospects-2010. *Archives of Toxicology*, *85*(5), 367–485. https://doi.org/10.1007/s00204-011-0693-2

Alavarse, A. C., Frachini, E. C. G., da Silva, R. L. C. G., Lima, V. H., Shavandi, A., & Petri, D. F. S. (2022). Crosslinkers for polysaccharides and proteins: Synthesis conditions, mechanisms, and crosslinking efficiency, a review. *International Journal of Biological Macromolecules*, *202*, 558–596. https://doi.org/10.1016/j.ijbiomac.2022.01.029

Alba, K., & Kontogiorgos, V. (2021). Chapter 2—Techniques for the chemical and physicochemical characterization of polysaccharides. In G. O. Phillips & P. A. Williams (Eds.), *Handbook of Hydrocolloids (Third Edition)* (pp. 27–74). Woodhead Publishing. https://doi.org/10.1016/B978-0-12-820104-6.00026-7

Alba, K., MacNaughtan, W., Laws, A. P., Foster, T. J., Campbell, G. M., & Kontogiorgos, V. (2018). Fractionation and characterisation of dietary fibre from blackcurrant pomace. *Food Hydrocolloids*, *81*, 398–408. https://doi.org/10.1016/j.foodhyd.2018.03.023

Alekseeva, A., Raman, R., Eisele, G., Clark, T., Fisher, A., Lee, S. L., Jiang, X., Torri, G., Sasisekharan, R., & Bertini, S. (2020). In-depth structural characterization of pentosan polysulfate sodium complex drug using orthogonal analytical tools. *Carbohydrate Polymers*, *234*, 115913. https://doi.org/10.1016/j.carbpol.2020.115913

Alépée, N., Leblanc, V., Adriaens, E., Grandidier, M. H., Lelièvre, D., Meloni, M., Nardelli, L., Roper, C. S., Santirocco, E., Toner, F., Van Rompay, A., Vinall, J., & Cotovio, J. (2016). Multi-laboratory validation of SkinEthic HCE test method for testing serious eye damage/eye irritation using liquid chemicals. *Toxicology in Vitro: An International Journal Published in Association with BIBRA*, *31*, 43–53. https://doi.org/10.1016/j.tiv.2015.11.012

Alotaibi, W. M., Abusharha, A., Pearce, E. I., Althomali, M., Afsar, T., & Razak, S. (2024). Assessment of Tamarind Seed Polysaccharide (TSP) and Hyaluronic Acid (HA) Containing Ophthalmic Solution to Maintain Tear Osmolarity, Ocular Surface

Temperature (OST) and Tear Production. *Clinical Ophthalmology*, *18*, 3503–3513. https://doi.org/10.2147/OPTH.S493336

Al-Sibani, M., Al-Harrasi, A., & Neubert, R. H. H. (2016). Study of the effect of mixing approach on cross-linking efficiency of hyaluronic acid-based hydrogel cross-linked with 1,4-butanediol diglycidyl ether. *European Journal of Pharmaceutical Sciences*, *91*, 131–137. https://doi.org/10.1016/j.ejps.2016.06.010

Amnuaikit, T., Khakhong, S., & Khongkow, P. (2019). Formulation Development and Facial Skin Evaluation of Serum Containing Jellose from Tamarind Seeds. *Journal of Pharmaceutical Research International*, 1–14. https://doi.org/10.9734/jpri/2019/v31i430306

Apperley, D. C., Harris, R. K., & Hodgkinson, P. (2012). *Solid-State NMR: Basic Principles and Practice*. Momentum Press. https://research.ebsco.com/linkprocessor/plink?id=ba7bccfc-a549-38c5-ba93-e029996b236f

Arruda, I. R. S., Albuquerque, P. B. S., Santos, G. R. C., Silva, A. G., Mourão, P. A. S., Correia, M. T. S., Vicente, A. A., & Carneiro-da-Cunha, M. G. (2015). Structure and rheological properties of a xyloglucan extracted from *Hymenaea courbaril* var. *Courbaril* seeds. *International Journal of Biological Macromolecules*, *73*, 31–38. https://doi.org/10.1016/j.ijbiomac.2014.11.001

Artursson, P., Palm, K., & Luthman, K. (2001). Caco-2 monolayers in experimental and theoretical predictions of drug transport1. *Advanced Drug Delivery Reviews*, *46*(1), 27–43. https://doi.org/10.1016/S0169-409X(00)00128-9

Bai, S., Wang, W., & Dybowski, C. (2010). Solid State NMR Spectroscopy. *Analytical Chemistry*, *82*(12), 4917–4924. https://doi.org/10.1021/ac100761m

Bedini, E., Laezza, A., Parrilli, M., & Iadonisi, A. (2017). A review of chemical methods for the selective sulfation and desulfation of polysaccharides. *Carbohydrate Polymers*, *174*, 1224–1239. https://doi.org/10.1016/j.carbpol.2017.07.017

Benalaya, I., Alves, G., Lopes, J., & Silva, L. R. (2024). A Review of Natural Polysaccharides: Sources, Characteristics, Properties, Food, and Pharmaceutical Applications. *International Journal of Molecular Sciences*, *25*(2), 1322. https://doi.org/10.3390/ijms25021322

Berezhnaya, Y. D., Kazachenko, A. S., Kazachenko, A. S., Malyar, Y. N., & Borovkova, V. S. (2024). Sulfation of Various Polysaccharide Structures: Different Methods and Perspectives. *Chemistry*, *6*(4), Article 4. https://doi.org/10.3390/chemistry6040038

Berne, B. J., & Pecora, R. (2013). *Dynamic Light Scattering: With Applications to Chemistry, Biology, and Physics*. Courier Corporation.

Berthomieu, C., & Hienerwadel, R. (2009). Fourier transform infrared (FTIR) spectroscopy. *Photosynthesis Research*, *101*(2), 157–170. https://doi.org/10.1007/s11120-009-9439-x

Bertini, S., Fareed, J., Madaschi, L., Risi, G., Torri, G., & Naggi, A. (2017). Characterization of PF4-Heparin Complexes by Photon Correlation Spectroscopy and Zeta Potential. *Clinical and Applied Thrombosis/Hemostasis: Official Journal of the International Academy of Clinical and Applied Thrombosis/Hemostasis*, *23*(7), 725–734. https://doi.org/10.1177/1076029616685430

Blanco, A., García-Abuín, A., Gómez-Díaz, D., & Navaza, J. M. (2013). Physicochemical characterization of chitosan derivatives. *CyTA - Journal of Food*, *11*(2), 190–197. https://doi.org/10.1080/19476337.2012.722565

Bouhlal, R., Haslin, C., Chermann, J.-C., Colliec-Jouault, S., Sinquin, C., Simon, G., Cerantola, S., Riadi, H., & Bourgougnon, N. (2011). Antiviral Activities of Sulfated Polysaccharides Isolated from Sphaerococcus coronopifolius (Rhodophytha, Gigartinales) and Boergeseniella thuyoides (Rhodophyta, Ceramiales). *Marine Drugs*, *9*(7), Article 7. https://doi.org/10.3390/md9071187

Bragd, P. L., van Bekkum, H., & Besemer, A. C. (2004). TEMPO-Mediated Oxidation of Polysaccharides: Survey of Methods and Applications. *Topics in Catalysis*, *27*(1), 49–66. https://doi.org/10.1023/B:TOCA.0000013540.69309.46

Buranaamnuay, K. (2021). The MTT assay application to measure the viability of spermatozoa: A variety of the assay protocols. *Open Veterinary Journal*, *11*(2), 251–269. https://doi.org/10.5455/OVJ.2021.v11.i2.9

Caputo, H. E., Straub, J. E., & Grinstaff, M. W. (2019). Design, synthesis, and biomedical applications of synthetic sulphated polysaccharides. *Chemical Society Reviews*, *48*(8), 2338–2365. https://doi.org/10.1039/C7CS00593H

Chakka, V. P., & Zhou, T. (2020). Carboxymethylation of polysaccharides: Synthesis and bioactivities. *International Journal of Biological Macromolecules*, *165*(Pt B), 2425–2431. https://doi.org/10.1016/j.ijbiomac.2020.10.178

Chawananorasest, K., Saengtongdee, P., & Kaemchantuek, P. (2016). Extraction and Characterization of Tamarind (Tamarind indica L.) Seed Polysaccharides (TSP) from Three Difference Sources. *Molecules*, *21*(6), Article 6. https://doi.org/10.3390/molecules21060775

Chen, X., Shen, M., Yu, Q., Chen, Y., & Xie, J. (2024). Recent advance in chemistry modified methods of natural polysaccharides and their applications. *Trends in Food Science & Technology*, *144*, 104317. https://doi.org/10.1016/j.tifs.2023.104317

Cheng, H. N., & and Neiss, T. G. (2012). Solution NMR Spectroscopy of Food Polysaccharides. *Polymer Reviews*, *52*(2), 81–114. https://doi.org/10.1080/15583724.2012.668154

Chiaregato, C. G., França, D., Messa, L. L., dos Santos Pereira, T., & Faez, R. (2022). A review of advances over 20 years on polysaccharide-based polymers applied as enhanced efficiency fertilizers. *Carbohydrate Polymers*, *279*, 119014. https://doi.org/10.1016/j.carbpol.2021.119014

Chinta, M. L., Gandam, P. K., Sivasankar, M. V., & Parcha, S. R. (2025). Tamarind *(Tamarindus indica L.)* Seed Polysaccharide: A promising biopolymer for drug delivery, wound healing, tissue engineering and beyond. *Carbohydrate Research*, *552*, 109454. https://doi.org/10.1016/j.carres.2025.109454

Crispín-Isidro, G., Hernández-Rodríguez, L., Ramírez-Santiago, C., Sandoval-Castilla, O., Lobato-Calleros, C., & Vernon-Carter, E. J. (2019). Influence of purification on physicochemical and emulsifying properties of tamarind (*Tamarindus indica* L.) seed gum. *Food Hydrocolloids*, *93*, 402–412. https://doi.org/10.1016/j.foodhyd.2019.02.046

Cui, H., Ai, L., Xiong, Z., Song, Z., Yuan, C., & Zhang, H. (2024). Synthesis and characterization of cationic tamarind seed polysaccharide: An effective flocculating agent. *Colloids and Surfaces A: Physicochemical and Engineering Aspects*, *696*, 134404. https://doi.org/10.1016/j.colsurfa.2024.134404

da Silva, A. C. C., de Almeida, R. R., Vidal, C. S., Neto, J. F. C., da Cruz Sousa, A. C., Martínez, F. N. A., Pinheiro, D. P., Sales, S. L. A., Pessoa, C., Denardin, J. C., de Morais, S. M., & Ricardo, N. M. P. S. (2022). Sulfated xyloglucan-based magnetic nanocomposite for preliminary evaluation of theranostic potential. *International Journal of Biological Macromolecules*, *216*, 520–527. https://doi.org/10.1016/j.ijbiomac.2022.06.197

Damiri, F., Fatimi, A., Liu, Y., Musuc, A. M., Fajardo, A. R., Gowda, B. H. J., Vora, L. K., Shavandi, A., & Okoro, O. V. (2025). Recent advances in 3D bioprinted polysaccharide hydrogels for biomedical applications: A comprehensive review. *Carbohydrate Polymers*, *348*, 122845. https://doi.org/10.1016/j.carbpol.2024.122845

De Boulle, K., Glogau, R., Kono, T., Nathan, M., Tezel, A., Roca-Martinez, J.-X., Paliwal, S., & Stroumpoulis, D. (2013). A review of the metabolism of 1,4-butanediol diglycidyl ether-crosslinked hyaluronic acid dermal fillers. *Dermatologic Surgery:*

Official Publication for American Society for Dermatologic Surgery [et Al.], *39*(12), 1758–1766. https://doi.org/10.1111/dsu.12301

de Oliveira Cardoso, V. M., Gremião, M. P. D., & Cury, B. S. F. (2020). Mucin-polysaccharide interactions: A rheological approach to evaluate the effect of pH on the mucoadhesive properties. *International Journal of Biological Macromolecules*, *149*, 234–245. https://doi.org/10.1016/j.ijbiomac.2020.01.235

Dehabadi, L., & Wilson, L. D. (2014). Polysaccharide-based materials and their adsorption properties in aqueous solution. *Carbohydrate Polymers*, *113*, 471–479. https://doi.org/10.1016/j.carbpol.2014.06.083

Deng, Q., Wang, X., Chen, H., Zhao, C., Gong, X., & Zhou, X. (2020). Structural characterization, modification and hepatoprotective effects of polysaccharide from *Mori Fructus*. *International Journal of Biological Macromolecules*, *153*, 357–363. https://doi.org/10.1016/j.ijbiomac.2020.02.300

Dharmaraja, A. T. (2017). Role of Reactive Oxygen Species (ROS) in Therapeutics and Drug Resistance in Cancer and Bacteria. *Journal of Medicinal Chemistry*, *60*(8), 3221–3240. https://doi.org/10.1021/acs.jmedchem.6b01243

Doneanu, C. E., Chen, W., & Gebler, J. C. (2009). Analysis of oligosaccharides derived from heparin by ion-pair reversed-phase chromatography/mass spectrometry. *Analytical Chemistry*, *81*(9), 3485–3499. https://doi.org/10.1021/ac802770r

Dumitriu, S. (Ed.). (2004). *Polysaccharides: Structural Diversity and Functional Versatility, Second Edition* (2nd ed.). CRC Press. https://doi.org/10.1201/9781420030822

Dunleavy, K. A., Raffals, L. E., & Camilleri, M. (2023). Intestinal Barrier Dysfunction in Inflammatory Bowel Disease: Underpinning Pathogenesis and Therapeutics. *Digestive Diseases and Sciences*, *68*(12), 4306–4320. https://doi.org/10.1007/s10620-023-08122-w

Ediriweera, M. K., Tennekoon, K. H., & Samarakoon, S. R. (2019). In vitro assays and techniques utilized in anticancer drug discovery. *Journal of Applied Toxicology*, *39*(1), 38–71. https://doi.org/10.1002/jat.3658

Eisele, G., Alekseeva, A., Bertini, S., Gardini, C., Paganini, D., Fonseca, E. C. M., Guerrini, M., & Naggi, A. (2023). Further advances in identification of pentosan polysulfate monosaccharide composition by NMR. *Journal of Pharmaceutical and Biomedical Analysis*, *235*, 115672. https://doi.org/10.1016/j.jpba.2023.115672

Ejaz, U., Sohail, M., & Ghanemi, A. (2021). Cellulases: From Bioactivity to a Variety of Industrial Applications. *Biomimetics (Basel, Switzerland)*, *6*(3), 44. https://doi.org/10.3390/biomimetics6030044

Esposito, L., Barbosa, A. I., Moniz, T., Costa Lima, S., Costa, P., Celia, C., & Reis, S. (2020). Design and Characterization of Sodium Alginate and Poly(vinyl) Alcohol Hydrogels for Enhanced Skin Delivery of Quercetin. *Pharmaceutics*, *12*(12), Article 12. https://doi.org/10.3390/pharmaceutics12121149

Faivre, J., Pigweh, A. I., Iehl, J., Maffert, P., Goekjian, P., & Bourdon, F. (2021). Crosslinking hyaluronic acid soft-tissue fillers: Current status and perspectives from an industrial point of view. *Expert Review of Medical Devices*, *18*(12), 1175–1187. https://doi.org/10.1080/17434440.2021.2014320

Fallacara, A., Manfredini, S., Durini, E., & Vertuani, S. (2017). Hyaluronic Acid Fillers in Soft Tissue Regeneration. *Facial Plastic Surgery: FPS*, *33*(1), 87–96. https://doi.org/10.1055/s-0036-1597685

Fan, S., Zhang, J., Nie, W., Zhou, W., Jin, L., Chen, X., & Lu, J. (2017). Antitumor effects of polysaccharide from *Sargassum fusiforme* against human hepatocellular carcinoma HepG2 cells. *Food and Chemical Toxicology*, *102*, 53–62. https://doi.org/10.1016/j.fct.2017.01.020

Feng, X., Huang, G., Qiu, J., Peng, L., Luo, K., Liu, D., & Han, P. (2023). Dynamic light scattering in flowing dispersion. *Optics Communications*, *531*. https://doi.org/10.1016/j.optcom.2022.129225

Fenn, L. S., & McLean, J. A. (2011). Structural resolution of carbohydrate positional and structural isomers based on gas-phase ion mobility-mass spectrometry. *Physical Chemistry Chemical Physics: PCCP*, *13*(6), 2196–2205. https://doi.org/10.1039/c0cp01414a

Ferreira, L. M. B., Cardoso, V. M. O., dos Santos Pedriz, I., Souza, M. P. C., Ferreira, N. N., Chorilli, M., Gremião, M. P. D., & Zucolotto, V. (2023). Understanding mucus modulation behavior of chitosan oligomers and dextran sulfate combining light scattering and calorimetric observations. *Carbohydrate Polymers*, *306*, 120613. https://doi.org/10.1016/j.carbpol.2023.120613

Fidalgo, J., Deglesne, P.-A., Arroyo, R., Sepúlveda, L., Ranneva, E., & Deprez, P. (2018). Detection of a new reaction by-product in BDDE cross-linked autoclaved hyaluronic acid hydrogels by LC-MS analysis. *Medical Devices (Auckland, N.Z.)*, *11*, 367–376. https://doi.org/10.2147/MDER.S166999

Foston, M. (2014). Advances in solid-state NMR of cellulose. *Current Opinion in Biotechnology*, *27*, 176–184. https://doi.org/10.1016/j.copbio.2014.02.002

Gandhi, N. S., & Mancera, R. L. (2008). The Structure of Glycosaminoglycans and their Interactions with Proteins. *Chemical Biology & Drug Design*, *72*(6), 455–482. https://doi.org/10.1111/j.1747-0285.2008.00741.x

Gao, X., Qu, H., Gao, Z., Zeng, D., Wang, J., Baranenko, D., Li, Y., & Lu, W. (2019). Protective effects of *Ulva pertusa* polysaccharide and polysaccharide-iron (III) complex on cyclophosphamide induced immunosuppression in mice. *International Journal of Biological Macromolecules*, *133*, 911–919. https://doi.org/10.1016/j.ijbiomac.2019.04.101

Gardini, C., Bisio, A., Mazzini, G., Guerrini, M., Naggi, A., & Alekseeva, A. (2021). Saturated tetrasaccharide profile of enoxaparin. An additional piece to the heparin biosynthesis puzzle. *Carbohydrate Polymers*, *273*, 118554. https://doi.org/10.1016/j.carbpol.2021.118554

Geethalaxmi, M., Sunil, C. K., & Venkatachalapathy, N. (2024). Tamarind seed polysaccharides, proteins, and mucilage: Extraction, modification of properties, and their application in food. *Sustainable Food Technology*, *2*(6), 1670–1685. https://doi.org/10.1039/D4FB00224E

Ghaffaripour, S., Van den Bilcke, N., & Samson, R. (2017). The importance of seed reserve on performance and breeding of tamarind seedlings. *Scientia Horticulturae*, *222*, 145–152. https://doi.org/10.1016/j.scienta.2017.04.032

Ghasemi, M., Turnbull, T., Sebastian, S., & Kempson, I. (2021). The MTT Assay: Utility, Limitations, Pitfalls, and Interpretation in Bulk and Single-Cell Analysis. *International Journal of Molecular Sciences*, *22*(23), 12827. https://doi.org/10.3390/ijms222312827

Ghiorghita, C.-A., Dinu, M. V., Lazar, M. M., & Dragan, E. S. (2022). Polysaccharide-Based Composite Hydrogels as Sustainable Materials for Removal of Pollutants from Wastewater. *Molecules*, *27*(23), Article 23. https://doi.org/10.3390/molecules27238574

Glish, G. L., & Vachet, R. W. (2003). The basics of mass spectrometry in the twenty-first century. *Nature Reviews Drug Discovery*, *2*(2), 140–150. https://doi.org/10.1038/nrd1011

Goldstein, J., Newbury, D. E., Joy, D. C., Lyman, C. E., Echlin, P., Lifshin, E., Sawyer, L., & Michael, J. R. (2012). *Scanning Electron Microscopy and X-Ray Microanalysis: Third Edition*. Springer Science & Business Media.

Gopinath, V., Kamath, S. M., Priyadarshini, S., Chik, Z., Alarfaj, A. A., & Hirad, A. H. (2022). Multifunctional applications of natural polysaccharide starch and cellulose: An update on recent advances. *Biomedicine & Pharmacotherapy*, *146*, 112492. https://doi.org/10.1016/j.biopha.2021.112492

Gopinath, V., Saravanan, S., Al-Maleki, A. R., Ramesh, M., & Vadivelu, J. (2018). A review of natural polysaccharides for drug delivery applications: Special focus on cellulose, starch and glycogen. *Biomedicine & Pharmacotherapy*, *107*, 96–108. https://doi.org/10.1016/j.biopha.2018.07.136

Graça, A., Gonçalves, L. M., Raposo, S., Ribeiro, H. M., & Marto, J. (2018). Useful In Vitro Techniques to Evaluate the Mucoadhesive Properties of Hyaluronic Acid-Based Ocular Delivery Systems. *Pharmaceutics*, *10*(3), Article 3. https://doi.org/10.3390/pharmaceutics10030110

Guo, Q., Ai, L., & Cui, S. (2019). *Methodology for Structural Analysis of Polysaccharides* (1st ed. 2018 edition). Springer.

Guo, R., Li, X., Sun, X., Kou, Y., Zhang, J., Li, D., Liu, Y., Zhao, T., Zhang, H., Song, Z., & Wu, Y. (2022). Molecular aggregation *via* partial Gal removal affects physicochemical and macromolecular properties of tamarind kernel polysaccharides. *Carbohydrate Polymers*, *285*, 119264. https://doi.org/10.1016/j.carbpol.2022.119264

Han, C. D. (2007). *Rheology and Processing of Polymeric Materials: Volume 2: Polymer Processing*. Oxford University Press, USA.

Hans, N., Malik, A., & Naik, S. (2021). Antiviral activity of sulfated polysaccharides from marine algae and its application in combating COVID-19: Mini review. *Bioresource Technology Reports*, *13*, 100623. https://doi.org/10.1016/j.biteb.2020.100623

Heuckeroth, S., Damiani, T., Smirnov, A., Mokshyna, O., Brungs, C., Korf, A., Smith, J. D., Stincone, P., Dreolin, N., Nothias, L.-F., Hyötyläinen, T., Orešič, M., Karst, U., Dorrestein, P. C., Petras, D., Du, X., van der Hooft, J. J. J., Schmid, R., & Pluskal, T. (2024). Reproducible mass spectrometry data processing and compound annotation in MZmine 3. *Nature Protocols*, *19*(9), 2597–2641. https://doi.org/10.1038/s41596-024-00996-y

Hoffmann, E. de, & Stroobant, V. (2007). *Mass spectrometry: Principles and applications* (Third edition, Vol. 1–1 online resource (xii, 489 pages) : illustrations). J. Wiley.

http://www.dawsonera.com/depp/reader/protected/external/AbstractView/S9780470512135

Huang, X., Ai, C., Yao, H., Zhao, C., Xiang, C., Hong, T., & Xiao, J. (2022). Guideline for the extraction, isolation, purification, and structural characterization of polysaccharides from natural resources. *eFood*, *3*(6), e37. https://doi.org/10.1002/efd2.37

Irgens, F. (2013). *Rheology and Non-Newtonian Fluids*. Springer Science & Business Media.

Jabeen, N., & Atif, M. (2024). Polysaccharides based biopolymers for biomedical applications: A review. *Polymers for Advanced Technologies*, *35*(1), e6203. https://doi.org/10.1002/pat.6203

Jana, S., Mukherjee, S., Ribelato, E. V., Darido, M. L., Faccin-Galhardi, L. C., Ray, B., & Ray, S. (2021). The heparin-mimicking arabinogalactan sulfates from *Anogeissus latifolia* gum: Production, structures, and anti-herpes simplex virus activity. *International Journal of Biological Macromolecules*, *183*, 1419–1426. https://doi.org/10.1016/j.ijbiomac.2021.05.107

Jang, K., Hong, Y. E., Moon, Y., Jeon, S., Angalet, S., & Kweon, M. (2018). Exploring the applicability of tamarind gum for making gluten-free rice bread. *Food Science and Biotechnology*, *27*(6), 1639–1648. https://doi.org/10.1007/s10068-018-0416-z

Kailemia, M. J., Ruhaak, L. R., Lebrilla, C. B., & Amster, I. J. (2014). Oligosaccharide analysis by mass spectrometry: A review of recent developments. *Analytical Chemistry*, *86*(1), 196–212. https://doi.org/10.1021/ac403969n

Kang, J., Jia, X., Wang, N., Xiao, M., Song, S., Wu, S., Li, Z., Wang, S., Cui, S. W., & Guo, Q. (2022). Insights into the structure-bioactivity relationships of marine sulfated polysaccharides: A review. *Food Hydrocolloids*, *123*, 107049. https://doi.org/10.1016/j.foodhyd.2021.107049

Kaur, H., Yadav, S., Ahuja, M., & Dilbaghi, N. (2012). Synthesis, characterization and evaluation of thiolated tamarind seed polysaccharide as a mucoadhesive polymer. *Carbohydrate Polymers*, *90*(4), 1543–1549. https://doi.org/10.1016/j.carbpol.2012.07.028

Kenne, L., Gohil, S., Nilsson, E., Karlsson, A., Ericsson, D., Kenne, A., & Nord, L. (2013). Modification and cross-linking parameters in hyaluronic acid hydrogels-Definitions and analytical methods. *Carbohydrate Polymers*, *91*, 410–418. https://doi.org/10.1016/j.carbpol.2012.08.066

Khan, S. A., Khan, S. B., Khan, L. U., Farooq, A., Akhtar, K., & Asiri, A. M. (2018). Fourier Transform Infrared Spectroscopy: Fundamentals and Application in Functional Groups and Nanomaterials Characterization. In S. K. Sharma (Ed.), *Handbook of*

Materials Characterization (pp. 317–344). Springer International Publishing. https://doi.org/10.1007/978-3-319-92955-2_9

Khongkow, P., Khakhong, S., Thammarat, C., & Amnuaikit, T. (2024). Potential Bioactivities of Tamarind Seed Jellose at the Cellular Level for Cosmetic Product Development. *Sustainability*, *16*(8), Article 8. https://doi.org/10.3390/su16083114

Kohler, I., Verhoeven, M., Haselberg, R., & Gargano, A. F. G. (2022). Hydrophilic interaction chromatography – mass spectrometry for metabolomics and proteomics: State-of-the-art and current trends. *Microchemical Journal*, *175*, 106986. https://doi.org/10.1016/j.microc.2021.106986

Kwan, A., & Davidov-Pardo, G. (2018). Controlled release of flavor oil nanoemulsions encapsulated in filled soluble hydrogels. *Food Chemistry*, *250*, 46–53. https://doi.org/10.1016/j.foodchem.2017.12.089

La Gatta, A., Bedini, E., Aschettino, M., Finamore, R., & Schiraldi, C. (2022). Hyaluronan Hydrogels: Rheology and Stability in Relation to the Type/Level of Biopolymer Chemical Modification. *Polymers*, *14*(12), Article 12. https://doi.org/10.3390/polym14122402

Ladiè, R., Cosentino, C., Tagliaro, I., Antonini, C., Bianchini, G., & Bertini, S. (2021). Supramolecular Structuring of Hyaluronan-Lactose-Modified Chitosan Matrix: Towards High-Performance Biopolymers with Excellent Biodegradation. *Biomolecules*, *11*(3), Article 3. https://doi.org/10.3390/biom11030389

Lang, P., Masci, G., Dentini, M., Crescenzi, V., Cooke, D., Gidley, M. J., Fanutti, C., & Reid, J. S. G. (1992). Tamarind seed polysaccharide: Preparation, characterisation and solution properties of carboxylated, sulphated and alkylaminated derivatives. *Carbohydrate Polymers*, *17*(3), 185–198. https://doi.org/10.1016/0144-8617(92)90003-9

Larramendy, M., & Soloneski, S. (2018). *Genotoxicity: A Predictable Risk to Our Actual World*. BoD – Books on Demand.

Lee, J. H. (2018). Injectable hydrogels delivering therapeutic agents for disease treatment and tissue engineering. *Biomaterials Research*, *22*(1), 27. https://doi.org/10.1186/s40824-018-0138-6

Li, Z., & Lin, Z. (2021). Recent advances in polysaccharide-based hydrogels for synthesis and applications. *Aggregate*, *2*(2), e21. https://doi.org/10.1002/agt2.21

Liang, L., Ao, L., Ma, T., Ni, Y., Liao, X., Hu, X., & Song, Y. (2018). Sulfated modification and anticoagulant activity of pumpkin (*Cucurbita pepo*, Lady Godiva)

polysaccharide. *International Journal of Biological Macromolecules*, *106*, 447–455. https://doi.org/10.1016/j.ijbiomac.2017.08.035

Limsangouan, N., Milasing, N., Thongngam, M., Khuwijitjaru, P., & Jittanit, W. (2019). Physical and chemical properties, antioxidant capacity, and total phenolic content of xyloglucan component in tamarind (Tamarindus indica) seed extracted using subcritical water. *Journal of Food Processing and Preservation*, *43*(10). Scopus. https://doi.org/10.1111/jfpp.14146

Liu, T., Ren, Q., Wang, S., Gao, J., Shen, C., Zhang, S., Wang, Y., & Guan, F. (2023). Chemical Modification of Polysaccharides: A Review of Synthetic Approaches, Biological Activity and the Structure–Activity Relationship. *Molecules*, *28*(16), Article 16. https://doi.org/10.3390/molecules28166073

Liu, Y., Sun, Y., Li, D., Li, P., Yang, N., He, L., & Nishinari, K. (2024). Influence of Temperatures on Physicochemical Properties and Structural Features of Tamarind Seed Polysaccharide. *Molecules*, *29*(11), Article 11. https://doi.org/10.3390/molecules29112622

Liu, Z., Jiao, Y., Wang, Y., Zhou, C., & Zhang, Z. (2008). Polysaccharides-based nanoparticles as drug delivery systems. *Advanced Drug Delivery Reviews*, *60*(15), 1650–1662. https://doi.org/10.1016/j.addr.2008.09.001

London, J. (2022). *Analysis of Complex Polysaccharides of Biological and Industrial Relevance via Nuclear Magnetic Resonance Spectroscopy: Structure, Modification and Protein Interactions.* [Dphil, University of Liverpool]. https://livrepository.liverpool.ac.uk/3165135

Lough, W. J., & Wainer, I. W. (1995). *High Performance Liquid Chromatography: Fundamental Principles and Practice*. CRC Press.

Lynch, C., Kondiah, P. P. D., Choonara, Y. E., du Toit, L. C., Ally, N., & Pillay, V. (2019). Advances in Biodegradable Nano-Sized Polymer-Based Ocular Drug Delivery. *Polymers*, *11*(8), 1371. https://doi.org/10.3390/polym11081371

Madsen, F., Eberth, K., & Smart, J. D. (1998). A rheological examination of the mucoadhesive/mucus interaction: The effect of mucoadhesive type and concentration. *Journal of Controlled Release*, *50*(1), 167–178. https://doi.org/10.1016/S0168-3659(97)00138-7

Maiti, S., Maji, B., & Yadav, H. (2024). Progress on green crosslinking of polysaccharide hydrogels for drug delivery and tissue engineering applications. *Carbohydrate Polymers*, *326*, 121584. https://doi.org/10.1016/j.carbpol.2023.121584

Majeed, H., Bhatti, H. N., & Bhatti, I. A. (2019). Replacement of sodium alginate polymer, urea and sodium bicarbonate in the conventional reactive printing of cellulosic cotton. *Journal of Polymer Engineering*, *39*(7), 661–670. https://doi.org/10.1515/polyeng-2019-0076

Maji, B. (2019). 1—Introduction to natural polysaccharides. In S. Maiti & S. Jana (Eds.), *Functional Polysaccharides for Biomedical Applications* (pp. 1–31). Woodhead Publishing. https://doi.org/10.1016/B978-0-08-102555-0.00001-7

Malik, M., Steele, S. A., Mitra, D., Long, C. J., & Hickman, J. J. (2025). Trans-epithelial/endothelial electrical resistance (TEER): Current state of integrated TEER measurements in organ-on-a-chip devices. *Current Opinion in Biomedical Engineering*, *34*, 100588. https://doi.org/10.1016/j.cobme.2025.100588

Mallick, P. K. (2023). *Fundamentals of molecular spectroscopy* (Vol. 1–1 online resource (496 p.)). Springer. https://public.ebookcentral.proquest.com/choice/PublicFullRecord.aspx?p=30616862

Mansingh, B. B., Binoj, J. S., Sai, N. P., Hassan, S. A., Siengchin, S., Sanjay, M. R., & Liu, Y. C. (2021). Sustainable development in utilization of *Tamarindus indica* L. and its by-products in industries: A review. *Current Research in Green and Sustainable Chemistry*, *4*, 100207. https://doi.org/10.1016/j.crgsc.2021.100207

Manzoor, A., Dar, A. H., Pandey, V. K., Shams, R., Khan, S., Panesar, P. S., Kennedy, J. F., Fayaz, U., & Khan, S. A. (2022). Recent insights into polysaccharide-based hydrogels and their potential applications in food sector: A review. *International Journal of Biological Macromolecules*, *213*, 987–1006. https://doi.org/10.1016/j.ijbiomac.2022.06.044

Marathe, R. M., Annapure, U. S., Singhal, R. S., & Kulkarni, P. R. (2002). Gelling behaviour of polyose from tamarind kernel polysaccharide. *Food Hydrocolloids*, *16*(5), 423–426. https://doi.org/10.1016/S0268-005X(01)00118-7

Martins, A., Alves, C., Silva, J., Pinteus, S., Gaspar, H., & Pedrosa, R. (2023). Sulfated Polysaccharides from Macroalgae—A Simple Roadmap for Chemical Characterization. *Polymers*, *15*(2), Article 2. https://doi.org/10.3390/polym15020399

Mazepa, E., Biscaia, S. M. P., de L. Bellan, D., da S. Trindade, E., & Simas, F. F. (2022). Structural characteristics of native and chemically sulfated polysaccharides from seaweed and their antimelanoma effects. *Carbohydrate Polymers*, *289*, 119436. https://doi.org/10.1016/j.carbpol.2022.119436

Menchicchi, B., Fuenzalida, J. P., Hensel, A., Swamy, M. J., David, L., Rochas, C., & Goycoolea, F. M. (2015). Biophysical analysis of the molecular interactions between polysaccharides and mucin. *Biomacromolecules*, *16*(3), 924–935. https://doi.org/10.1021/bm501832y

Mezger, T. G. (2015). *Applied rheology: With Joe Flow on Rheology Road* (1st edition.). Anton Paar.

Mohammed, A. S. A., Naveed, M., & Jost, N. (2021). Polysaccharides; Classification, Chemical Properties, and Future Perspective Applications in Fields of Pharmacology and Biological Medicine (A Review of Current Applications and Upcoming Potentialities). *Journal of Polymers and the Environment*, *29*(8), 2359–2371. https://doi.org/10.1007/s10924-021-02052-2

Mohanty, S., Swarup, J., Priya, S., Jain, R., & Singhvi, G. (2024). Exploring the potential of polysaccharide-based hybrid hydrogel systems for their biomedical and therapeutic applications: A review. *International Journal of Biological Macromolecules*, *256*, 128348. https://doi.org/10.1016/j.ijbiomac.2023.128348

Moore, E. (2017). *Fourier transform infrared spectroscopy (FTIR): Methods, analysis, and research insights* (Vol. 1–1 online resource.). Nova Science Publishers, Inc. http://search.ebscohost.com/login.aspx?direct=true&scope=site&db=nlebk&db=nlabk&AN=1419216

Morales, D., Smiderle, F. R., Villalva, M., Abreu, H., Rico, C., Santoyo, S., Iacomini, M., & Soler-Rivas, C. (2019). Testing the effect of combining innovative extraction technologies on the biological activities of obtained β-glucan-enriched fractions from *Lentinula edodes*. *Journal of Functional Foods*, *60*, 103446. https://doi.org/10.1016/j.jff.2019.103446

Mori, S. (with Internet Archive). (1999). *Size exclusion chromatography*. Berlin ; New York : Springer. http://archive.org/details/sizeexclusionchr0000mori

Mukherjee, S., Jana, S., Khawas, S., Kicuntod, J., Marschall, M., Ray, B., & Ray, S. (2022). Synthesis, molecular features and biological activities of modified plant polysaccharides. *Carbohydrate Polymers*, *289*, 119299. https://doi.org/10.1016/j.carbpol.2022.119299

Mukherjee, S., Pujol, C. A., Jana, S., Damonte, E. B., Ray, B., & Ray, S. (2021). Chemically sulfated arabinoxylans from *Plantago ovata* seed husk: Synthesis, characterization and antiviral activity. *Carbohydrate Polymers*, *256*, 117555. https://doi.org/10.1016/j.carbpol.2020.117555

Muthukumar, J., Chidambaram, R., & Sukumaran, S. (2021). Sulfated polysaccharides and its commercial applications in food industries—A review. *Journal of Food Science and Technology*, *58*(7), 2453–2466. https://doi.org/10.1007/s13197-020-04837-0

Muthusamy, S., Udayakumar, G. P., & Narala, V. R. (2021). Recent advances in the extraction and characterization of seed polysaccharides, and their bioactivities: A review. *Bioactive Carbohydrates and Dietary Fibre*, *26*, 100276. https://doi.org/10.1016/j.bcdf.2021.100276

Nagar, C. K., Dash, S. K., & Rayaguru, K. (2022). Tamarind seed: Composition, applications, and value addition: A comprehensive review. *Journal of Food Processing & Preservation*, *46*(10), 1–18. https://doi.org/10.1111/jfpp.16872

Nakashima, A., Yamada, K., Iwata, O., Sugimoto, R., Atsuji, K., Ogawa, T., Ishibashi-Ohgo, N., & Suzuki, K. (2018). β-Glucan in Foods and Its Physiological Functions. *Journal of Nutritional Science and Vitaminology*, *64*(1), 8–17. https://doi.org/10.3177/jnsv.64.8

Ngo, D.-H., & Kim, S.-K. (2013). Sulfated polysaccharides as bioactive agents from marine algae. *International Journal of Biological Macromolecules*, *62*, 70–75. https://doi.org/10.1016/j.ijbiomac.2013.08.036

Ngohang, F. E., Gay, L., & Bourbigot, S. (2015). Smoke composition using MLC/FTIR/ELPI: Application to flame retarded ethylene vinyl acetate. *Polymer Degradation and Stability*, *115*. https://doi.org/10.1016/j.polymdegradstab.2015.03.002

Nguyen, M. T. H., Tran, C. V., Nguyen, P. H., Tran, Q. D., Kim, M.-S., Jung, W.-K., & Nguyen, P. T. M. (2021). In vitro osteogenic activities of sulfated derivative of polysaccharide extracted from Tamarindus indica L. *Biological Chemistry*, *402*(10), 1213–1224. https://doi.org/10.1515/hsz-2021-0200

Niu, C., Liu, Y., Yang, Y., Wang, R., & Li, T. (2023). Advances in sulfonated modification and bioactivity of polysaccharides. *International Journal of Biological Macromolecules*, *253*, 126400. https://doi.org/10.1016/j.ijbiomac.2023.126400

Nizzolo, S., Esposito, E., Ni, M.-H., Bertocchi, L., Bianchini, G., Freato, N., Zanzoni, S., Guerrini, M., & Bertini, S. (2024). A novel biomimetic probe for galectin-3 recognition: Chemical synthesis and structural characterization of a β-galactose branched sodium hyaluronate. *Proteoglycan Research*, *2*(1), e19. https://doi.org/10.1002/pgr2.19

Noraphaiphipaksa, N., Sochu, W., Manonukul, A., & Kanchanomai, C. (2016). Experimental and numerical investigations to determine the modulus and fracture

mechanics of tamarind seed (*Tamarindus indica* L.). *Biosystems Engineering*, *151*, 17–27. https://doi.org/10.1016/j.biosystemseng.2016.08.021

Nozari, N., & Ramin, S. (2021). The effect of tamarind seed polysaccharide containing eye drop in dry eye syndrome: Results of an interventional, comparative, clinical study. *Medical Hypothesis, Discovery & Innovation in Optometry*, *2*(2), Article 2. https://doi.org/10.51329/mehdioptometry128

Osborne-Richards, M., Ring, D., Wang, X., Wall, S., Edmondson, S., & Saunders, B. R. (2025). Converting high modulus water-based elastomeric core–shell nanoparticle films from viscoelastic to predominantly elastic using di-epoxide crosslinking. *Polymer Chemistry*, *16*(2), 181–191. https://doi.org/10.1039/D4PY01073F

Øvrebø, Ø., Giorgi, Z., De Lauretis, A., Vanoli, V., Castiglione, F., Briatico-Vangosa, F., Ma, Q., Perale, G., Haugen, H. J., & Rossi, F. (2024). Characterisation and biocompatibility of crosslinked hyaluronic acid with BDDE and PEGDE for clinical applications. *Reactive and Functional Polymers*, *200*, 105920. https://doi.org/10.1016/j.reactfunctpolym.2024.105920

Paiva, M. T. P., Kishima, J. O. F., Silva, J. B. M. D., Mantovan, J., Colodi, F. G., & Mali, S. (2024). Crosslinking Methods in Polysaccharide-Based Hydrogels for Drug Delivery Systems. *Biomedical Materials & Devices*, *2*(1), 288–306. https://doi.org/10.1007/s44174-023-00118-4

Pal, K., Paulson, A. T., & Rousseau, D. (2013). 14—Biopolymers in Controlled-Release Delivery Systems. In S. Ebnesajjad (Ed.), *Handbook of Biopolymers and Biodegradable Plastics* (pp. 329–363). William Andrew Publishing. https://doi.org/10.1016/B978-1-4557-2834-3.00014-8

Privar, Y., Skatova, A., Maiorova, M., Golikov, A., Boroda, A., & Bratskaya, S. (2024). Tuning Mechanical Properties, Swelling, and Enzymatic Degradation of Chitosan Cryogels Using Diglycidyl Ethers of Glycols with Different Chain Length as Cross-Linkers. *Gels*, *10*(7), Article 7. https://doi.org/10.3390/gels10070483

Qi, X., Tong, X., Pan, W., Zeng, Q., You, S., & Shen, J. (2021). Recent advances in polysaccharide-based adsorbents for wastewater treatment. *Journal of Cleaner Production*, *315*, 128221. https://doi.org/10.1016/j.jclepro.2021.128221

Qin, Z., Jia, X.-W., Liu, Q., Kong, B., & Wang, H. (2019). Fast dissolving oral films for drug delivery prepared from chitosan/pullulan electrospinning nanofibers. *International Journal of Biological Macromolecules*, *137*, 224–231. https://doi.org/10.1016/j.ijbiomac.2019.06.224

Raj, V., & Lee, S. (2024). State-of-the-art progress on tamarind seed polysaccharide (*Tamarindus indica*) and its diverse potential applications, a review with insight. *Carbohydrate Polymers*, *331*, 121847. https://doi.org/10.1016/j.carbpol.2024.121847

Ramli, H., Zainal, N. F. A., Hess, M., & Chan, C. H. (2022). Basic principle and good practices of rheology for polymers for teachers and beginners. *Chemistry Teacher International*, *4*(4), 307–326. https://doi.org/10.1515/cti-2022-0010

Ray, B., Schütz, M., Mukherjee, S., Jana, S., Ray, S., & Marschall, M. (2021). Exploiting the Amazing Diversity of Natural Source-Derived Polysaccharides: Modern Procedures of Isolation, Engineering, and Optimization of Antiviral Activities. *Polymers*, *13*(1), Article 1. https://doi.org/10.3390/polym13010136

Reddy, N., Reddy, R., & Jiang, Q. (2015). Crosslinking biopolymers for biomedical applications. *Trends in Biotechnology*, *33*(6), 362–369. https://doi.org/10.1016/j.tibtech.2015.03.008

Ren, L., Yang, Y., Bian, X., Li, X., Wang, B., Wang, D., Su, D., Liu, L., Yu, D., Guo, X., Zhang, X., & Zhang, N. (2022a). Physicochemical, Rheological, Structural, Antioxidant, and Antimicrobial Properties of Polysaccharides Extracted from Tamarind Seeds. *Journal of Food Quality*, *2022*. https://doi.org/10.1155/2022/9788248

Ren, L., Yang, Y., Bian, X., Li, X., Wang, B., Wang, D., Su, D., Liu, L., Yu, D., Guo, X., Zhang, X., & Zhang, N. (2022b). Physicochemical, Rheological, Structural, Antioxidant, and Antimicrobial Properties of Polysaccharides Extracted from Tamarind Seeds. *Journal of Food Quality*, *2022*(1), 9788248. https://doi.org/10.1155/2022/9788248

Ren, Y., Bai, Y., Zhang, Z., Cai, W., & Del Rio Flores, A. (2019). The Preparation and Structure Analysis Methods of Natural Polysaccharides of Plants and Fungi: A Review of Recent Development. *Molecules*, *24*(17), Article 17. https://doi.org/10.3390/molecules24173122

Rizkyana, A. D., Ho, T. C., Roy, V. C., Park, J.-S., Kiddane, A. T., Kim, G.-D., & Chun, B.-S. (2022). Sulfation and characterization of polysaccharides from Oyster mushroom *(Pleurotus ostreatus)* extracted using subcritical water. *The Journal of Supercritical Fluids*, *179*, 105412. https://doi.org/10.1016/j.supflu.2021.105412

Rosen, S. L. (1993). *Fundamental principles of polymeric materials* (2nd ed.). Wiley.

Saeidnia, S., Manayi, A., & Abdollahi, M. (2015). From in vitro Experiments to in vivo and Clinical Studies; Pros and Cons. *Current Drug Discovery Technologies*, *12*(4), 218–224.

Saidin, N. M., Anuar, N. K., & Affandi, M. M. R. M. M. (2018). Roles of Polysaccharides in Transdermal Drug Delivery System and Future Prospects. *Journal of Applied Pharmaceutical Science*, *8,*(3), 141–157. https://doi.org/10.7324/JAPS.2018.8320

Salehi, M., & Rashidinejad, A. (2025). Multifaceted roles of plant-derived bioactive polysaccharides: A review of their biological functions, delivery, bioavailability, and applications within the food and pharmaceutical sectors. *International Journal of Biological Macromolecules*, *290*, 138855. https://doi.org/10.1016/j.ijbiomac.2024.138855

Salwowska, N. M., Bebenek, K. A., Żądło, D. A., & Wcisło-Dziadecka, D. L. (2016). Physiochemical properties and application of hyaluronic acid: A systematic review. *Journal of Cosmetic Dermatology*, *15*(4), 520–526. https://doi.org/10.1111/jocd.12237

Sanyasi, S., Kumar, A., Goswami, C., Bandyopadhyay, A., & Goswami, L. (2014). A carboxy methyl tamarind polysaccharide matrix for adhesion and growth of osteoclast-precursor cells. *Carbohydrate Polymers*, *101*, 1033–1042. https://doi.org/10.1016/j.carbpol.2013.10.047

Sasisekharan, R., Raman, R., & Prabhakar, V. (2006). GLYCOMICS APPROACH TO STRUCTURE-FUNCTION RELATIONSHIPS OF GLYCOSAMINOGLYCANS. *Annual Review of Biomedical Engineering*, *8*(Volume 8, 2006), 181–231. https://doi.org/10.1146/annurev.bioeng.8.061505.095745

Schepetkin, I. A., & Quinn, M. T. (2006). Botanical polysaccharides: Macrophage immunomodulation and therapeutic potential. *International Immunopharmacology*, *6*(3), 317–333. https://doi.org/10.1016/j.intimp.2005.10.005

Semenzato, A., Costantini, A., & Baratto, G. (2015). Green Polymers in Personal Care Products: Rheological Properties of Tamarind Seed Polysaccharide. *Cosmetics*, *2*(1), Article 1. https://doi.org/10.3390/cosmetics2010001

Separovic, F., & Sani, M.-A. (2020). *Solid-State NMR: Applications in biomembrane structure*. IOP Publishing. https://iopscience-iop-org.unimib.idm.oclc.org/book/edit/978-0-7503-2532-5

Serra, M., Casas, A., Toubarro, D., Barros, A. N., & Teixeira, J. A. (2023). Microbial Hyaluronic Acid Production: A Review. *Molecules*, *28*(5), 2084. https://doi.org/10.3390/molecules28052084

Shafqat, A., Tahir, A., Mahmood, A., Tabinda, A. B., Yasar, A., & Pugazhendhi, A. (2020). A review on environmental significance carbon foot prints of starch based bio-

plastic: A substitute of conventional plastics. *Biocatalysis and Agricultural Biotechnology*, *27*, 101540. https://doi.org/10.1016/j.bcab.2020.101540

Shao, H., Zhang, H., Tian, Y., Song, Z., Lai, P. F. H., & Ai, L. (2019). Composition and Rheological Properties of Polysaccharide Extracted from Tamarind (Tamarindus indica L.) Seed. *Molecules*, *24*(7), Article 7. https://doi.org/10.3390/molecules24071218

Shi, D., Sheng, A., & Chi, L. (2021). Glycosaminoglycan-Protein Interactions and Their Roles in Human Disease. *Frontiers in Molecular Biosciences*, *8*, 639666. https://doi.org/10.3389/fmolb.2021.639666

Sinha, V. R., & Kumria, R. (2001). Polysaccharides in colon-specific drug delivery. *International Journal of Pharmaceutics*, *224*(1), 19–38. https://doi.org/10.1016/S0378-5173(01)00720-7

Sinnott, M. (2013). *Carbohydrate Chemistry and Biochemistry: Structure and Mechanism* (2nd edition). Royal Society of Chemistry.

Sonawane, S., Bagul, M., & Arya, S. (2015). Tamarind seeds: Chemistry, technology, applications and health benefits: A review. *Indian Food Industry*.

Sri, R., Ghosh, T., B. V., B., & P., L. P. (2025). Tamarind seed polymer-based formulations: Advances and applications in biomedical science. *Journal of Biomaterials Science, Polymer Edition*, 1–24. https://doi.org/10.1080/09205063.2025.2491604

Srinivasan, B., Kolli, A. R., Esch, M. B., Abaci, H. E., Shuler, M. L., & Hickman, J. J. (2015). TEER measurement techniques for in vitro barrier model systems. *Journal of Laboratory Automation*, *20*(2), 107–126. https://doi.org/10.1177/2211068214561025

Stetefeld, J., McKenna, S. A., & Patel, T. R. (2016). Dynamic light scattering: A practical guide and applications in biomedical sciences. *Biophysical Reviews*, *8*(4), 409–427. https://doi.org/10.1007/s12551-016-0218-6

Stojkov, G., Niyazov, Z., Picchioni, F., & Bose, R. K. (2021). Relationship between Structure and Rheology of Hydrogels for Various Applications. *Gels*, *7*(4), 255. https://doi.org/10.3390/gels7040255

Sudjaroen, Y., Haubner, R., Würtele, G., Hull, W. E., Erben, G., Spiegelhalder, B., Changbumrung, S., Bartsch, H., & Owen, R. W. (2005). Isolation and structure elucidation of phenolic antioxidants from Tamarind (*Tamarindus indica* L.) seeds and pericarp. *Food and Chemical Toxicology*, *43*(11), 1673–1682. https://doi.org/10.1016/j.fct.2005.05.013

Sun, P., Laurent, C. V. F. P., Scheiblbrandner, S., Frommhagen, M., Kouzounis, D., Sanders, M. G., van Berkel, W. J. H., Ludwig, R., & Kabel, M. A. (2020). Configuration

of active site segments in lytic polysaccharide monooxygenases steers oxidative xyloglucan degradation. *Biotechnology for Biofuels*, *13*(1), 95. https://doi.org/10.1186/s13068-020-01731-x

Sun, X., Guo, R., Kou, Y., Song, H., Zhan, T., Wu, J., Song, L., Zhang, H., Xie, F., Wang, J., Song, Z., & Wu, Y. (2023). Inhibition of ice recrystallization by tamarind (*Tamarindus indica* L.) seed polysaccharide and molecular weight effects. *Carbohydrate Polymers*, *301*, 120358. https://doi.org/10.1016/j.carbpol.2022.120358

Szilágyi, B. Á., Mammadova, A., Gyarmati, B., & Szilágyi, A. (2020). Mucoadhesive interactions between synthetic polyaspartamides and porcine gastric mucin on the colloid size scale. *Colloids and Surfaces B: Biointerfaces*, *194*, 111219. https://doi.org/10.1016/j.colsurfb.2020.111219

Tang, D.-Q., Zou, L., Yin, X.-X., & Ong, C. N. (2016). HILIC-MS for metabolomics: An attractive and complementary approach to RPLC-MS. *Mass Spectrometry Reviews*, *35*(5), 574–600. https://doi.org/10.1002/mas.21445

Tang, S., Chi, K., Xu, H., Yong, Q., Yang, J., & Catchmark, J. M. (2021). A covalently cross-linked hyaluronic acid/bacterial cellulose composite hydrogel for potential biological applications. *Carbohydrate Polymers*, *252*, 117123. https://doi.org/10.1016/j.carbpol.2020.117123

Tian, H., Liu, H., Song, W., Zhu, L., Zhang, T., Li, R., & Yin, X. (2020). Structure, antioxidant and immunostimulatory activities of the polysaccharides from *Sargassum carpophyllum*. *Algal Research*, *49*, 101853. https://doi.org/10.1016/j.algal.2020.101853

Tiernan, H., Byrne, B., & Kazarian, S. G. (2020). ATR-FTIR spectroscopy and spectroscopic imaging for the analysis of biopharmaceuticals. *Spectrochimica Acta Part A: Molecular and Biomolecular Spectroscopy*, *241*, 118636. https://doi.org/10.1016/j.saa.2020.118636

Tu, W., Zhu, J., Bi, S., Chen, D., Song, L., Wang, L., Zi, J., & Yu, R. (2016). Isolation, characterization and bioactivities of a new polysaccharide from *Annona squamosa* and its sulfated derivative. *Carbohydrate Polymers*, *152*, 287–296. https://doi.org/10.1016/j.carbpol.2016.07.012

Tudu, M., & Samanta, A. (2023). Natural polysaccharides: Chemical properties and application in pharmaceutical formulations. *European Polymer Journal*, *184*, 111801. https://doi.org/10.1016/j.eurpolymj.2022.111801

Tuomivaara, S. T., Yaoi, K., O'Neill, M. A., & York, W. S. (2015). Generation and structural validation of a library of diverse xyloglucan-derived oligosaccharides,

including an update on xyloglucan nomenclature. *Carbohydrate Research*, *402*, 56–66. https://doi.org/10.1016/j.carres.2014.06.031

Uccello-Barretta, G., Balzano, F., Vanni, L., & Sansò, M. (2013). Mucoadhesive properties of tamarind-seed polysaccharide/hyaluronic acid mixtures: A nuclear magnetic resonance spectroscopy investigation. *Carbohydrate Polymers*, *91*, 568–572. https://doi.org/10.1016/j.carbpol.2012.07.085

Uccello-Barretta, G., Nazzi, S., Zambito, Y., Di Colo, G., Balzano, F., & Sansò, M. (2010). Synergistic interaction between TS-polysaccharide and hyaluronic acid: Implications in the formulation of eye drops. *International Journal of Pharmaceutics*, *395*(1–2), 122–131. https://doi.org/10.1016/j.ijpharm.2010.05.031

Uman, S., Dhand, A., & Burdick, J. A. (2020). Recent advances in shear-thinning and self-healing hydrogels for biomedical applications. *Journal of Applied Polymer Science*, *137*(25), 48668. https://doi.org/10.1002/app.48668

Vatanpour, V., Yavuzturk Gul, B., Zeytuncu, B., Korkut, S., İlyasoğlu, G., Turken, T., Badawi, M., Koyuncu, I., & Saeb, M. R. (2022). Polysaccharides in fabrication of membranes: A review. *Carbohydrate Polymers*, *281*, 119041. https://doi.org/10.1016/j.carbpol.2021.119041

Vega, M. P., Lima, E. L., & Pinto, J. C. (2001). In-line monitoring of weight average molecular weight in solution polymerizations using intrinsic viscosity measurements. *Polymer*, *42*(8), 3909–3914. https://doi.org/10.1016/S0032-3861(00)00780-1

Vernon-Parry, K. D. (2000). Scanning electron microscopy: An introduction. *III-Vs Review*, *13*(4), 40–44. https://doi.org/10.1016/S0961-1290(00)80006-X

Wang, A., Liu, Y., Zeng, S., Liu, Y., Li, W., Wu, D., Wu, X., Zou, L., & Chen, H. (2023). Dietary Plant Polysaccharides for Cancer Prevention: Role of Immune Cells and Gut Microbiota, Challenges and Perspectives. *Nutrients*, *15*(13), 3019. https://doi.org/10.3390/nu15133019

Wang, L., Li, X., & Chen, Z. (2009). Sulfated modification of the polysaccharides obtained from defatted rice bran and their antitumor activities. *International Journal of Biological Macromolecules*, *44*(2), 211–214. https://doi.org/10.1016/j.ijbiomac.2008.12.006

Wang, Y., Peng, Y., Wei, X., Yang, Z., Xiao, J., & Jin, Z. (2010). Sulfation of tea polysaccharides: Synthesis, characterization and hypoglycemic activity. *International Journal of Biological Macromolecules*, *46*(2), 270–274. https://doi.org/10.1016/j.ijbiomac.2009.12.007

Wang, Z., Xie, J., Shen, M., Nie, S., & Xie, M. (2018). Sulfated modification of polysaccharides: Synthesis, characterization and bioactivities. *Trends in Food Science & Technology*, *74*, 147–157. https://doi.org/10.1016/j.tifs.2018.02.010

Wang, Z.-B., Pei, J.-J., Ma, H.-L., Cai, P.-F., & Yan, J.-K. (2014). Effect of extraction media on preliminary characterizations and antioxidant activities of *Phellinus linteus* polysaccharides. *Carbohydrate Polymers*, *109*, 49–55. https://doi.org/10.1016/j.carbpol.2014.03.057

Wende, F. J., Gohil, S., Nord, L. I., Helander Kenne, A., & Sandström, C. (2017). 1D NMR methods for determination of degree of cross-linking and BDDE substitution positions in HA hydrogels. *Carbohydrate Polymers*, *157*, 1525–1530. https://doi.org/10.1016/j.carbpol.2016.11.029

Wu, C.-S. (Ed.). (2003). *Handbook Of Size Exclusion Chromatography And Related Techniques: Revised And Expanded* (2nd ed.). CRC Press. https://doi.org/10.1201/9780203913321

Xie, F., Ren, X., Zhu, Z., Luo, J., Zhang, H., Xiong, Z., Wu, Y., Song, Z., & Ai, L. (2023). Tamarind seed polysaccharide-assisted fabrication of stable emulsion-based oleogel structured with gelatin: Preparation, interaction, characterization, and application. *Food Hydrocolloids*, *142*, 108761. https://doi.org/10.1016/j.foodhyd.2023.108761

Xie, F., Zhang, H., Nie, C., Zhao, T., Xia, Y., & Ai, L. (2021). Structural characteristics of tamarind seed polysaccharides treated by high-pressure homogenization and their effects on physicochemical properties of corn starch. *Carbohydrate Polymers*, *262*, 117661. https://doi.org/10.1016/j.carbpol.2021.117661

Xie, F., Zhang, H., Xia, Y., & Ai, L. (2020). Effects of tamarind seed polysaccharide on gelatinization, rheological, and structural properties of corn starch with different amylose/amylopectin ratios. *Food Hydrocolloids*, *105*, 105854. https://doi.org/10.1016/j.foodhyd.2020.105854

Xu, B., Li, S., Ding, W., Zhang, C., Rehman, M., Tareen, M., Wang, L., & Huang 黄淑成, S.-C. (2024). From structure to function: A comprehensive overview of polysaccharide roles and applications. *Food Frontiers*, *6*, 15–39. https://doi.org/10.1002/fft2.490

Yamatoya, K., & Shirakawa, M. (2003). Xyloglucan: Structure, rheological properties, biological functions and enzymatic modification. *Curr. Trends Polym. Sci.*, *8*, 27–72.

Yamatoya, K., Tabuchi, A., Suzuki, Y., & Yamada, H. (2020). Chapter 20 - Tamarind seed polysaccharide: Unique profile of properties and applications. In K. Pal, I. Banerjee, P. Sarkar, D. Kim, W.-P. Deng, N. K. Dubey, & K. Majumder (Eds.), *Biopolymer-Based Formulations* (pp. 445–461). Elsevier. https://doi.org/10.1016/B978-0-12-816897-4.00020-5

Yang, M., Ren, W., Li, G., Yang, P., Chen, R., & He, H. (2022). The effect of structure and preparation method on the bioactivity of polysaccharides from plants and fungi. *Food & Function*, *13*(24), 12541–12560. https://doi.org/10.1039/D2FO02029G

Yang, Q., Peng, J., Xiao, H., Xu, X., & Qian, Z. (2022). Polysaccharide hydrogels: Functionalization, construction and served as scaffold for tissue engineering. *Carbohydrate Polymers*, *278*, 118952. https://doi.org/10.1016/j.carbpol.2021.118952

Yau, W. W. (with Internet Archive). (1979). *Modern size-exclusion liquid chromatography: Practice of gel permeation and gel filtration chromatography*. New York : Wiley. http://archive.org/details/modernsizeexclus0000yauw

Yermak, I. M., Davydova, V. N., Kravchenko, A. O., Chistyulin, D. A., Pimenova, E. A., & Glazunov, V. P. (2020). Mucoadhesive properties of sulphated polysaccharides carrageenans from red seaweed families Gigartinaceae and Tichocarpaceae. *International Journal of Biological Macromolecules*, *142*, 634–642. https://doi.org/10.1016/j.ijbiomac.2019.10.005

Yermak, I. M., Davydova, V. N., & Volod'ko, A. V. (2022). Mucoadhesive Marine Polysaccharides. *Marine Drugs*, *20*(8), 522. https://doi.org/10.3390/md20080522

Yoon, W. H., & Lee, K. H. (2019). Rheological properties and efficacy of the formulation of hyaluronic acid with tamarind seed polysaccharide for arthritis. *Biorheology*, *56*(1), 31–38. https://doi.org/10.3233/BIR-190208

York, W. S., Harvey, L. K., Guillen, R., Albersheim, P., & Darvill, A. G. (1993). Structural analysis of tamarind seed xyloglucan oligosaccharides using beta-galactosidase digestion and spectroscopic methods. *Carbohydrate Research*, *248*, 285–301. https://doi.org/10.1016/0008-6215(93)84135-s

Yu, Y., Shen, M., Song, Q., & Xie, J. (2018). Biological activities and pharmaceutical applications of polysaccharide from natural resources: A review. *Carbohydrate Polymers*, *183*, 91–101. https://doi.org/10.1016/j.carbpol.2017.12.009

Yu, Y., Shen, M., Wang, Z., Wang, Y., Xie, M., & Xie, J. (2017). Sulfated polysaccharide from *Cyclocarya paliurus* enhances the immunomodulatory activity of macrophages. *Carbohydrate Polymers*, *174*, 669–676. https://doi.org/10.1016/j.carbpol.2017.07.009

Yu, Y., Xu, S., Li, S., & Pan, H. (2021). Genipin-cross-linked hydrogels based on biomaterials for drug delivery: A review. *Biomaterials Science*, *9*(5), 1583–1597. https://doi.org/10.1039/D0BM01403F

Zafar, S., Hanif, M., Azeem, M., Mahmood, K., & Gondal, S. A. (2022). Role of crosslinkers for synthesizing biocompatible, biodegradable and mechanically strong hydrogels with desired release profile. *Polymer Bulletin*, *79*(11), 9199–9219. https://doi.org/10.1007/s00289-021-03956-8

Zaia, J. (2004). Mass spectrometry of oligosaccharides. *Mass Spectrometry Reviews*, *23*(3), 161–227. https://doi.org/10.1002/mas.10073

Zhang, B., Lan, W., & Xie, J. (2022). Chemical modifications in the structure of marine polysaccharide as serviceable food processing and preservation assistant: A review. *International Journal of Biological Macromolecules*, *223*, 1539–1555. https://doi.org/10.1016/j.ijbiomac.2022.11.034

Zhang, C., Sui, Y., Liu, S., & Yang, M. (2024). In vitro and in vivo experimental models for cancer immunotherapy study. *Current Research in Biotechnology*, *7*, 100210. https://doi.org/10.1016/j.crbiot.2024.100210

Zhang, D. (2014). *2D NMR Characterization of Cellobiose Sulfate Hydrolyzed from Cellulose Nanocrystals* [Masters]. Auburn University.

Zhang, F., Xu, S., & Wang, Z. (2011). Pre-treatment optimization and properties of gelatin from freshwater fish scales. *Food and Bioproducts Processing*, *89*(3), 185–193. https://doi.org/10.1016/j.fbp.2010.05.003

Zhang, H., Cui, H., Xie, F., Song, Z., & Ai, L. (2024a). Tamarind seeds polysaccharide: Structure, properties, health benefits, modification and food applications. *Food Hydrocolloids*, *155*, 110222. https://doi.org/10.1016/j.foodhyd.2024.110222

Zhang, H., Cui, H., Xie, F., Song, Z., & Ai, L. (2024b). Tamarind seeds polysaccharide: Structure, properties, health benefits, modification and food applications. *Food Hydrocolloids*, *155*, 110222. https://doi.org/10.1016/j.foodhyd.2024.110222

Zhang, H., Zhao, T., Wang, J., Xia, Y., Song, Z., & Ai, L. (2020). An amendment to the fine structure of galactoxyloglucan from Tamarind (Tamarindus indica L.) seed. *International Journal of Biological Macromolecules*, *149*, 1189–1197. https://doi.org/10.1016/j.ijbiomac.2020.01.284

Zhang, T., Zhao, S., Chen, Y., Wang, J., Zhang, W., Liu, J., Kan, Y., Li, J., Guo, X., & Li, H. (2023). In-depth characterization of 1,4-butanediol diglycidyl ether substituted

hyaluronic acid hydrogels. *Carbohydrate Polymers*, *307*, 120611. https://doi.org/10.1016/j.carbpol.2023.120611

Zhang, X., Qin, M., Xu, M., Miao, F., Merzougui, C., Zhang, X., Wei, Y., Chen, W., & Huang, D. (2021). The fabrication of antibacterial hydrogels for wound healing. *European Polymer Journal*, *146*, 110268. https://doi.org/10.1016/j.eurpolymj.2021.110268

Zhou, W., Apkarian, R., Wang, Z. L., & Joy, D. (2007). Fundamentals of Scanning Electron Microscopy (SEM). In W. Zhou & Z. L. Wang (Eds.), *Scanning Microscopy for Nanotechnology: Techniques and Applications* (pp. 1–40). Springer. https://doi.org/10.1007/978-0-387-39620-0_1

Ziliani, S., Alekseeva, A., Antonini, C., Esposito, E., Neggiani, F., Sansò, M., Guerrini, M., & Bertini, S. (2024). Synthesis and Physiochemical Properties of Sulphated Tamarind (Tamarindus indica L.) Seed Polysaccharide. *Molecules*, *29*(23), Article 23. https://doi.org/10.3390/molecules29235510

Zong, A., Cao, H., & Wang, F. (2012). Anticancer polysaccharides from natural resources: A review of recent research. *Carbohydrate Polymers*, *90*(4), 1395–1410. https://doi.org/10.1016/j.carbpol.2012.07.026

La borsa di dottorato cofinanziata con risorse dell'Unione europea-*NextGeneration EU*
Piano Nazionale di Ripresa e Resilienza Missione 4 – Componente 1 – Riforma 4.1
Riforma dei Dottorati – Inv. 4.1 Borse PNRR patrimonio Culturale –
CUPH41J22000230009

RINGRAZIAMENTI

Questo lavoro di dottorato non sarebbe stato possibile senza l'aiuto e il supporto di molte persone che vorrei ringraziare.

Grazie al Prof. Carlo Antonini per avermi guidato al meglio in questo percorso e per essere sempre stato presente e disponibile ad ogni evenienza.

Vorrei inoltre ringraziare il Dott. Marco Sansò per l'opportunità che mi ha dato di svolgere questo percorso in collaborazione con IFBS e per la gentilezza e disponibilità dimostrati durante questi anni.

Un grazie speciale va alla Dott.ssa Sabrina Bertini per tutto quello che mi ha insegnato in questo percorso e per il sostegno non solo a livello lavorativo ma anche personale.

Un grande grazie va anche al gruppo di laboratorio dell'Università Milano-Bicocca per la grande disponibilità e i consigli che mi hanno dato. Uno speciale ringraziamento va alla Dott.ssa Irene Tagliaro per l'aiuto dato per la realizzazione di questo progetto.

Un enorme grazie va a tutti i collaboratori dell'Istituto Ronzoni che mi hanno insegnato tutto quello che ho imparato presso l'Istituto e che sono stati di grande supporto durante questi anni. Un ringraziamento speciale è per i miei due compagni di dottorato Marco e Sofia, per il supporto, le risate, i lamenti e il conforto nei momenti più disperati ma soprattutto per il legame di amicizia che si è creato.

Uno speciale ringraziamento anche per Arianna per il sostegno, i lamenti condivisi e per esserci sempre stata.

Un grande grazie va a Veronica, avermi sempre ascoltata e consigliata e per aver alleggerito anche i momenti più difficili.

Non sarei mai riuscita a completare questo percorso senza ovviamente la vicinanza dei miei amici.

Un grande grazie va al gruppo capodannos, per i bellissimi momenti passati insieme tra feste, compleanni e silent che mi hanno permesso di divertirmi e svagarmi anche nei momenti più complicati.

In particolare, vorrei ringraziare i miei amici di una vita Anna, Ari, Cami, Cozzo, Davide, Fede e Gallo senza i quali non saprei proprio cosa fare. Grazie per esserci sempre amici.

Vorrei inoltre ringraziare Emi, che mi è sempre stata vicina e mi ha sempre ascoltata quando ne avevo più bisogno.

Un ringraziamento gigante è per Silvio, che mi supporta e soprattutto mi sopporta in ogni occasione. Non potrei essere più grata di averti nella mia vita.
Questo mio traguardo non sarebbe inoltre stato di certo possibile senza il supporto di tutta la mia famiglia.
Un grande grazie alla mia nonna social Giselda, per le storie che mi raccontava da bambina, per tuti i piatti che ci cucini che ti risollevano sempre il morale e che mi è sempre stata vicina in ogni momento.
Un grazie speciale a mia zia Orianna per avermi sempre supportata, consigliata e incoraggiata.
Un grandissimo grazie anche ai miei zii Michela e Franco, per il sostegno e la vicinanza dimostrati in ogni momento.
Un ringraziamento gigante ai miei cugini Riccardo e Noemi, per tutti i bei momenti passati in famiglia, le risate, i film, le partite per essermi stata accanto sempre.
Un ringraziamento a Mario che ormai è come un fratello, che riesce sempre a farci ridere, per tutte le vacanze passate insieme e per esserci sempre nel momento del bisogno.
Un grazie al mio cognatino Alessandro per le risate, le prese in giro e per il sostegno in tutti questi anni.
Uno speciale grazie a mia sorella Fabiana, che è sempre stata un esempio per me e mi è sempre stata vicina e incoraggiata in ogni momento.
Un grazie gigante alla mia mamma Alberta, per essere sempre stata la nostra roccia e per averci sostenute sempre e in ogni caso.
Infine, un ringraziamento speciale è per le persone che vorrei che fossero qui con me a festeggiare questo traguardo.
A mio nonno Gino, per avermi fatta giocare da bambina, per averci fatto divertire e per esserci sempre stato.
A mio zio Beppe, che ha sempre incoraggiata nelle mie decisioni e che mi è sempre stato vicino nei traguardi importanti nella mia vita.
A mio papà Mario, per sempre stato il mio modello, per avermi sempre supportata in qualunque decisione e per essere stato il miglior papà che avrei mai potuto desiderare.
Ci mancate.